SYNTHESIS, CHARACTERIZATION, AND ANTIMICROBIAL STUDIES OF MANGANESE (II) AND EUROPIUM (III) METAL ION DOPED ZINC OXIDE NANOPARTICLES FOR POTENTIAL CLINICAL APPLICATIONS

A thesis presented to the faculty of the Graduate School of
Western Carolina University in partial fulfillment of the
requirements for the degree of Master of Science in Chemistry.

By

Nicole Ann Dragan

Director: Dr. Channa De Silva
Assistant Professor of Chemistry
Department of Chemistry and Physics

Committee Members: Dr. Indrani Bose, Biology
Dr. David Evanoff, Jr., Chemistry

June 2016

ACKNOWLEDGEMENTS

First and foremost, I would like to thank the Department of Chemistry and Physics at Western Carolina University, Cullowhee, NC for giving me the opportunity to further my education in the Masters of Chemistry program. I would like to give special thanks to my director, Dr. Channa De Silva for his encouragement and advice throughout the progress of my degree. Thank you to my other TRAC committee members, Dr. David Evanoff and Dr. Indrani Bose for their help throughout my project and their willingness to answer numerous questions. Without my TRAC members, the completion of this project would not be possible and I appreciate all of the advice they have offered throughout this process. I would also like to acknowledge Dr. Indika Arachchige and Virginia Commonwealth University, Richmond, VA for their collaboration on the band gap studies. Additional acknowledgements to Dr. Carmen Huffman and Stephen Printz for their collaboration and guidance for the cotton modification studies. Thanks to the Clemson University Electron Microscope Facility for allowing access to their facility to obtain images. My sincerest gratitude goes to all of the faculty and staff who have supported me along the way in the WCU Department of Chemistry and Physics and the Department of Biology at WCU. Thank you to all of my friends and family who have supported and encouraged the pursuit of my graduate degree, and particular thanks to Matt Burleson for his enthusiasm and support for my degree and for always being willing to study with me and to accompany me to campus. Without the guidance and assistance of these extraordinary people, my success would not be possible.

TABLE OF CONTENTS

LIST OF TABLES

LIST OF FIGURES

LIST OF ABBREVIATIONS

AST .....antimicrobial susceptibility testing

ATR.....attenuated total reflectance

a.u.....arbitrary units

CFU.....colony forming units

EDX .....energy dispersive X-ray spectroscopy

EPA.....Environmental Protection Agency

EUCAST .....European Committee on Antimicrobial Susceptibility Testing

eV.....electron volts

HAI .....hospital associated infection

ICP-OES .....inductively coupled plasma-optical emission spectroscopy

MH .....Mueller Hinton

MHA .....Mueller Hinton agar

MHB .....Mueller Hinton broth

MIC.....minimum inhibitory concentration

OD.....optical density

PVP .....poly(vinylpyrrolidinone)

ROS.....reactive oxygen species

SEM .....scanning electron microscopy

TEM .....transmission electron microscopy

UV-Vis.....ultraviolet-visible spectroscopy

XRD .....X-ray powder diffraction

ABSTRACT

SYNTHESIS, CHARACTERIZATION, AND ANTIMICROBIAL STUDIES OF MANGANESE (II) AND EUROPIUM (III) METAL-DOPED ZINC OXIDE NANOPARTICLES FOR POTENTIAL CLINICAL APPLICATIONS

Nicole Ann Dragan, M.S.

Western Carolina University (June 2016)

Director: Dr. Channa De Silva

Zinc oxide (ZnO) nanomaterials have a unique set of properties making them desirable for a variety of industrial applications including optical, electronic and biomedical technology. Our research is focused on enhancing the antimicrobial activity of ZnO nanoparticles. Our previous research used a precipitation method for making ZnO nanoparticles with manganese doping and subsequently, the particles were introduced into cotton fabric for possible clinical use. However, these particles lacked monodispersity and after three washes, the cotton fabric no longer possessed the antimicrobial properties. The following research proposes a comparative study of synthetic methods by developing a selective precipitation method for manganese (II) doped ZnO nanoparticles and adapting a literature precipitation method for europium (III) doped ZnO nanoparticles. Herein, the purpose of the research is focused on doping ZnO nanoparticles with Mn^{2+} and Eu^{3+} metal ions to explore the effects of metal ion doping and the particle size on the electronic structure and antimicrobial properties. The nanoparticles were characterized using absorption and luminescence spectroscopy, X-ray powder diffraction (XRD), transmission electron microscopy (TEM), dynamic light scattering (DLS), diffuse reflectance spectroscopy, and inductively coupled plasma-optical emission spectroscopy (ICP-OES). Nanoparticle attachment

to cotton was performed using two methods, a literature attachment method using 2-propanol, and a collaborative cotton modification method using β-cyclodextrin as a crosslinker. Antimicrobial activity of the metal-doped nanoparticles was evaluated using two antimicrobial susceptibility testing techniques: agar diffusion and minimum inhibitory concentration (MIC) against *Escherichia coli* (*E. coli*), *Staphylococcus aureus* (*S. aureus*), and *Staphylococcus epidermidis* (*S. epidermidis*). 5% Eu^{3+} doped ZnO (E5) nanoparticles demonstrated the lowest MIC across all three bacterial species resulting in an MIC value range of 1.25 – 0.625 mg/mL, 2.50 – 1.25 mg/mL, and 0.625 – 0.313 mg/mL for *E. coli*, *S. aureus* and *S. epidermidis*, respectively. Agar diffusion and time-dependent studies evaluated the nanoparticle attachment to cotton textiles against *S. aureus* bacteria species. Time-dependent testing showed that antimicrobial activity was retained even after three washes for nanoparticles attached to the modified cotton, improving upon our previous research.

CHAPTER 1. BACKGROUND

1.1 Hospital Acquired Infections and Current Preventative Measures

One of the most potentially devastating global problems is that of antimicrobial resistance which is made even more devastating by hospital-acquired infections. Hospital-acquired infections (HAI) are infections that develop subsequent to hospitalization, and specifically those that begin after 48 hours and were not manifested at the time of admission.[1] The United States alone combats 1.7 million hospital-acquired infections annually, 16% of which are antibiotic resistant to the common therapies.[2,3] This results in a cost of approximately $9.8 billion per year.[3] Magill, *et al.* found that in a 183 hospital survey, 4% of patients out of the 11,282 had at least one hospital-associated infection.[4] HAI can lengthen hospitalization, increase the probability for complications and raise the cost of medical bills significantly.[1]

Research has shown that there are several prevalent pathogens which account for 84% of HAIs: coagulase-negative staphylococci, *Staphylococcus aureus, Enterococci, Candida* species, *Escherichia coli, Pseudomonas aeruginosa, Klebsiella pneumonia, Enterobacter* species, *Acinetobacter baumannii*, and *Klebsiella oxytoca.*[2] *Staphylococci* and *Staphylococcus aureus* account for the most infections at 30%.[2] Several methods to prevent the transmission of these common pathogens are in place in modern hospitals. One of the most fundamental ways to prevent HAIs is proper hand hygiene.[5] The World Health Organization (WHO) recommends clinicians wash their hands before touching patients, after touching patients or after touching patients' surroundings with soap and water for at least 15 seconds, or with alcohol based hand sanitizer containing chlorhexidine.[5]

Other preventive measures include personal protective equipment like gloves, gowns, masks and shoe coverings.[5] Care equipment that is non-disposable must be sterilized properly prior to its next use.[5]

The hospital environment must be cleaned on a regular schedule with high-quality disinfecting agents.[5] This is especially important to things that the patient will be in contact with frequently like the bedrails, bedside tables, doors and knobs, and the care equipment. Due to the lengthy survival period for some pathogens, like methicillin-resistant *Staphylococcus aureus* (MRSA), and *Clostridium difficile*, disinfectants registered by the Environmental Protection Agency (EPA) must be used for hospital environment cleaning.[5] Textiles, on the other hand, have less stringent guidelines for cleaning and disinfection, leading to the potential for spread of pathogens from patient to patient with hospital turnover rates.[6] Lack of stringency on these materials has led to research on the survival rate and time for clinically-important pathogenic species.

1.1.1 Hospital Fabrics and Bacterial Growth/Viability

Millions of microorganisms are encountered on hospital and healthcare facility textiles every day. Hospital textiles include commonly used items like bed sheets, towels, hospital gowns, scrubs/uniforms, surgical drapes and blankets.[6] These items are often woven textiles which are susceptible to bacterial growth under the right environmental conditions.[7] Moisture and temperature are two of the most important conditions for the proliferation of bacteria.[7] Patient bed sheets and blankets are the most susceptible to proliferation since the patient's body heat and the humidity make appropriate conditions for bacterial growth.[7] Due to this, and the patients contact with the bed linens, it is likely that microorganisms can survive on the fabrics for long periods of time, especially when laundering conditions do not reach high enough

temperatures to destroy bacterial cells.[7] *Staphylococcus aureus*, a clinically important gram-positive bacterium, can survive up to 19 days on cotton fabric and 21 days on blends.[8] It is also reported that *Staphylococcus aureus* can survive a 10 minute wash cycle at 54 °C, even after drying.[6]

1.2 Antimicrobial Materials

These staggering statistics for pathogen survival on textiles and other surfaces, has highlighted the field of antimicrobial materials, especially as antibiotics become more and more resistant. Antimicrobials are defined as materials that can kill or prevent the proliferation of microorganisms, like bacteria and fungi.[9] Some commonly used antimicrobial agents include ethanol (50-70%), isopropanol (50-70%), formaldehyde, silver salts, hypochlorite, and ethylene oxide gas.[9] These antimicrobials are defined by two different categories: antiseptic and disinfectants.[9] Antiseptics, like ethanol, are considered relatively harmless and can be applied externally.[9] Disinfectants kill microorganisms but may not kill their spores and are used for cleaning of countertops, floors, and other surfaces[9]. Disinfectants like sodium hypochlorite or bleach, are safe for these surfaces but not the body.[9]

Metal oxides have also been found to have antimicrobial activity, and much research has focused on using these materials in the clinical settings for wound dressings, biofilm coatings, dental fillings and in urinary catheters to prevent common infections.[10,11] Metal oxides with antimicrobial activity include iron oxide (Fe_3O_4), titanium dioxide (TiO_2), copper oxide (CuO) and zinc oxide (ZnO).[10] ZnO and TiO_2 have been studied widely in the literature for their antimicrobial activity.[10–13] The advantages of these materials as antimicrobial agents is their relative low cost and limited toxicity[10]. ZnO, specifically, has been shown to be an effective antimicrobial agent against a broad range of bacteria.[11] Zinc oxide is also used often in many

everyday materials from sunscreen, to diaper rash ointment and even as a food additive. ZnO is also approved by the Food and Drug Administration (FDA) for its antimicrobial activity and low toxicity to the host. As a food additive, ZnO has been shown to be effective against food-borne pathogens, like *E. coli* (O157:H7).[11] Due to metal oxide's antimicrobial activity, and the flourish of nano-research, metal oxide nanomaterials as antimicrobial agents has come into light.

1.2.1 Antimicrobial Nanomaterials

Antimicrobial nanomaterials have been the frequent subject of research efforts in recent years. Nanomaterials have dimensions of less than 100 nanometers (nm) in size, and at this small size they often exhibit enhanced chemical and physical properties when compared to their bulk counterparts.[10,11,14] Metal and metal oxide nanomaterials are currently in use today as antimicrobial agents and have numerous mechanisms for action. ZnO has been shown to have an antibacterial effect in both light and dark conditions, and nano-ZnO has a greater antimicrobial effect due to the larger number of surface defects and greater surface area.[12] The two most common pathways for nanomaterials' bactericidal mechanism are damage to the membrane of the bacterial cell, and production of reactive oxygen species (ROS), or oxygen radicals.[10,12] Oxygen radicals potential for disrupting the proliferation of bacteria is a result of several different effects. The ROS can cause oxidative stress for the bacteria cell, leading to damage to macromolecules within the cell, peroxidation of cell lipids, enzyme inhibition and can cause damage to both DNA and RNA. Concentration dependent, when many ROS are available the cell will die, but if concentration is on the lower range, the cell will undergo DNA damage leading to mutations.[10] Recently, Prassana and Vijavaraghavan studied the mechanism of the antibacterial activity of ZnO specifically and found that ROS are produced in both light and dark, while exposure to UV or ambient light toxicity of nanomaterials is considered photocatalytic, in

the dark, ROS are still produced, especially in aqueous suspensions of ZnO.[12] They found conclusively that reactive oxygen species including hydroxyl radical ($^{\bullet}OH$), superoxide anion ($^{\bullet}O_2^-$), and hydrogen peroxide (H_2O_2) are significantly produced from aqueous suspensions of ZnO.[12] The ROS are formed in UV light excitation, under ambient light, and in the dark, at room temperature. In the dark, singlet oxygen formation is not possible because this requires electron excitation to the conduction band which cannot occur without a photon.[8] Furthermore, they also found that surface defects are a core contributor to the production of ROS.[12] Nanocrystalline ZnO is abundant in surface defects, therefore, providing the opportunity for more contact to exist between the nanomaterial surface and the microbes.[12] The mechanism of ROS generation in the dark is described below.[12]

$$O_2 + e^- \rightarrow {}^{\bullet}O_2^- \quad (1)$$

$$^{\bullet}O_2^- + H^+ \rightarrow {}^{\bullet}HO_2 \quad (2)$$

$$^{\bullet}HO_2 + {}^{\bullet}HO_2 \rightarrow H_2O_2 + O_2 \quad (3)$$

$$H_2O_2 + {}^{\bullet}O_2^- \rightarrow O_2 + {}^{\bullet}OH + OH^- \quad (4)$$

In addition to metal oxides, a variety of materials have been shown to exhibit these antimicrobial properties, from organic based materials like carbon nanotubes, to inorganic salts like ammonium chloride to bio-synthesized nanomaterials.[9,15–17] Single-walled carbon nanotubes with an average diameter of 0.9 nm exhibited antimicrobial activity against *Escherichia coli* (*E. coli*) bacterial cells by physically damaging the outer cell membrane, however, cells must be in direct contact with the carbon nanotubes for the cell death to occur.[15] Composite nanomaterials have also been shown to exhibit tunable antimicrobial activity, Sambhy, *et al.* developed a

composite with silver bromide (AgBr) with synthesized polymer poly(4-vinylpyridine-*co*-poly(4-vinyl-*N*-hexylpyridinium bromide) shortened NPVP that was found to be effective against gram-positive, *Bacillus cereus* and *Staphylococcus aureus*, and gram-negative, *Escherichia coli* and *Pseudomonas aeruginosa*, bacterial species. These nanomaterials were tunable as the research group found they were able to control the release of silver ions (Ag^+) by controlling the size of the AgBr nanoparticles.[18] Gold and silver nanoparticles with antimicrobial activity have been synthesized through bio-inspired means.[17,19] Gold nanoparticles were synthesized with an average diameter of 150 nm by bioreduction of chloroauric acid using the extract from *Mentha piperita* and were effective against *E. coli*.[19]

1.3 Zinc Oxide Nanomaterials: Synthetic Methods

ZnO nanoparticles are an example of a semiconductor nanostructure.[20] ZnO is classified as a group II-VI semiconductor, referencing zinc and oxygen's respective positions in the periodic table, and is often used because of its wide direct band gap of 3.37 electron volts (eV) and its generally low toxicity, cost-effectiveness and ability to biodegrade.[20] ZnO nanoparticles can be synthesized in a myriad of ways, often resulting in different sizes and shapes.[20] One of the most common shapes is the hexagonal crystal structure, known as the Wurtzite crystal structure.[20] Common synthetic methods include precipitation, thermal decomposition , microwave, and solvothermal methods.[20]

Precipitation methods generally involve the use of a zinc salt and a base to induce precipitation. Several research groups have investigated the precipitation method to make ZnO nanomaterials, often with the goal for different applications.[20–24] Lanje *et al*., has reported a precipitation method using zinc nitrate and sodium hydroxide, as precursors, with a 0.3% starch solution as a stabilizing agent, resulting in nearly consistent spherical particles with a diameter of

40 nm.[21] Other precipitation methods utilize zinc acetate with ammonium carbonate[24] or potassium hydroxide[25] resulting in particle sizes of 30 nm, and 160-500 nm, respectively. Zinc sulfate with ammonium hydroxide and ammonium bicarbonate with diameters between 100 and 1000 nm have also been reported for synthesis of ZnO.[26] Precipitation methods have the advantage that they are often cost-effective, have relatively short reaction times, but can produce polydisperse particle sizes, as the previous examples indicate. Thermal decomposition methods can help to eliminate the issue of polydispersity. For example, a thermal decomposition method using zinc acetate has been reported resulting in uniform particle size between 20 and 30 nm.[27]

1.3.1 Metal Doping and its Effect on the Antimicrobial Activity of ZnO Nanomaterials

Previous research has shown that introducing a metal dopant can alter the band gap of ZnO, therefore, increasing the antimicrobial activity.[28] The band gap is the energy difference between the valence band and conduction band of a semiconductor, where the valence band is fully occupied with valence electrons but the conduction band is unoccupied.[29] When electrons are excited enough, they form an electron-hole pair, where the electrons are promoted to the conduction band, therefore creating a void, or *hole*, in the valence band.[29] Electrons and holes are mobile charge carriers, where the electrons in the conduction band are referred to as conduction electrons because once they break loose they are free to move in the crystal.[29] Electrons moving along the same axis within the crystal structure is what is considered an electrical current.[6] Introducing a dopant into the semiconductor structure creates impurities resulting in an increase in conduction electrons.[29]

Manganese, Mn^{2+}, (5 and 10%) doped ZnO has been studied for its effect on the antimicrobial activity and structure of ZnO. The researchers found that the Mn^{2+} doping increased the crystalline size with increasing concentrations of Mn^{2+} and showed greater

antimicrobial activity against several bacterial species compared to undoped ZnO prepared the same way, but was most effective against *E. coli*.[13] Tin (Sn) doped ZnO has also been evaluated for its antibacterial activity.[30] Sn doped ZnO was synthesized by a co-precipitation method and the resulting nanoparticles were evaluated against *E. coli*, *Psuedomonas aeruginosa* and *S. aureus*.[30] Sn doping increased particle size from 17 nm for undoped ZnO to 36 nm for 6% Sn-doped ZnO.[30] All doping percentages (2, 4 and 6% Sn) were found to exhibit antimicrobial activity but no pattern was found.[30] The 2% Sn doped ZnO had a smaller zone of inhibition when compared to undoped ZnO, but 4% Sn doped had a greater inhibition zone compared to undoped ZnO against all three bacterial species.[30]

Lanthanide doping of ZnO has also been reported in the literature with several lanthanides used for doping including Sm^{3+}, Eu^{3+}, Gd^{3+}, Yb^{3+}, and Nd^{3+}.[31–35] Sm^{3+} doped ZnO based thin films were evaluated for their photocatalytic activity and sterilization properties.[31] Sm^{3+} doped ZnO was synthesized with an average particle diameter of 35 nm, and its sterilizing properties were evaluated against *S. aureus*.[31] The authors found that *S. aureus* applied to the surface of the thin films reduced to an insignificant level after 240 minutes under UV light, but in dark conditions, was only reduced by approximately 11.7%.[31] Though Eu^{3+} doped ZnO has been studied for its effects on optical and electronic properties of ZnO, antimicrobial studies have not yet been reported, to our knowledge.[26,36,37]

1.4 Nanomaterials and their Attachment to Textiles

Nanotechnology applied to textiles has become an increasing demand to make textiles more durable, UV-resistant, stain-resistant, wrinkle-resistant, antimicrobial, or to eliminate static.[20] Antimicrobial properties of nanomaterials can improve fabric and help prevent HAI. Several different nanomaterials have been researched for their ability to be attached to textiles

for antimicrobial activity, including metal oxides TiO_2 and ZnO, and metals like silver and gold.[38] Poly[(allyl glycidyl ether)-*co*-(dimethyl diallyl ammonium chloride)]/ZnO, abbreviated P(AGE-DMDAAC)/nano ZnO, with average diameter between 70 and 100 nm were attached to cotton textiles and found to be effective against *E. coli*, *S. aureus* and *C. albicans*.[16] The attachment method involved treating the cotton samples with varying amount of P(AGE-DMDAAC)/ZnO and P(AGE-DMDAAC) separately, and separate sample prepared in solutions containing no P(AGE-DMDAAC)/ZnO or P(AGE-DMDAAC) as a control. Even after washing 10 times, cotton treated with 5 g/L of the P(AGE-DMDAAC)/ZnO were 97% effective against *E. coli.*[16]

1.5 Antimicrobial Activity Testing

Antimicrobial susceptibility tests (AST) are clinical microbiology tests which are used to detect potential drug resistance of common pathogens but is also used to evaluate the efficacy of drugs for individual pathogenic infections.[39] In nanomaterials research, these tests are often employed to test the potential of synthesized materials for their effectiveness as antimicrobial agents. These tests are divided into qualitative and quantitative testing methods. Qualitative AST testing in nanomaterial research is used to establish whether or not a material does or does not exhibit antimicrobial activity. An example of a qualitative test is the so-called agar diffusion testing method, which involves introducing nanomaterials into wells in the agar plates. This method is based off of the commonly used disc diffusion method which is performed by applying bacterial inoculum at a concentration of ca. 1-2 x 10^8 CFU/mL to the surface of a Mueller-Hinton agar plate, and paper antibiotic disks are placed on the inoculated surface of the agar, then incubated at 37° C for 16-24 hours before evaluating the results.[39]

A quantitative test, such as the minimum inhibitory concentration (MIC) test, evaluates the minimum concentration of antimicrobial agent required to destroy bacterial cells.[39] This test is performed manually using a bioassay which evaluates the reducing environment of the living cell.[40] The MIC test is used in nanomaterial research to determine the minimum number of nanoparticles needed to inhibit the growth of clinically-important pathogens. The visual color change indicates the viability of bacterial cells, cells that are viable are indicated by the color change from blue to pink.

CHAPTER 2. INTRODUCTION TO RESEARCH

ZnO nanoparticles can be synthesized in a myriad of ways, often resulting in different sizes and shapes.[20] One of the most common shapes is the hexagonal crystal structure, known as the Wurtzite crystal structure.[12] These particles exhibit strong antimicrobial properties which are most commonly attributed to formation of reactive oxygen species (ROS).[12,28,41] Due to this, much research has been focused on how to enhance the antimicrobial activity. Researchers have investigated this by altering the synthetic methods for ZnO nanoparticles, and through the introduction of a metal dopant into the inorganic semiconductor.[42] Transition metal doping has been studied widely in the literature, however, lanthanide doping specifically for antimicrobial purposes is limited to only a few studies.[30,31,43]

Lanthanide doping has the potential to influence the recombination of electron-hole pairs in the valence band, leading to more electrons available in the conduction band.[31,42] The greater the number of electrons in the conduction band, the more potential for the formation of ROS. Introducing a dopant can also increase the surface defects in nano-ZnO which can aid in increased contact between the nanomaterial and bacterium.[12] Europium (Eu^{3+}) doping was chosen for our research purposes for two reasons: (1) multiple studies of europium (Eu^{3+}) doped ZnO have been reported in literature, but none have investigated Eu^{3+} doping as an antibacterial agent and (2) Eu^{3+} doping has the potential to be used as an imaging agent due to its luminescent properties.[36,37,26] Our current study is focused on studying the antibacterial activity of ZnO nanoparticles as a function of Eu^{3+} metal ion doping. An imaging agent with antimicrobial activity would be advantageous for minimizing bacterial infections during clinical practices.

The purpose of this research is to (1) synthesize Mn^{2+} and Eu^{3+} doped ZnO nanoparticles and characterize the particles using a variety of analytical techniques, (2) examine the effect of Mn2+ and Eu 3+ metal ion doping and the particle size on both antimicrobial activity and the electronic properties of ZnO nanoparticles (3) investigate the effect of different ZnO synthetic methods on the antimicrobial activity and (4) to develop a preliminary method to functionalize the Eu^{3+} doped ZnO nanoparticles for incorporation into cotton fabric. The Eu^{3+} doped nanoparticles were synthesized via a modified low temperature precipitation method.[22] The goal of the Eu^{3+} ion doped ZnO nanoparticles is to potentially enhance the antimicrobial capability of ZnO and compare lanthanide doping to transition metal doping. Mn^{2+} doped ZnO nanoparticles will be synthesized following a previously developed synthetic method in our laboratory with size separation via selective precipitation.[44]

Antimicrobial susceptibility testing (AST) will be employed to determine the extent of the antimicrobial activity of the nanoparticles on *E. coli*, *S. aureus* and *S. epidermidis* bacteria species. The first test is called the "agar diffusion test" where the bacterial growth inhibition is qualitatively measured in the presence of the nanoparticles. The second AST is the minimum inhibitory concentration test (MIC). The MIC test encompasses inoculating the bacterial species into a liquid media and introducing a suspension of nanoparticles in varying dilutions across the wells. Resazurin (sodium salt), also the main ingredient in Alamar Blue dye, is incorporated into the MIC test to serve as an indicator dye.[40] Alamar Blue, active ingredient, resazurin sodium salt, is a good choice for this assay since it is non-toxic, easily dissolved in water, stable in culture medium and can penetrate cell membranes.[40] The solution of resazurin sodium salt is reduced upon bacterial growth to resorufin, visually seen as a change from blue to pink in color (Figure 1).[40] The final examination of antimicrobial activity will be performed as a time-

dependent test. The time-dependent test involves introducing the nanoparticles into a liquid bacteria culture, and monitoring the optical density over a period of time to evaluate the modified cotton samples.

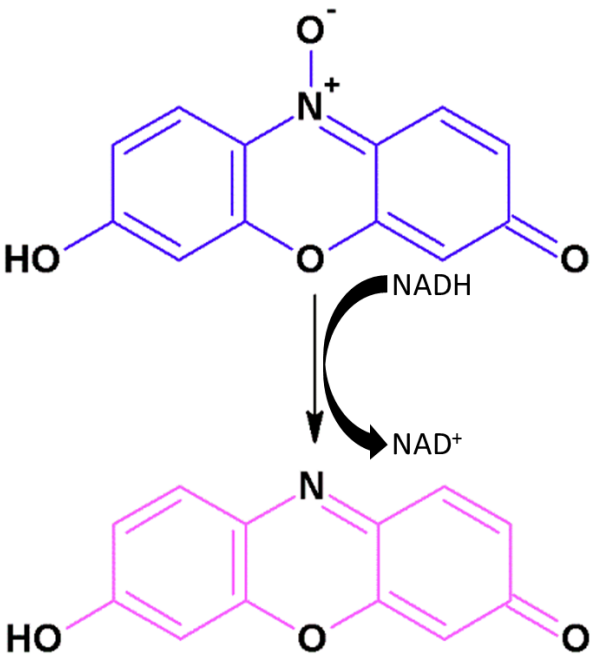

Resazurin
Indicates there are no viable bacteria cells

Resorufin
Indicates there are viable bacteria cells

Figure 1. Reduction of Resazurin to Resorufin indicating the presence of viable bacterial cells.[40]

CHAPTER 3. EXPERIMENTAL

3.1 Materials

Zinc nitrate hexahydrate ($Zn(NO_3)_2 \cdot 6H_2O$), manganese (II) sulfate monohydrate ($MnSO_4 \cdot H_2O$), ammonium carbonate $(NH_4)_2CO_3$) and europium nitrate hexahydrate ($Eu(NO_3)_3 \cdot 6H_2O$) (99.9%) were purchased from Fisher Scientific and all metal salts were reagent grade, unless otherwise noted. Zinc sulfate hexahydrate ($ZnSO_4 \cdot 7H_2O$) was purchased from Mallinkrodt. Mueller Hinton broth and BD Difco™ Mueller Hinton Agar were purchased from Becton Dickinson. Barium chloride dihydrate ($BaCl_2 \cdot 2H_2O$) (99.8%) and sulfuric acid (96%) were purchased from Fisher Scientific. Absolute ethanol (99.5%), nitric acid (69.6%) and acetone were obtained from Fisher Scientific. All reagents were used without further purification, as received.

Quantitative Fisherbrand Q2 (fine porosity and slow flow rate) filter paper with a diameter of 7.0 cm was purchased from Fisher Scientific. Sartorius Minisart® nylon syringe filters with a diameter of 15 mm and a 0.45 μm pore size were obtained from Fisher Scientific. Nanopure water with a resistivity of 18.2 MΩ-cm was obtained from a Barnstead E-Pure system with a 0.2 μm hollow fiber filter. Copper grids (200 mesh) were purchased from Electron Microscopy Sciences and used for TEM imaging.

3.2 Synthesis of Mn^{2+} doped ZnO Nanoparticles

Mn^{2+} doped ZnO nanoparticles were prepared via a modified precipitation method.[13] Different metal-doping percentages of ZnO nanoparticles were prepared based on molar ratios of manganese to zinc ions, including undoped ZnO, 5%, 10% and 15% Mn^{2+} doped ZnO. For undoped ZnO nanoparticles, a 0.225 M solution of zinc sulfate heptahydrate ($ZnSO_4 \cdot 7H_2O$) (0.0034 mol, 2.912 g) was prepared in nanopure water (45 mL). This solution was heated with

stirring in a 250 mL Erlenmeyer flask on a magnetic hot plate, until it reached a temperature of 65 °C. In a separate container, a 0.725 M solution of potassium hydroxide (KOH) (0.0109 mol, 0.610 g) was prepared in nanopure water (15 mL). Once the $ZnSO_4 \cdot 7H_2O$ (aq) solution had reached the desired temperature, KOH solution was added dropwise at a rate of 2 mL/minute until a milky color was observed. For 45 mL of total solution, the volume of KOH (aq) added was approximately 1 mL. The KOH solution induces the precipitation of ZnO nanoparticles. The solutions were then heated at a constant temperature of 65 °C for 2 hours and subsequently aged for 48 hours at room temperature prior to centrifugation.

For all the manganese ion doping percentages, an identical preparative method was followed with varying amounts of manganese. For example, 5% Mn^{2+} doped ZnO nanoparticles were prepared using the following modification. A solution of 0.225 M $ZnSO_4 \cdot 7H_2O$ (0.01013 mol, 2.912 g) was prepared in nanopure water (45 mL). In a separate container, a 0.012 M solution of manganese (II) sulfate monohydrate ($MnSO_4 \cdot H_2O$) (0.00053 mol, 0.090 g) was prepared in nanopure water (45 mL). The two solutions were then combined into a 250 mL Erlenmeyer flask, fitted with stirrer, and heated until they reached the desired temperature (65 °C). The 0.725 M KOH was added dropwise in the same manner described above. To the 90 mL total solution, a volume of approximately 2 mL of KOH was added.

10% and 15% Mn^{2+} doped ZnO nanoparticles were synthesized by using 0.024 M (0.00106 mol, 0.180 g) and 0.035 M (0.00160 mol, 0.270 g) aqueous solutions of $MnSO_4 \cdot H_2O$, respectively.

3.2.1 Selective Precipitation via Centrifugation

The size separation of ZnO and Mn^{2+} ZnO nanoparticles was performed via a selective centrifugation technique. The nanoparticle suspension was separated into 15 mL conical tubes,

and placed in a Becton Dickinson Adams Compact II Centrifuge which has a fixed rotation at 3500 rpm. The first centrifugation was held for 8 seconds. The supernatant solution was then transferred into a separate 15 mL conical tube (B), resulting in isolated large particles in the conical tubes from the first centrifugation. Tube B was then returned to the centrifuge and the same step was repeated to isolate the medium sized particles. The second supernatant solution, which would contain the small particles, was then transferred to a 50 mL conical tube to be isolated at a higher centrifugation speed (3724 g for 15 minutes). All isolated particles were re-suspended in nanopure water and centrifuged on a Beckman Coulter Allegra X-15R Centrifuge at 3724 g for 15 minutes, with a two-step wash cycle. The nanoparticles were washed three times with nanopure water and three times with a 95% ethanol solution. Finally, the precipitated particles were dried at room temperature, with a final step of oven drying at 100 °C for 24 hours prior to use.

3.3 Synthesis of Eu^{3+} doped ZnO Nanoparticles

Eu^{3+} doped zinc oxide nanoparticles were prepared via a modified literature precipitation method.[36] For undoped ZnO, a 0.242 M solution of ammonium carbonate ($(NH_4)_2CO_3$) (0.00605 mol, 0.581 g) was prepared in nanopure water (25 mL). Additionally, a 0.161 M solution of zinc nitrate hexahydrate ($Zn(NO_3)_2 \cdot 6H_2O$) (0.00403 mol, 1.199 g) was prepared in a separate flask (25 mL). The $(NH_4)_2CO_3$ (aq) solution was added to a 100 mL round bottom flask equipped with a magnetic stir bar, and the zinc nitrate hexahydrate solution was added slowly dropwise until all 25 mL of solution were added. The solution was stirred at room temperature (~21 °C) for 2 hours. The reaction mixture was then filtered through Fisherbrand Q2 fine porosity (particle retention 1 to 5 μm) filter paper to yield the precursor. The precursor was dried

in the oven at 100 °C for 6 hours and the particles were annealed at 200 °C for 4 hours to form the ZnO nanoparticles.

For the synthesis of Eu^{3+} doped ZnO nanoparticles, an identical preparative and purification method was followed with the subsequent exceptions: a solution of europium nitrate hexahydrate ($Eu(NO_3)_3 \cdot 6H_2O$) (Table 1) was prepared in nanopure water (15 mL) while a separate solution of zinc nitrate hexahydrate was prepared in nanopure water (10 mL). The two solutions were combined prior to adding to the 0.242 M $(NH_4)_2CO_3$ (aq) solution, in an identical manner as described above.

Table 1. Amounts of europium nitrate hexahydrate and zinc nitrate hexahydrate used for Eu^{3+} doping.

Calculated Eu^{3+} doping Percentage	Moles of $Eu(NO_3)_3 \cdot 6H_2O$ (mol)	Moles of $Zn(NO_3)_2 \cdot 6H_2O$ (mol)	Mass of $Eu(NO_3)_3 \cdot 6H_2O$ (g)	Mass of $Zn(NO_3)_2 \cdot 6H_2O$ (g)
1%	4.03×10^{-5}	0.00399	0.018	1.187
5%	2.02×10^{-5}	0.00383	0.090	1.139
10%	4.03×10^{-4}	0.00363	0.180	1.078
15%	6.05×10^{-4}	0.00343	0.270	1.019
20%	8.06×10^{-4}	0.00322	0.360	0.959

3.4 Materials Characterization

Nanoparticles were characterized via X-ray powder diffraction, ICP-OES, absorption spectroscopy, luminescence spectroscopy, dynamic light scattering particle size analysis, and transmission electron microscopy. Both ZnO, Mn^{2+} and Eu^{3+} doped ZnO nanoparticles were subjected to antimicrobial activity testing using three testing protocols: agar diffusion testing, minimum inhibitory concentration (MIC) testing, and time-dependent testing against three bacterial species *S. aureus*, *S. epidermidis* and *E. coli.*

3.4.1 X-ray Powder Diffraction Studies

X-ray powder diffraction was performed using a desktop X-ray diffractometer "MiniFlex+," with a Co-Kα (λ = 1.78899 Å) radiation source and a scan speed of 0.5° per minute. The X-ray diffraction pattern is compared to a literature diffraction pattern for ZnO to ensure that the particles were synthesized correctly. The diffraction pattern also gives the necessary components to calculate crystallite size. X-ray powder diffraction studies were performed by suspending the nanoparticles in acetone and applying suspension dropwise to the XRD well plate. The acetone was allowed to evaporate before adding additional drops. The process was continued until a flat and even layer of particles was achieved on the surface of the well plate. Diffraction data were collected from 2θ = 10 ° to 2θ =90 °. The diffraction data was analyzed using Materials Data Jade 7 software and the diffraction pattern was converted to Cu-Kα (λ=1.54059 Å) for data analysis.

3.4.2 Quantification of Eu^{3+} Doping Using ICP-OES

A Perkin Elmer 4100DV inductively coupled plasma optical emission spectrometer was used to determine the actual doping percentages of Zn^{2+} and Eu^{3+} ions in ZnO nanoparticles. The samples were prepared by weighing out a small amount of the nanoparticles (25 mg) and placing them in 15 mL conical tubes. The particles were then digested in 700 µL of concentrated nitric acid (15.7 M) (HNO_3), and diluted with nanopure water to make a 7% nitric acid solution (10 mL). Standards were prepared by performing serial dilutions with 7% nitric acid using a stock solution of zinc nitrate hexahydrate and europium nitrate hexahydrate to yield the desired standard range. The stock solution was prepared by adding 10 mg of zinc nitrate hexahydrate and europium nitrate hexahydrate to a 100 mL volumetric flask and adding nanopure water up to the line.

3.4.3 Absorption Spectroscopy

An Agilent 8453 UV-visible spectrometer was used to characterize the nanoparticles by looking for a shift in the extinction maxima. Absorption spectroscopy measurements were taken by suspending a low concentration (0.05 mg/mL - 0.077 mg/mL) of each doping percentage of nanoparticles in nanopure water and samples were sonicated for 15 minutes to ensure even dispersion of particles. The nanoparticle suspensions (3 mL) were transferred to a 1 cm quartz cell for measurements. Each spectrum was analyzed to determine the extinction maximum.

3.4.4 Luminescence Spectroscopy

Luminescence spectra were obtained using a Perkin Elmer LS-55 Fluorescence Spectrometer with a 5 nm slit width using a quartz cuvette to examine the electronic properties of the nanoparticles. Luminescence spectroscopy measurements were performed by suspending the nanoparticles in nanopure water (20 mg/mL). The samples were sonicated at room temperature for 15 minutes before collecting spectra. Samples were measured using an excitation wavelength of 365 nm and emission spectra were collected from 300 to 750 nm with a scan speed of 200 nm/minute.

3.4.5 Dynamic Light Scattering Particle Size Analysis

Particle size in aqueous suspension was determined using a Zetasizer Nano-ZS dynamic light scattering instrument with a Helium-Neon (He-Ne) source with a wavelength of 632.8 nm. Particle size was collected using the Non-Invasive Backscatter optics at an angle of 173º. Nanoparticle suspensions were prepared at a concentration 0.1 mg/mL in 50 mL conical tubes (typically 3-4 mg of particles was added to 30-40 mL of nanopure water). The nanoparticle suspensions were sonicated for 5 minutes, and then filtered using a 0.45 μm nylon syringe filter into a clean 15 mL conical tube. The filtered particle suspension (1 mL) was transferred to a

disposable cuvette and fitted with a lid. The filtered particle suspensions were analyzed to obtain an approximate particle size for each doping percentage in nanopure water.

3.4.6 Transmission Electron Microscopy (TEM) and Scanning Electron Microscopy (SEM)/Energy Dispersive X-ray Spectroscopy (EDX) Studies

Electron microscopy images were obtained using a Hitachi HR-9500 transmission electron microscope in order to determine particle size. Samples for TEM studies were prepared by suspending nanoparticles in HPLC grade acetone (1 – 5 mg/mL) and dropping 20 µL of the suspension onto a carbon-coated copper grid, then letting sample dry for 10 minutes to evaporate the solvent. Another 20 µL of the suspension was added and the evaporation process was repeated. The Eu^{3+} doped ZnO nanoparticles were prepared in the same manner using a 50:50 mixture of acetone (HPLC grade) and nanopure water. The prepared grid was placed inside the storage box for transportation to the Clemson University electron microscope facility. SEM images were obtained using a Hitachi FE-SEM SU6600 to visualize nanoparticle coverage on cotton samples.

3.5 Antimicrobial Activity Testing

Three antimicrobial activity tests were used to evaluate the antimicrobial effect of the Mn^{2+} and Eu^{3+} doped ZnO nanoparticles, the agar diffusion test, minimum inhibitory concentration (MIC) test and time-dependent studies. The agar diffusion test is a qualitative test which tells whether or not antimicrobial activity is present. MIC tests determine the lowest concentration of nanoparticles which prevents bacterial growth, and the time-dependent test shows how the nanoparticles affect bacterial growth over a period of time. All antimicrobial activity tests were repeated in triplicate simultaneously against three different bacterial species (*S. aureus, S. epidermidis,* and *E. coli*).

3.5.1 Preparation of Mueller Hinton Agar (MHA) Plates

Mueller Hinton (MH) agar is a nutrient culture medium commonly used for antimicrobial disc diffusion susceptibility testing appropriate for rapidly growing bacteria.[45] MH agar plates were prepared by suspending the dehydrated culture medium (19 g) in nanopure water (500 mL) in a sterilized Pyrex® bottle (1 L). The suspension was heated gently to boiling in order to dissolve the dehydrated culture medium. The prepared medium was then autoclaved at 121 °C for 20 minutes. The medium was allowed to cool to 45 °C and was then distributed into sterile petri dishes (100 mm x 15 mm). The medium was allowed to solidify after pouring to a depth of approximately 4 mm then the petri dishes were inverted to prevent condensation from dripping onto the surface of the medium. The inverted petri dishes were left to dry for 24 hours at room temperature. The prepared plates were then stored in a storage bag in stacks of 20 at 4 °C.

3.5.2 Preparation of Mueller Hinton Broth (MHB)

MH broth was prepared by suspending the dehydrated medium (10.5 g) in nanopure water (500 mL) in a Pyrex® bottle (1 L). The solution was warmed gently with stirring to dissolve the dehydrated medium. The solution was then autoclaved at 121 °C for 20 minutes. Upon cooling, the MH broth was stored at room temperature. MHB was used as the liquid culture medium for MIC and time dependent testing. MHB was chosen due to its reproducibility and growth support of the majority of pathogens.[45]

3.5.3 Preparation of 0.9% Saline

A 0.9% saline solution was used as the medium for bacteria suspension for the agar diffusion testing method. The solution was prepared by suspending sodium chloride (4.5 g) in nanopure water (500 mL). The solution was then autoclaved at 121 °C for 20 minutes. The solution was then stored at room temperature.

3.5.4 Preparation of McFarland 0.5 Turbidity Standard

The McFarland 0.5 turbidity standard was prepared according to the EUCAST v. 4.0 manual protocol.[46] A solution of barium chloride, $BaCl_2$ (0.048 M) was prepared in nanopure water. A separate solution of 1% sulfuric acid (1% v/v, 0.18 M) was prepared in nanopure water (100 mL). The standard was prepared by mixing 1% sulfuric acid solution (99.5 mL) and the barium chloride solution (0.5 mL). The optical density of the suspension was checked through absorption spectroscopy using a 1 cm cuvette. The absorbance at 625 nm needs to be in the range of 0.08 to 0.13. The suspension was then distributed into 15 mL conical tubes at volumes of 2-3 mL. The tubes were stored at room temperature in the dark, and vortexed before use. The standard absorbance was checked after 6 months of storage.

3.5.5 Preparation of Bacterial Suspensions for Agar Diffusion

S. aureus, S. epidermidis, and *E. coli* bacterial suspensions were prepared using the direct colony suspension method. The direct colony suspension method involves taking several colonies directly from an overnight growth plate and suspending the colonies in saline with a sterile inoculating loop.[45] The optical density (OD) of a 0.5 turbidity McFarland standard is measured at 600 nm using a spectrophotometer. The bacterial species of interest was then inoculated into 0.9% saline, and the OD of the bacterial suspension is measured and adjusted until the OD value of the bacterial suspension matches the standard. The bacterial adjustment results in a suspension that contains 1-2 x 10^8 CFU/mL for *E. coli*.[46]

3.5.6 Agar Diffusion Antimicrobial Testing Method

The agar diffusion testing method was performed by inoculating the bacteria species of interest, either *E. coli, S. aureus, or S. epidermidis*, into a 0.9 % saline solution. The bacterial solution was then applied to Mueller-Hinton (MH) agar plates with a sterile cotton swab. After

the bacteria had been inoculated on to the plate, a 1000 µL pipette tip was used to make the 8 mm wells in the agar. The wells were then filled with 50 µL of additional MH agar. The final step was to introduce the nanoparticles into the wells (25 mg). For 1% and 5% Eu^{3+} doping the approximate number of nanoparticles introduced to the wells were 3 ± 2 and $4 \pm 3 \times 10^{16}$, respectively. The nanoparticles were introduced by applying the solid powder directly into the well using a sterile spatula. After preparing the plates, they were incubated at 37 °C for 24 hours prior to measuring the zone of inhibition.

3.5.7 Minimum Inhibitory Concentration Antimicrobial Testing Method

3.5.7.1 Preparation of Resazurin Dye (Alamar Blue)

Resazurin sodium salt was used to prepare the dye solution (100 µg/mL) in autoclaved nanopure water. To prepare the solution, resazurin sodium salt (4.0 mg) was dissolved in autoclaved nanopure water (40 mL) in a 50 mL conical tube. The conical tube was wrapped with aluminum foil to prevent degradation of the dye from any ambient or ultraviolet light. During testing, the bacterial culture (1 mL) was combined with the Alamar blue dye solution (5 mL) to yield a 5-fold dilution of the dye, yielding a final concentration of 5 µg/mL once applied to the wells.

3.5.7.2 Preparation of Nanoparticle Suspension and Dilution for MIC Tests

Nanoparticles were suspended in MH broth (3 mL) at various concentrations for the MIC testing. After adding the nanoparticles to the broth, the suspension was sonicated using a sonic dismembrator (30% power) for 30 to 60 seconds to fully disperse the nanoparticles. Table 1 indicates the concentrations across the wells prepared for each doping percentage of nanoparticles for Eu^{3+} doped ZnO, and Table 2 shows the concentrations used to find the MIC of the Mn^{2+} doped ZnO nanoparticles. Concentrations are varied because the same concentration

range did not yield clear MIC values for all doping percentages with each bacteria. Concentration ranges listed were the range that yielded clear results.

Table 2. Concentration range for MIC testing for Eu^{3+} doped ZnO nanoparticles.

Nanoparticle	Concentrations for MIC Testing (mg/mL)		
	E. coli	*S. aureus*	*S. epidermidis*
ZnO	40.00 - 0.08	40.00 - 0.08	40.00 - 0.08
1% Eu doped ZnO	40.00 - 0.08	40.00 - 0.08	40.00 - 0.08
5% Eu doped ZnO	80.00 - 0.15	80.00 - 0.15	40.00 - 0.08
10% Eu doped ZnO	20.00 - 2.00	50.00 - 5.00	40.00 - 0.08
15% Eu doped ZnO	20.00 - 2.00	20.00 - 2.00	40.00 - 0.08
20% Eu doped ZnO	40.00 - 0.08	40.00 - 0.08	40.00 - 0.08

Table 3. Concentration range for MIC testing for Mn^{2+} doped ZnO nanoparticles

Nanoparticle	Concentrations for MIC Testing (mg/mL)		
	E. coli	*S. aureus*	*S. epidermidis*
ZnO	10.00 – 0.50	10.00 – 0.50	10.00 – 0.50
10% Mn doped ZnO	10.00 – 0.50	10.00 – 0.50	10.00 – 0.50

3.5.6.3 Preparation of Bacterial Suspension for MIC Tests

The bacterial suspensions were prepared after the nanoparticle dilutions were prepared across the 96 well plate. The bacteria of interest was suspended in MH broth and using a spectrophotometer the OD value of the bacterial suspension was checked and adjusted until the OD value was around 0.100. MH broth was used as the blank.

3.5.6.4 Preparation of 96 Well Plates for MIC Tests

In a laminar flow hood, a 96 well plate was used to prepare the assay using Alamar blue dye (100 μg/mL). First MH broth (50 μL) was applied to all wells (1-12). Then to well 1, 50 μL of the nanoparticle suspension was added and a two-fold dilution was carried out across all wells until well number 10. Wells 11 and 12 served as the control wells (well 11: Alamar blue dye and MH broth and well 12: MH broth). Subsequently, 50 μL of the bacteria/dye solution was added to wells 1-10. Two control rows were also introduced into the 96 well plate: one with nanoparticles and Alamar blue dye but no bacteria, and one with medium and the same bacteria culture introduced into the dilution wells. These controls served to indicate whether contamination was present, or to indicate if the nanoparticles on their own caused a color change in the dye. The prepared 96 well plates were incubated at 37 °C for 24 hours and the MIC was determined by recording the last well that remained blue (no viable cells). The color change from pink to blue indicates that there are viable bacterial cells.[40]

3.6 Nanoparticle Attachment to Cotton Textile

3.6.1 Cotton Modification Method

Cotton textile samples were cut into 2 cm x 2 cm squares using a drawn pattern and the cut cotton pieces were then washed in nanopure water three times (for every 0.1 g of textile, 25 mL of water was used). After being washed, the samples were dried at 60 °C for 10 minutes. Once dry, the samples were ready to be modified.

The textiles were modified using a literature-based method, described by Ambika and Sundrarajan, with some adjustment.[47–51] For the cotton modification, textiles (0.1 g) were sonicated in a solution of 0.42 M sodium phosphate, 0.52 M citric acid, and 2.75 x 10^{-4} M β-cyclodextrin in nanopure water (25 mL) for 30 minutes. The textile samples were then

removed from the modification solution and dried in an oven at 110 °C for 5 minutes. The temperature was raised to 195 °C for another 5 minutes for curing. The samples were then removed from the oven and rinsed in a 60 °C water bath. Finally, the textiles were oven dried at 60 °C and were cut to 1 cm x 1 cm pieces prior to coating with nanoparticles.

3.6.1.1 Attachment of Nanoparticles to Modified Cotton

To attach nanoparticles to the modified cotton samples, 5% Eu^{3+} doped ZnO nanoparticles (312.5 mg) were suspended in nanopure water (12 mL) and sonicated for 5 minutes. Four 1 cm^2 pieces were added to the nanoparticle suspension, and rotated horizontally on a rotisserie for 4 hours. The cotton samples were then removed from the nanoparticle suspension and dried in an oven at 60 °C for 10 minutes.

3.6.2 Attachment of Nanoparticles to Unmodified Cotton

Following a literature method, 5% Eu^{3+} doped ZnO nanoparticles (500 mg) were suspended in 2-propanol (10 g) (5% w/w).[52] The cotton textile samples (1 cm x 1 cm) were then added into the dispersed particle suspension and were stirred for 10 minutes. After removal from the suspension, excess suspension was blotted onto a Kim wipe and the samples were placed on a watch glass for drying at 130 °C for 15 minutes.

3.6.3 Method Used for Cotton Washing

All cotton samples were washed in the same manner, as follows. Four 1 cm x 1 cm pieces were placed in nanopure water (12 mL) in a 20 mL scintillation vial fitted with a small magnetic stir bar. The cotton samples were then stirred in the nanopure water for five minutes. The samples were removed from the water and rinsed in clean nanopure water before hanging to air dry. For multiple washes, the samples were dried prior to each additional wash and washed as indicated previously.

3.7 Antimicrobial Test Methods for Cotton Samples

3.7.1 Agar Diffusion Test of Cotton Samples

Agar diffusion testing was performed by using the direct colony suspension method, as discussed in section 3.6.6. The bacteria of interest was inoculated onto the surface of the medium with a sterile cotton swab and the cotton samples were placed on the surface of the agar immediately using sterile tweezers. The plates were then incubated at 37 °C for 24 hours.

3.7.2 Time Dependent Antimicrobial Tests of Cotton Samples

First, a single colony of *S. aureus* was selected and inoculated into MH broth. The bacterial culture was incubated in a shaking incubator for 1 hour at 37 °C and 190 RPM. After one hour, 100 μL of the culture was added to each sample test tube along with MH broth (19.9 mL). These tubes were vortex mixed and the initial (Time=0) optical density was recorded using a spectrophotometer at 600 nm. The cotton samples were then added to each test tube and the tubes were placed in the shaking incubator (37 °C, 190 RPM). The control textiles included modified cotton with no nanoparticles attached, plain cotton, and *S. aureus* in MHB without addition of nanoparticles or cotton. The optical density was then recorded once per hour for 7 hours, at 10 hours and 24 hours.

CHAPTER 4. RESULTS AND DISCUSSION

4.1 ZnO Nanoparticle Synthesis

Two different synthetic methods for ZnO nanoparticles were used throughout this work. Mn^{2+} doped ZnO was synthesized using a modified precipitation method, continuing work completed previously in our lab.[44] The Mn^{2+} ZnO nanoparticles were selectively precipitated due to the previously established large polydispersibility. The molar doping percentages synthesized for Mn^{2+} doped ZnO were 0, 5%, 10% and 15% (experimental details can be found in Section 3.2). ZnO and Eu^{3+} doped ZnO nanoparticles were synthesized by modifying a literature precipitation method in the following molar doping percentages 0%, 1%, 5%, 15%, and 20% Eu^{3+} (experimental details can be found in Section 3.3).[22]

4.2 Characterization of Mn^{2+} doped ZnO Nanoparticles

The nanoparticles were characterized using transmission electron microscopy, UV-visible spectroscopy and photodegradation studies. Dynamic light scattering measurements were attempted on the selectively precipitated nanoparticles, but yielded unclear results. The nanoparticles were very polydisperse even with the selective precipitation technique used, and therefore, the research focus shifted to the new modified literature precipitation method of Eu^{3+} doped ZnO nanoparticles.[22]

4.2.1 Transmission Electron Microscopy

10% Mn^{2+} doped ZnO nanoparticles were synthesized and TEM images of small and large 10% Mn^{2+} doped ZnO were obtained. The TEM images indicated an average nanoparticle size of 8 ± 2 and 426 ± 82 nm, respectively. This result shows that the selective precipitation was successful in separating the nanoparticles into different sizes, however, the large

nanoparticles might be aggregates of nanoparticles formed either during synthesis or during preparation of the TEM grids. Figure 2 shows the TEM images obtained of the small and large 10% Mn^{2+} doped ZnO nanoparticles, and Figure 3 shows the obtained size distribution data for small 10% Mn^{2+} doped ZnO, with a size range of 4 to 10 nm.

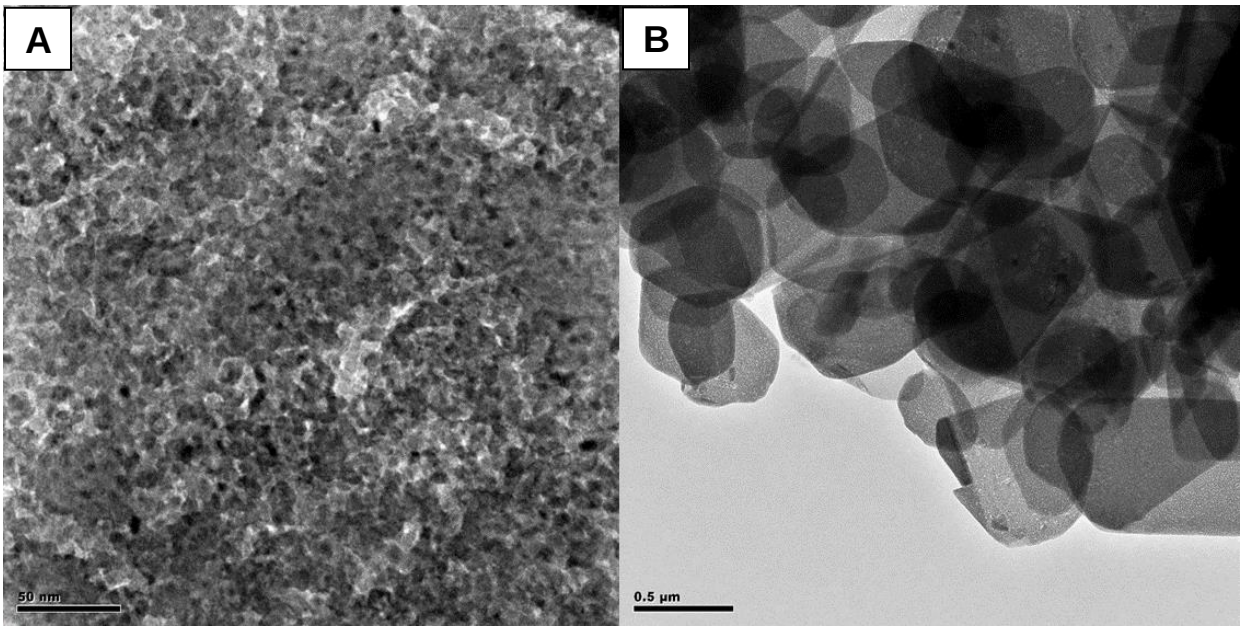

Figure 2. Transmission electron microscopy images of (A) Small 10% Mn^{2+} doped ZnO and (B) Large 10% Mn^{2+} doped ZnO nanoparticles.

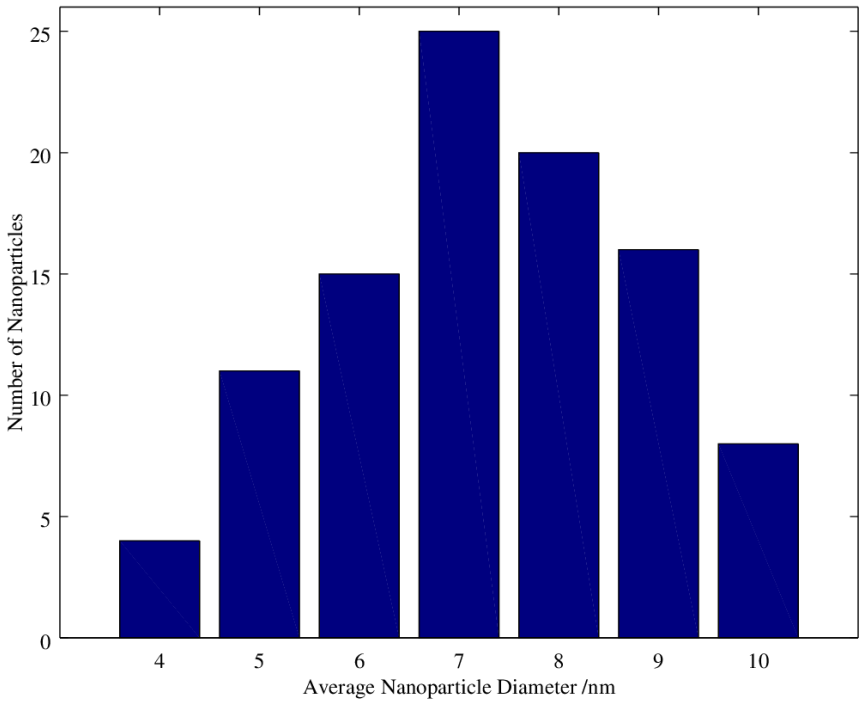

Figure 3. Size distribution of small 10% Mn^{2+} doped ZnO nanoparticles.

4.2.2 UV-Visible Spectroscopy of Mn^{2+} doped ZnO Nanoparticles

Figure 4 shows the UV-visible spectroscopy results obtained with the selectively precipitated Mn^{2+} doped ZnO nanoparticles. The extinction maxima for these particles were slightly blue shifted compared to the extinction maxima of ZnO nanoparticles found in the literature, typically around 355 nm.[23] This correlates to an increase in band gap energy. Shifts to lower wavelengths (higher energy) have been seen in the literature upon manganese doping, thus, our results agree with previous studies.[13]

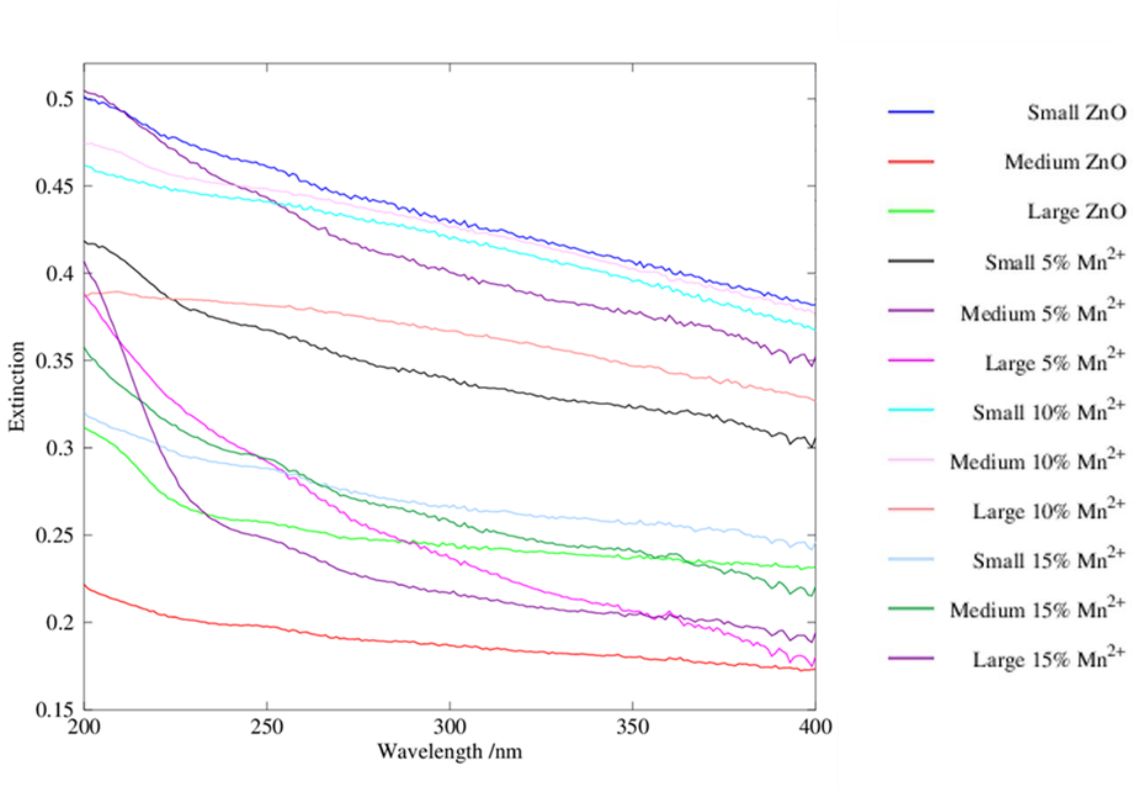

Figure 4. UV-Visible extinction spectra of Mn^{2+} doped ZnO nanoparticles.

4.2.3 Photodegradation Studies of Mn^{2+} doped ZnO Nanoparticles

Photodegradation studies of rhodamine-B dye were performed as an inner-group collaboration with an undergraduate student, Joseph Lee. The photodegradation studies of Mn^{2+} doped ZnO nanoparticles were performed using rhodamine-B dye at a concentration of 4.11×10^{-6} M in nanopure water (35 mL). The nanoparticles (50 mg) were added to the rhodamine-B dye solution and stirred under ultraviolet (UV) light. Aliquots were taken at various times and the extinction was measured. These studies show how ROS degrade the dye over time, since ROS are the main mechanism for photodegradation of the dye.[53,54] Due to this, these studies give an idea of whether or not the nanoparticles will be an effective antimicrobial agent, based on how quickly the dye is degraded. Figures 5 – 7 show the photodegradation

studies against ZnO, 5% Mn^{2+} doped ZnO, and 15% Mn^{2+} doped ZnO nanoparticles. Though antimicrobial testing was performed with ZnO and 10% Mn^{2+} ZnO, these studies give an idea of the other two doping percentages and their potential use as antimicrobial agents.

As seen in Figure 5, the small 5% Mn^{2+} doped ZnO nanoparticles were the most effective at degrading the dye. The extinction value almost flat lines at the extinction maxima of 554.3 nm after 180 minutes, compared to the large 5% Mn^{2+} doped ZnO nanoparticles. The degradation of the other doping percentages was not as pronounced, however, you can still see in the figures that the dye is being degraded in each case. The other doping percentages need more time to degrade the rhodamine-B dye, compared to the small 5% Mn^{2+} doped ZnO nanoparticles. Another trend seen in 5% and 15% Mn^{2+} doped ZnO nanoparticles photodegradation studies is that the small particles degrade the dye faster compared to the large particles. Undoped ZnO nanoparticles prepared the same way do not have as significant of a difference between the small and large degradation times. This indicates that the size separation of undoped ZnO does not drastically affect the efficiency of the nanoparticles degradation of rhodamine-B dye. Interestingly, a calculated surface area of small versus large 10% Mn^{2+} doped ZnO nanoparticles indicates that the small particles at the same mass have a significantly large surface area of 0.7 ± 0.3 m^2 compared to $2.52 \pm 0.02 \times 10^{-2}$ m^2 for large 10% Mn^{2+} doped ZnO. A larger surface area means there is more surface for ROS to be present, supporting the small Mn^{2+} doped ZnO nanoparticles degradation of the dye faster compared to the large Mn^{2+} doped ZnO nanoparticles.

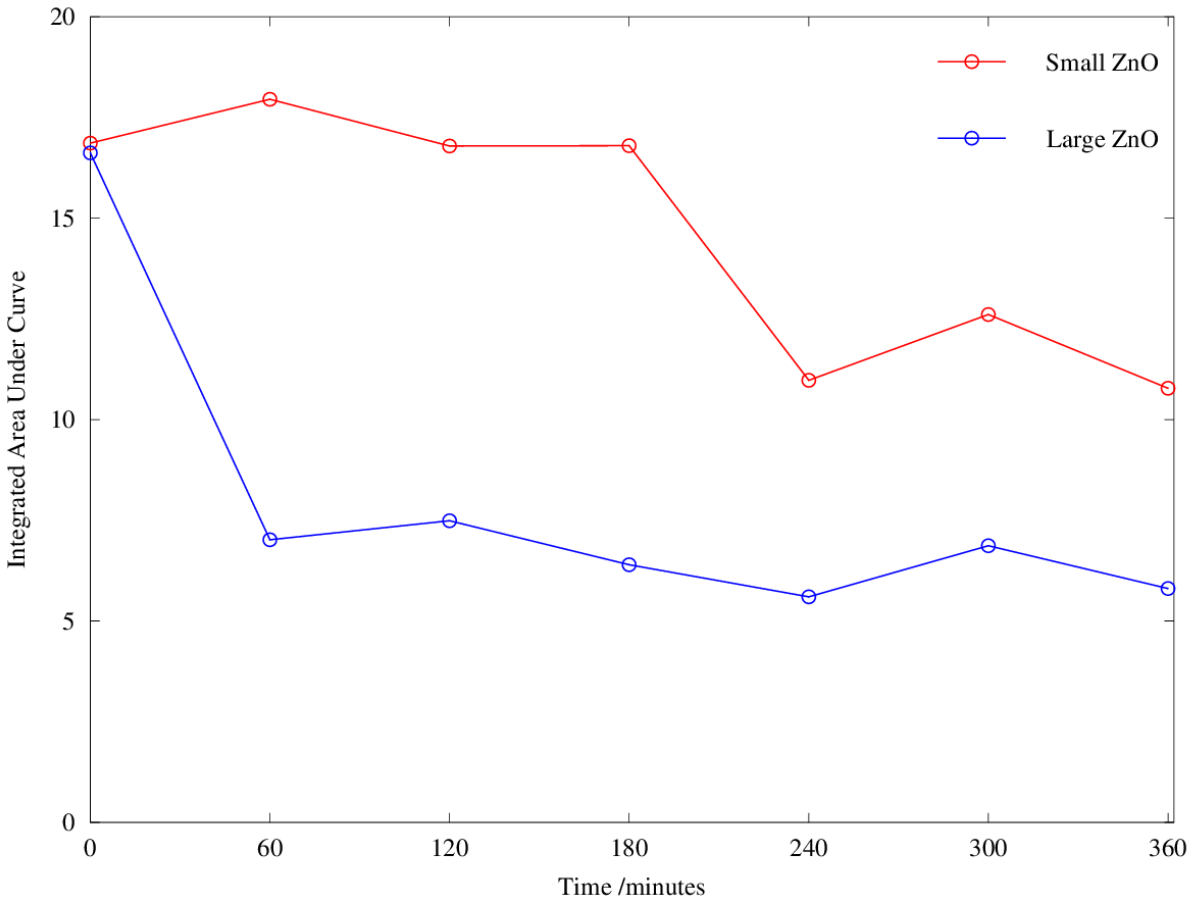

Figure 5. Photodegradation of rhodamine-B dye with Small and Large ZnO nanoparticles.

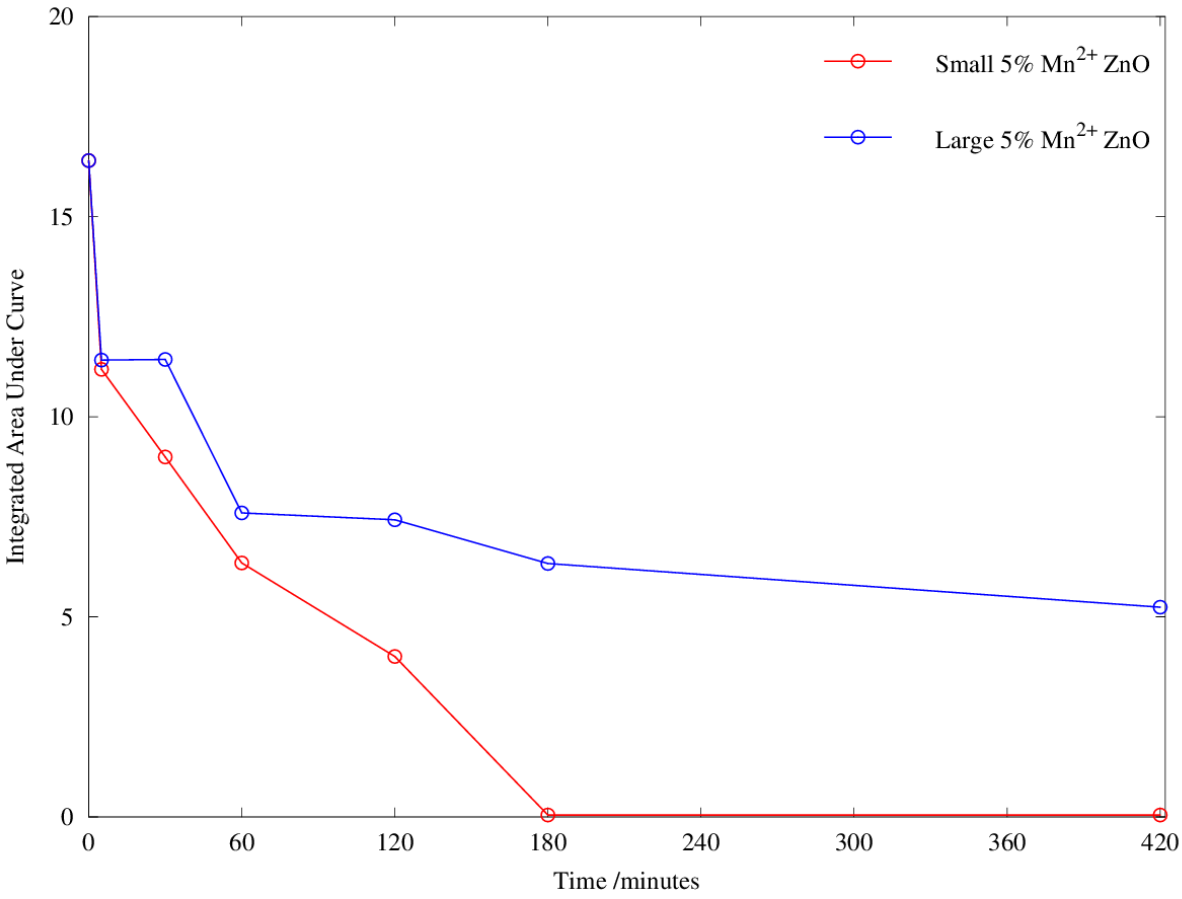

Figure 6. Photodegradation of rhodamine-B dye with Small and Large 5% Mn^{2+} doped ZnO nanoparticles.

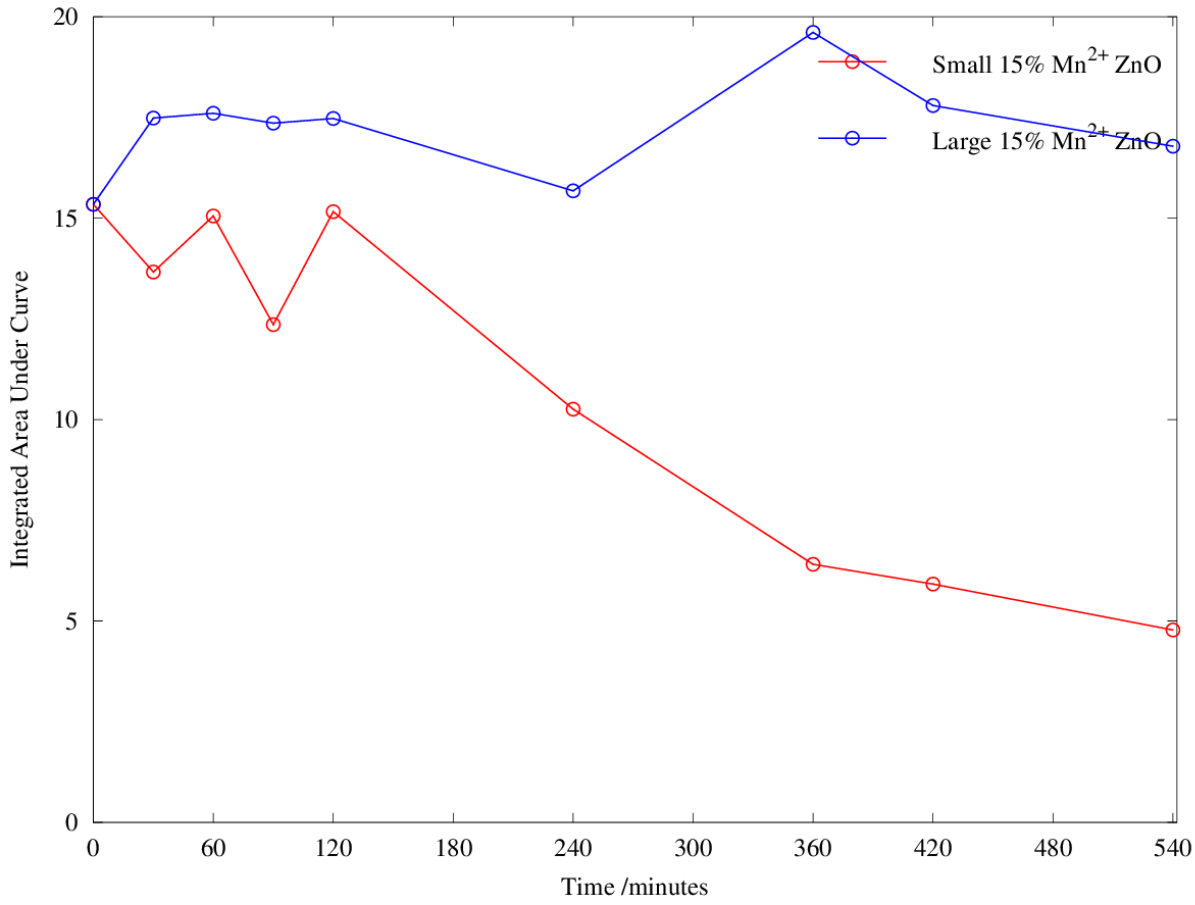

Figure 7. Photodegradation of rhodamine-B dye with Small and Large 5% Mn^{2+} doped ZnO nanoparticles.

4.3 Antimicrobial Susceptibility Testing for Mn^{2+} doped ZnO Nanoparticles

Antimicrobial susceptibility testing was performed on selectively precipitated Mn^{2+} doped ZnO nanoparticles against *E. coli* and *S. aureus* bacteria species including agar diffusion and MIC testing.

4.3.1 Agar Diffusion Test Results for Mn^{2+} doped ZnO Nanoparticles

Agar diffusion testing was performed on selectively precipitated ZnO and 10% Mn^{2+} doped ZnO nanoparticles, prepared using the same synthetic method. Figures 8 and 9 show the plates that were measured to obtain the agar diffusion results. Table 3 shows the measured zone

of inhibition data. From this data, there was indication that both ZnO and 10% Mn^{2+} doped ZnO both have an antimicrobial effect. It can also be noted that the small-sized nanoparticles for undoped and 10% Mn^{2+} ZnO nanoparticles each have slightly increased antimicrobial effect in *E. coli* in comparison to the large undoped and 10% Mn^{2+} doped ZnO. However, the zones are not significantly different from each other, with only a difference of 1 or 2 mm between the different sizes. Thus, further testing was necessary to make a conclusive statement about whether or not small particles are more effective, and this was explored through MIC testing.

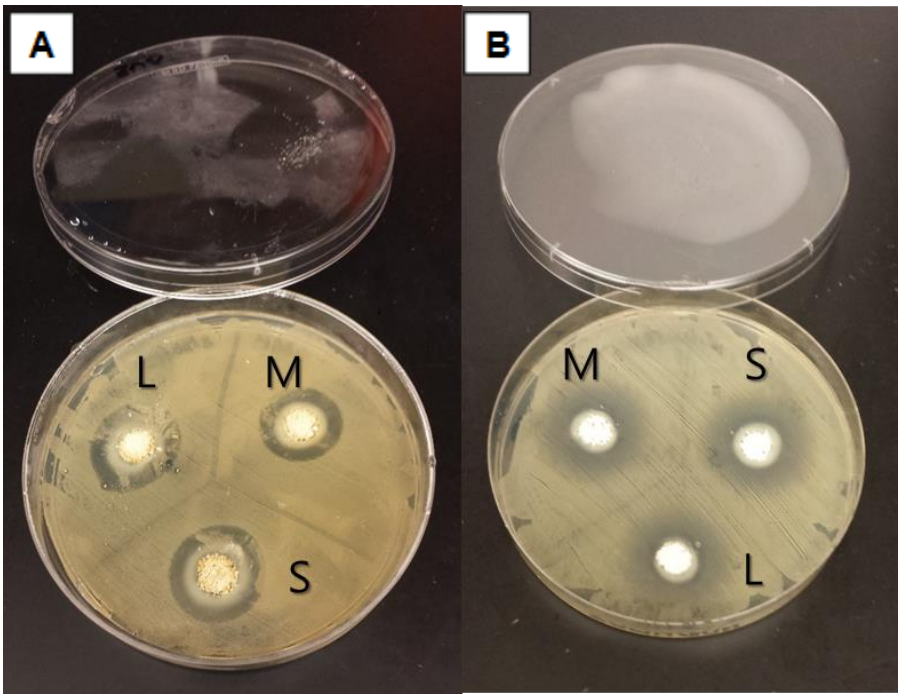

Figure 8. Agar diffusion testing for (A) Small, medium, and large ZnO and (B) Small, medium, and large 10% Mn^{2+} ZnO against *E. coli*.

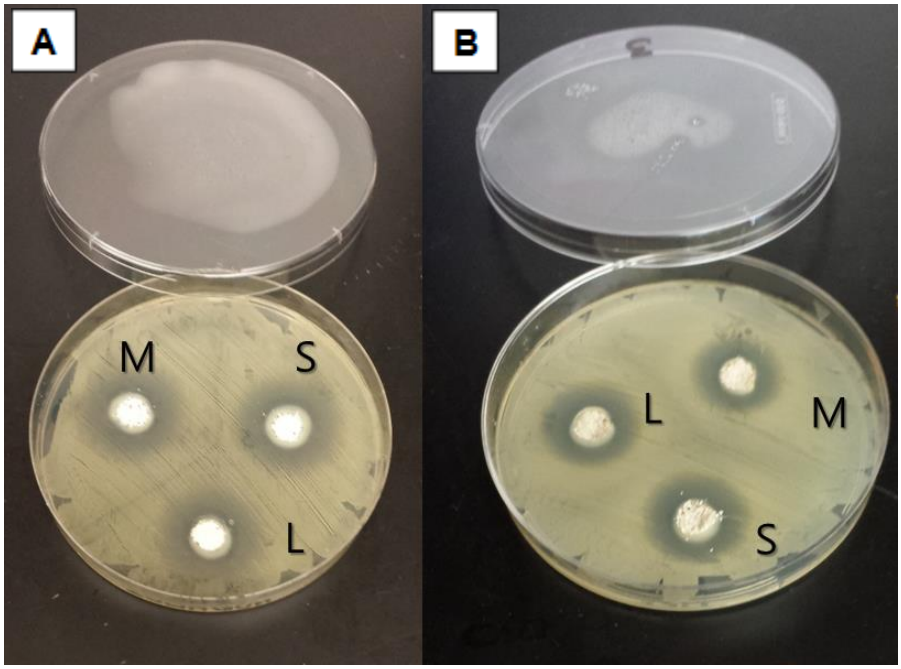

Figure 9. Agar diffusion testing for (A) Small, medium, and large ZnO and (B) Small, medium, and large 10% Mn^{2+} ZnO against *S. aureus*.

Table 4. Zone of Inhibition measurements of Mn^{2+} doped ZnO nanoparticles against *E. coli* and *S. aureus*.

		Zone of Inhibition (mm)	
Size	Doping Percentage	*E. coli*	*S. aureus*
S	0%	22	26
M	0%	20	25
L	0%	21	25
S	10%	18	22
M	10%	15	23
L	10%	16	24

4.3.2 Minimum Inhibitory Concentration Test Results for Mn^{2+} doped ZnO Nanoparticles

Minimum inhibitory concentration testing was performed against *E. coli* and *S. aureus*, to obtain a greater understanding of how size affects the antimicrobial activity. Figures 10 and 11 show the MIC test results obtained. Table 4 indicates the obtained MIC range for each of the nanoparticles. The results against *E. coli* were inconclusive across the four trials, since even the greatest nanoparticle concentration seems to only be inhibiting the growth partly, as indicated by the purple color. Therefore, the purple means that there are both viable and nonviable bacterial cells involved since the resazurin sodium salt monitors the living environment of the cell, and only turns to pink if there are viable bacteria cells.[40] This pink color, as discussed in the background section, is produced as a result of the reduction of rezasurin to resorufin. The purple color indicates a mixture of resazurin and resorufin. The tests against *S. aureus* showed a pattern over four trials. The medium ZnO nanoparticles produced the lowest MIC value of between 2.5 and 2.0 mg/mL, compared to 4 – 2.5 mg/mL and 5 – 4 mg/mL for small and large, respectively. Small 10% Mn^{2+} doped ZnO nanoparticles showed a higher MIC value of 4 mg/mL compared to 2.5 – 2.0 mg/mL for both medium and large nanoparticles.

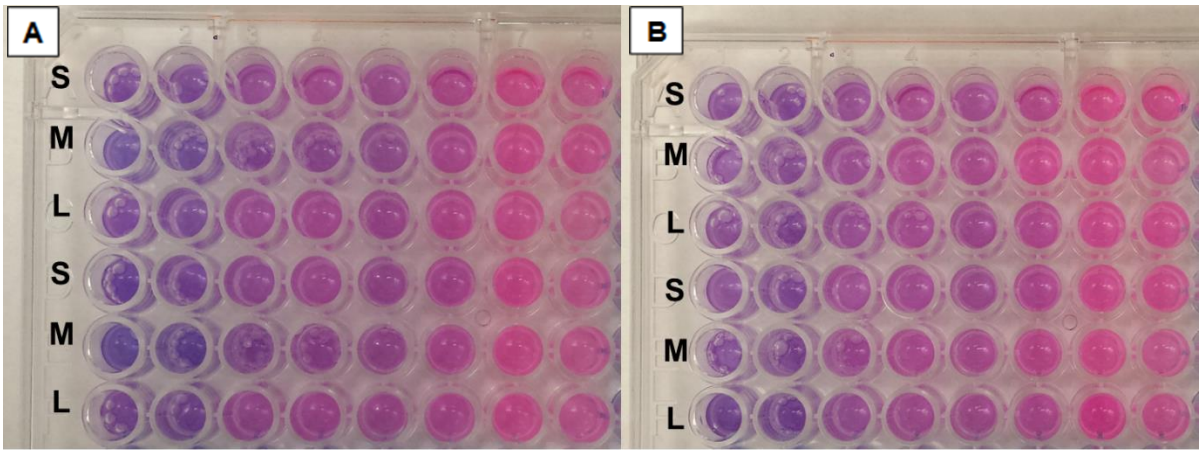

Figure 10. MIC test results for (A) Small, medium and large ZnO and (B) Small, medium and large 10% Mn^{2+} ZnO against *E. coli*.

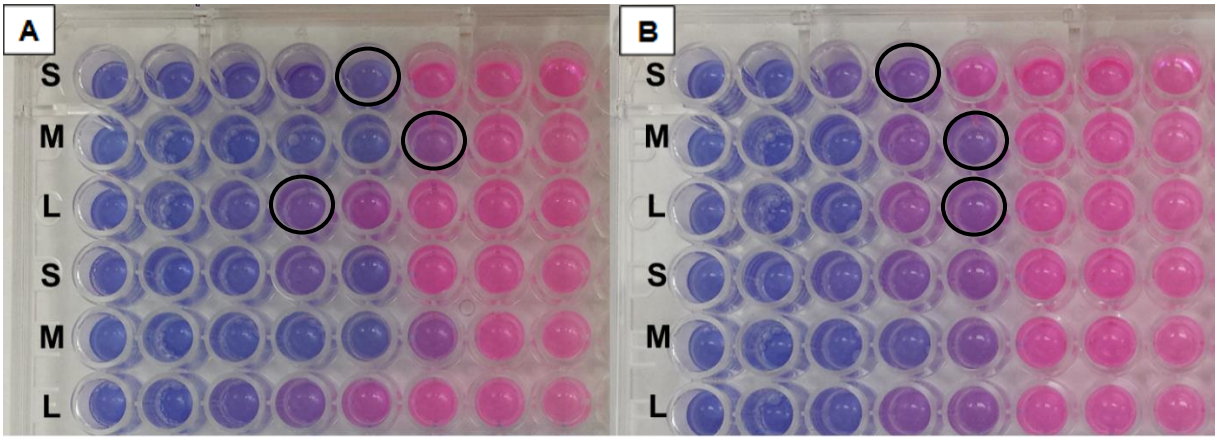

Figure 11. MIC test results for (A) Small, medium and large ZnO and (B) Small, medium and large 10% Mn^{2+} ZnO against *S. aureus*.

Table 5. MIC results for 10% Mn^{2+} doped ZnO nanoparticles.

Nanoparticle		**Minimum Inhibitory Concentration Range (mg/mL)**	
Calculated Mn^{2+} Doping %	**Nanoparticle Size**	***E. coli***	***S. aureus***
0	S	Inconclusive	4.0 - 2.5
0	M	Inconclusive	2.5 -2.0
0	L	Inconclusive	5.0 - 4.0
10	S	Inconclusive	4.0 - 2.5
10	M	Inconclusive	2.5 - 2.0
10	L	Inconclusive	2.5 - 2.0

4.4 Characterization of Eu^{3+} doped ZnO Nanoparticles

The following representative legend will be used throughout the discussion of the Eu^{3+} doped ZnO nanoparticles to describe the doping percentage of interest. The doping percentages will be represented by E0, E1, E5, E10, E15 and E20, where E0 is undoped ZnO nanoparticles,

E1 is 0.9% (1%) Eu^{3+} doped ZnO, E5 is 4.7% (5%) Eu^{3+} doped ZnO, E10 is 10% (10%) Eu^{3+} doped ZnO, E15 is 16% (15%) Eu^{3+} doped ZnO, and E20 is 20% (20%) Eu^{3+} doped ZnO. The average experimental doping percentage is indicated by these labels, and in parentheses is the theoretical doping percentage.

4.4.1 X-ray powder diffraction studies of Eu^{3+} doped ZnO Nanoparticles

Figure 12 shows the XRD spectrum of undoped and Eu^{3+} doped ZnO with annealing at 200 °C. The XRD spectrum of the synthesized ZnO matches that of the known Wurtzite crystal structure of ZnO.[22] A representative diffraction pattern of a literature reported diffraction pattern for ZnO is shown in Figure 13.[22] From comparing Figures 12 and 13, the experimentally obtained diffraction pattern matches that of the reference. Therefore, corresponding lattice planes at (100), (002), (101), (102), (110), (103) and (112) were assigned based on the literature reported diffraction pattern.[22] In this synthesis, ZnO is formed in a two-step process, by forming a precursor and then subsequently annealing the precursor at a high temperature. The precursor is the reaction mixture that is formed during the synthesis process. The precursor is proposed to be a form of zinc carbonate ($Zn_4(CO_3)(OH)_6 \cdot H_2O$).[22] Where upon heating, the precursor is decomposed and results in the formation of ZnO nanoparticles.[22]

The XRD pattern of the precursor indicates that the ZnO crystal is not formed until after the annealing process is complete, where the particles are heated in an oven at 100 °C for 6 hours and 200 °C for 4 hours. Additionally, it was observed that the Eu^{3+} doping did not result in any changes in the diffraction pattern, therefore, the basic crystal structure of ZnO remains unchanged between undoped and Eu^{3+} doped ZnO nanoparticles. The annealing temperature was also lowered in comparison with the optimum temperature found in the literature, to reduce the probability of burning, but the sharp peaks in the nanoparticles' diffraction patterns indicated that

the lowering of the temperature did not affect the formation of the ZnO crystal structure.[22,55] This has been observed in the literature with lanthanide doping including Eu^{3+} and Sm^{3+} doped ZnO.[31,36] The peak broadening seen in E5 nanoparticles could indicate changes in crystallite size, since smaller particles lead to broader peaks.[29] Since E5 nanoparticles were the smallest calculated crystallite size, the peak broadening explanation is reinforced by the decreased crystallite size. Crystallite size was calculated using the Debye-Scherrer equation (equation 1), and the following crystallite sizes were found for ZnO and Eu^{3+} doped ZnO, as summarized in Table 5.[22]

$$D = \frac{0.9\lambda}{\beta cos\theta} \quad (1)$$

D is crystallite size, λ is the wavelength of the X-ray (1.5418 Å), β is the full width at half max (FWHM, in radians) for the given diffraction peak, and θ is the angle of the peak. The most intense peak was used in the calculations, at approximately 36 ° (101).

Table 6. Crystallite size found for nanoparticles, calculated from the X-ray diffraction data.

Nanoparticle	Angle 2θ /Degrees	FWHM /Degrees	Mean Crystallite Size /nm
E0	35.937	0.607	13.7
E1	35.945	0.335	26.1
E5	36.079	0.763	10.9
E10	36.006	0.603	13.9
E15	35.957	0.374	22.3
E20	36.078	0.419	20.0

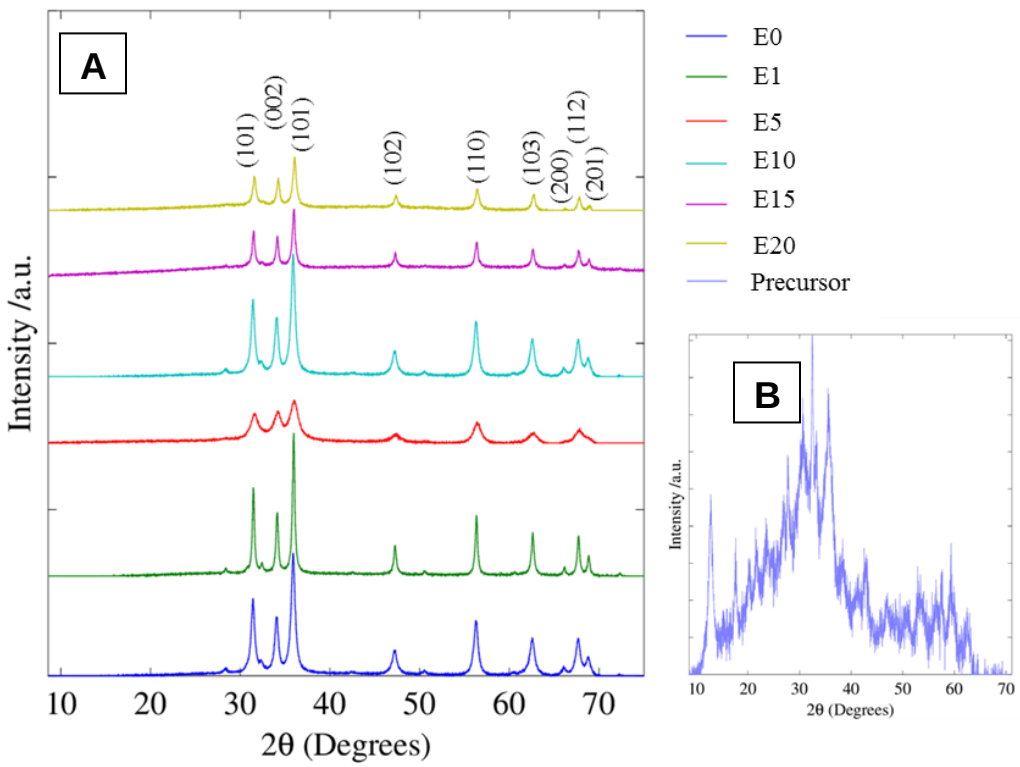

Figure 12. (A) X- ray diffraction patterns of nanoparticles and (B) X-ray diffraction pattern of the precursor, prior to being annealed.

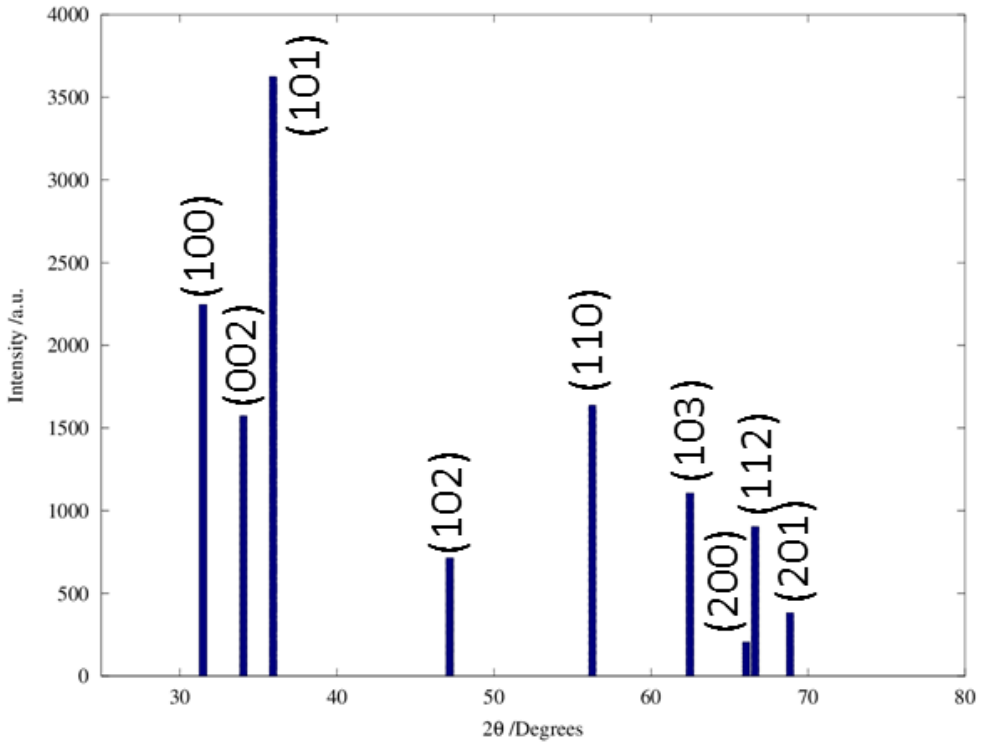

Figure 13. Representative reference X-ray diffraction pattern of ZnO nanoparticles.[22]

4.4.2 Transmission Electron Microscopy of Eu^{3+} Doped ZnO Nanoparticles

Transmission electron microscopy images of E1 and E5 nanoparticles were obtained and the average sizes were 9 ± 2 nm and 8 ± 2 nm, respectively (Figure 14). Figure 15 and 16 show the size distribution of the nanoparticles from the measurement of the TEM images. E1 nanoparticles had a range of 4 to 15 nm sizes, and the E5 nanoparticles had a range of 5 to 13 nm sizes. The distribution for E5 was slightly narrower compared to E1. As seen in the TEM images, the morphology of E5 nanoparticles is well ordered and the size distribution is better than E1 nanoparticles. E5 nanoparticles had a lattice spacing of 2.841 Å. As previously stated, the E5 nanoparticles have a better morphology compared to E1 nanoparticles. This could be

because the ratio of Eu^{3+} to Zn^{2+} ions is balanced and the synthesis of the E5 nanoparticles results in more controlled growth of the nanoparticles.

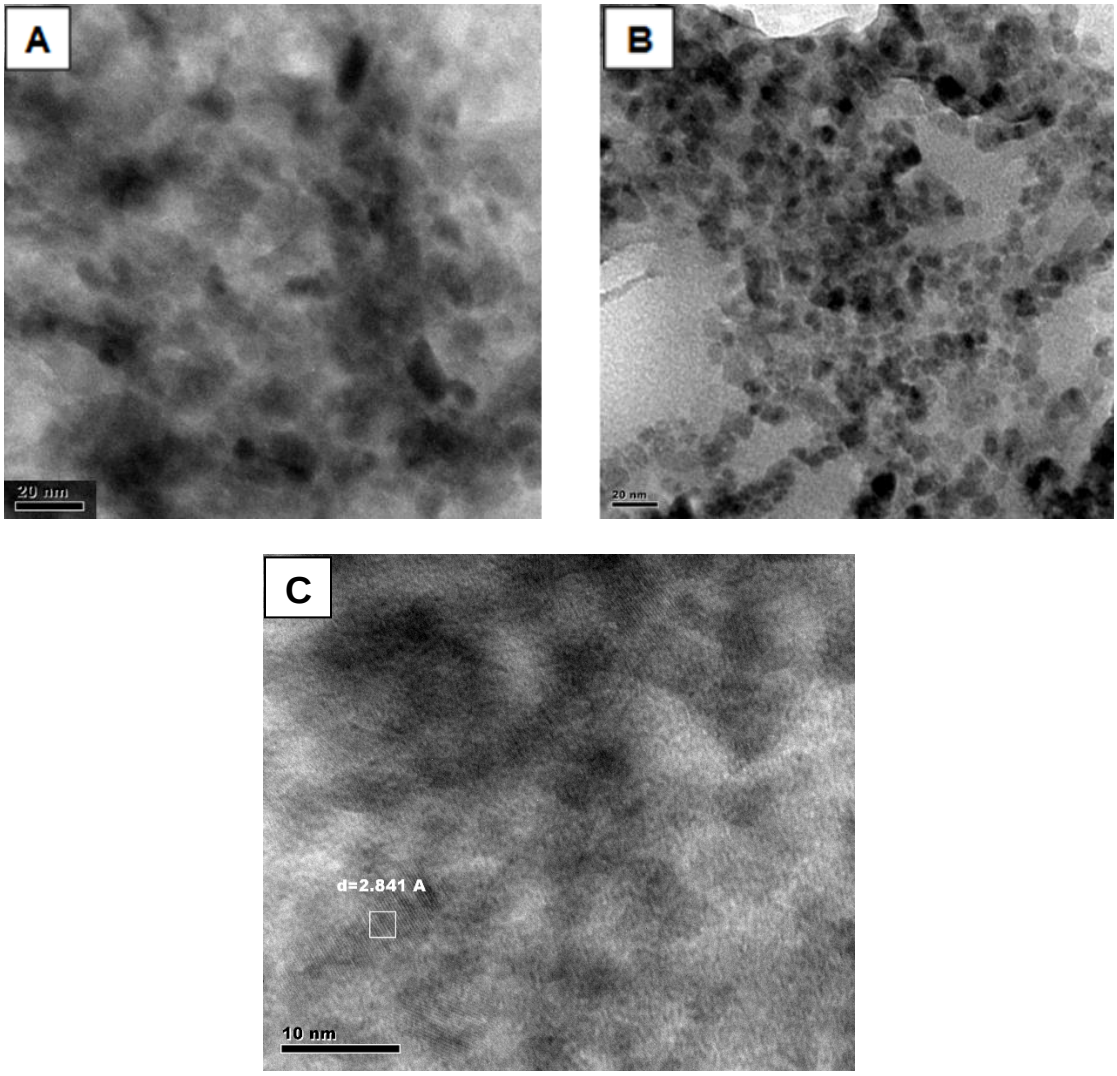

Figure 14. (A) Transmission electron microscopy image of E1 (0.9% Eu^{3+}) nanoparticles, (B) E5 (4.7% Eu^{3+}) nanoparticles and (C) lattice spacing for E5 nanoparticles.

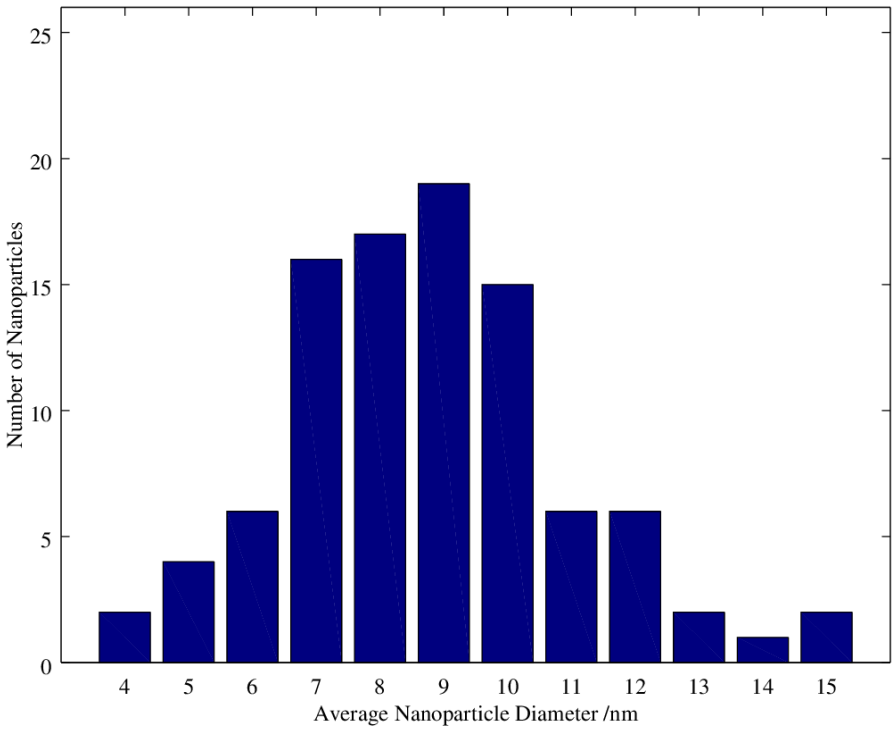

Figure 15. Size distribution data for E1 (0.9% Eu^{3+}) nanoparticles.

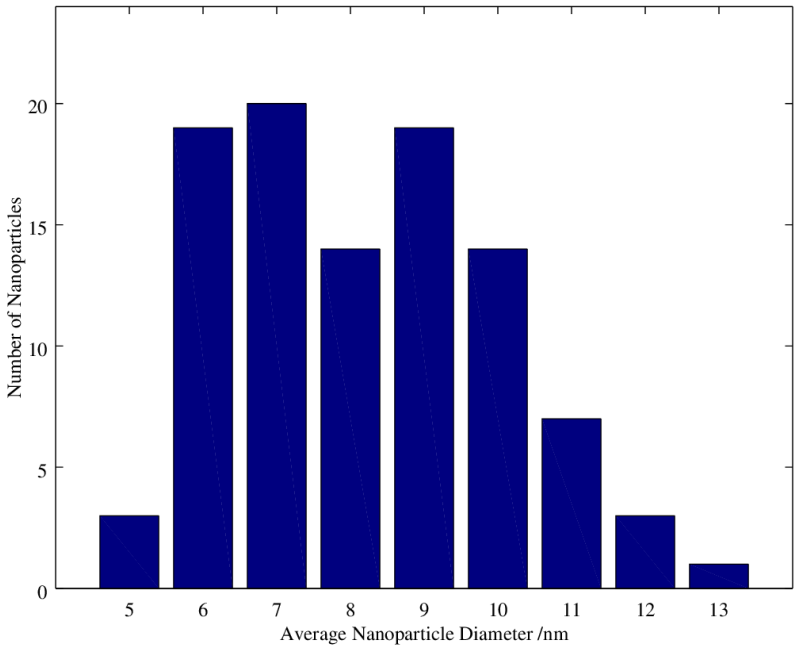

Figure 16. Size distribution data for E5 (4.7% Eu^{3+}) nanoparticles.

4.4.3 Nanoparticle Characterization via ICP-OES

In order to determine experimental doping percentages, ICP-OES was performed on the Eu^{3+} doped ZnO nanoparticles. Two data sets were obtained for the nanoparticles (1) the first synthesized batch of all nanoparticles and (2) the second synthesized batch of all nanoparticles, shown in Table 6. The two batches were analyzed to determine the Eu^{3+} doping percentages being used in the analytical and antimicrobial experiments. The average experimental doping percentages obtained, outlined in Table 6, were 0.9 Eu^{3+}, 4.7% Eu^{3+}, 10% Eu^{3+}, 16% Eu^{3+} and 20% Eu^{3+}, respectively. It should be noted that the experimental percentage of Eu^{3+} incorporated into the ZnO lattice is not significantly different than the calculated molar doping percentage.

The number of nanoparticles for E1 and E5 ZnO nanoparticles were calculated from the average particle diameter obtained from the TEM images, shown in Table 6. Several important assumptions were used in the calculations. The calculation assumes that the nanoparticles are fully spherical, and that the density of nano-sized ZnO is equivalent to the bulk density of 5.6 g/cm^3.[56] Another assumption is that all of the Eu^{3+} ions are incorporated into the ZnO lattice, and therefore only the values for zinc were used in the calculations. These numbers were used as a conversion factor for MIC data since 25 mg of the nanoparticles were massed and analyzed, therefore, we assume that the number of nanoparticles in that mass is consistent.

Table 7. Experimental Eu^{3+} doping percentages for two batches of nanoparticles, and the average experimental Eu^{3+} doping percentage.

Calculated Eu3+ doping Percentage /%	Experimental Eu3+ doping Percentage /%		
	Batch 1 (N=3)	Batch 2 (N=3)	Average (N=6)
1	0.687 ± 0.003	1.1 ± 0.1	0.9 ± 0.2
5	4.28 ± 0.04	5.20 ± 0.02	4.7 ± 0.7
10	8.60 ± 0.04	11.15 ± 0.05	10 ± 2
15	15.1 ± 0.2	17.35 ± 0.04	16 ± 2
20	17.40 ± 0.04	13.00 ± 0.1	20 ± 4

*Error listed is the calculated standard deviation of the experimental doping percentages with three replicates

Table 8. Calculated number of nanoparticles in 25 mg of massed nanoparticles with standard deviation.

Calculated Molar Doping Percentage of Eu^{3+} ions /%	Average Number of Nanoparticles (x 10^{16})[a]
1	3 ± 2
5	4 ± 3

[a]Error listed is the calculated standard deviation

4.4.4 Dynamic Light Scattering Particle Size Analysis

Table 8 shows the nanoparticles' hydrodynamic diameter. The particle size in suspension is significantly different than what was observed in the TEM images. This difference is likely due to the nanoparticles aggregating or sedimenting in aqueous suspension. From observation, we know that the nanoparticles fall out of suspension quite rapidly, and this could be due to particle aggregation. Since these nanoparticles are bare and lack a capping agent, they are more likely to aggregate.

Table 9. Hydrodynamic diameter of Eu^{3+} doped ZnO nanoparticles.

Eu^{3+} doping Percentage /%	Hydrodynamic Diameter /nm
E0	171 ± 70
E1	189 ± 70
E5	138 ± 60
E10	153 ± 70
E15	166 ± 80
E20	164 ± 82

4.4.5 Photophysical Property Characterization of Eu^{3+} Doped ZnO Nanoparticles

Figure 17 shows the obtained absorption and luminescence spectra of undoped and Eu^{3+} doped ZnO nanoparticles, respectively. In the absorption spectra, a shift to a longer maximum wavelength is observed when going from undoped to Eu^{3+} doped ZnO nanoparticles which typically corresponds to a decrease in the band gap. In the luminescence spectra, there are characteristic emission peaks for ZnO, though no europium emission peak is observed. The lack of the europium peak, usually seen at 614 nm, means that the selection rules have not been satisfied, thus not allowing for electronic transition between energy levels.[14,17] Whether or not a transition is allowed between electronic energy levels will depend on the symmetry, with respect to the center of inversion, and transitions with the same parity are forbidden.[17] Thus, the f to f electronic transitions for europium are therefore forbidden by the selection rules.[17] The other possibility is that there is no organic chromophore to allow for energy transfer which would overcome the forbidden transition.

Figure 18 shows the band gap energy obtained through a collaboration with Dr. Indika Arachchige's research group at Virginia Commonwealth University.[59] The results obtained do

not follow a clear pattern, however, the 5% Eu^{3+} doped ZnO nanoparticles (calculated molar doping percentage) have the smallest band gap energy of the six doping percentages. The labels in Figure 18 correspond to the calculated molar doping percentage, the experimental doping percentages are discussed in the figure caption. The extinction spectra corroborates this result with the shift to a longer wavelength. This result may indicate that this doping percentage would be advantageous since a smaller band gap would lead to the potential for greater production of reactive oxygen species. As discussed previously, ROS are the most common mechanism proposed for the antimicrobial activity of ZnO nanoparticles. If the band gap energy is lower, the electrons in the valence band have a higher probability of being able to overcome the band gap energy and be promoted to the conduction band.[12] Figure 19 shows an example of how some ROS are produced.[12] Conduction band electrons can combine with atmospheric oxygen to form superoxide anions, the holes left by the promoted electrons can combine with atmospheric moisture and form a hydroxyl radical.[12] In aqueous suspension, the superoxide anions can combine with water and form more hydroxyl radicals and hydroxide ions. If two hydroxyl radicals combine they can form peroxide, another reactive oxygen species.[12] These ROS combine to produce the antimicrobial activity of ZnO nanoparticles. Adding a dopant can decrease the recombination of electron-hole pairs, which would inhibit formation of the ROS.[60]

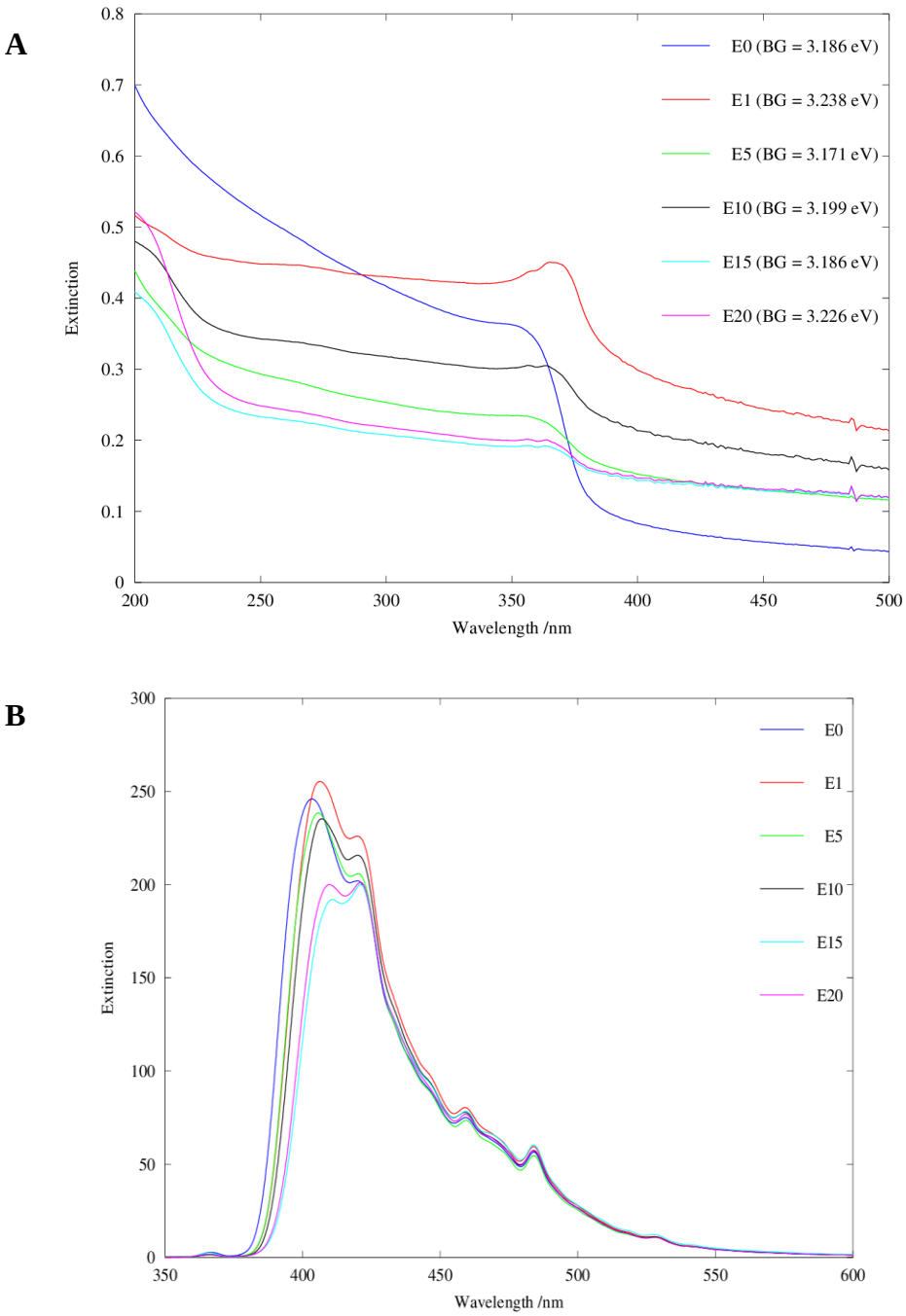

Figure 17. UV-Vis and luminescence studies of all nanoparticle doping percentages.

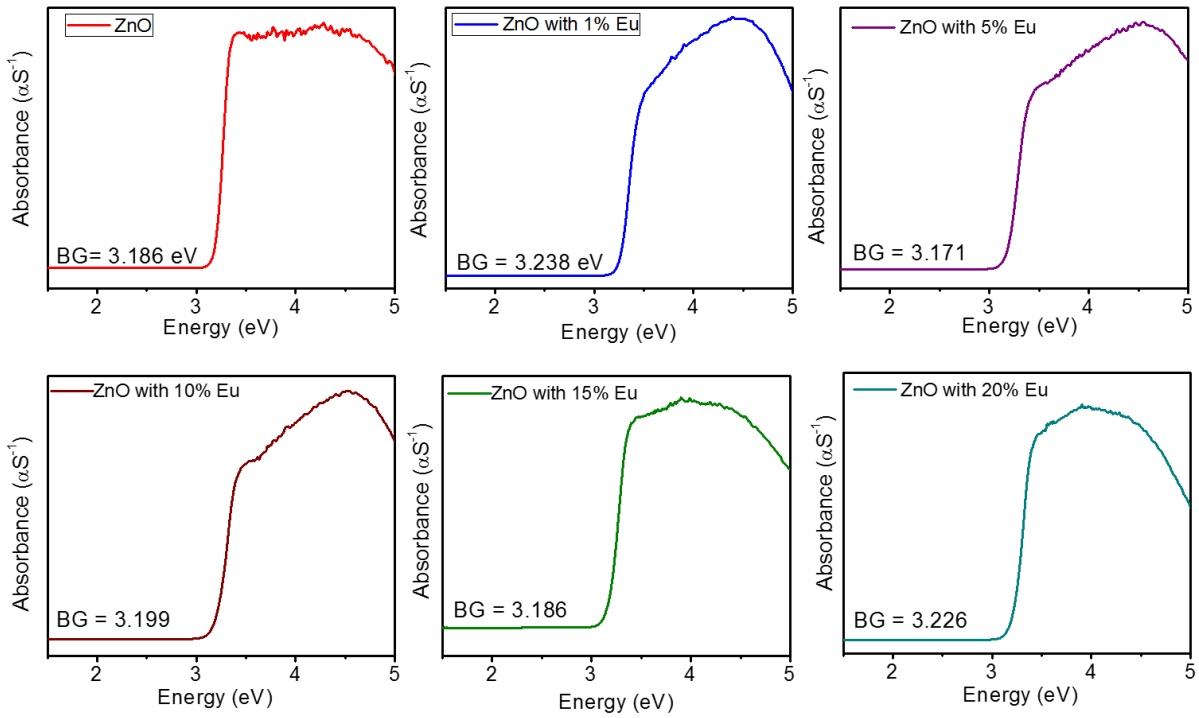

Figure 18. Diffuse reflectance spectroscopy of the synthesized doping percentages and their corresponding band gap energy. Labels indicate the calculated molar doping percentage, experimental doping percentages are 0.9% Eu^{3+} (1%), 4.7% Eu^{3+} (5%), 10% Eu^{3+} (10%), 16% Eu^{3+} (15%) and 20% Eu^{3+} (20%).

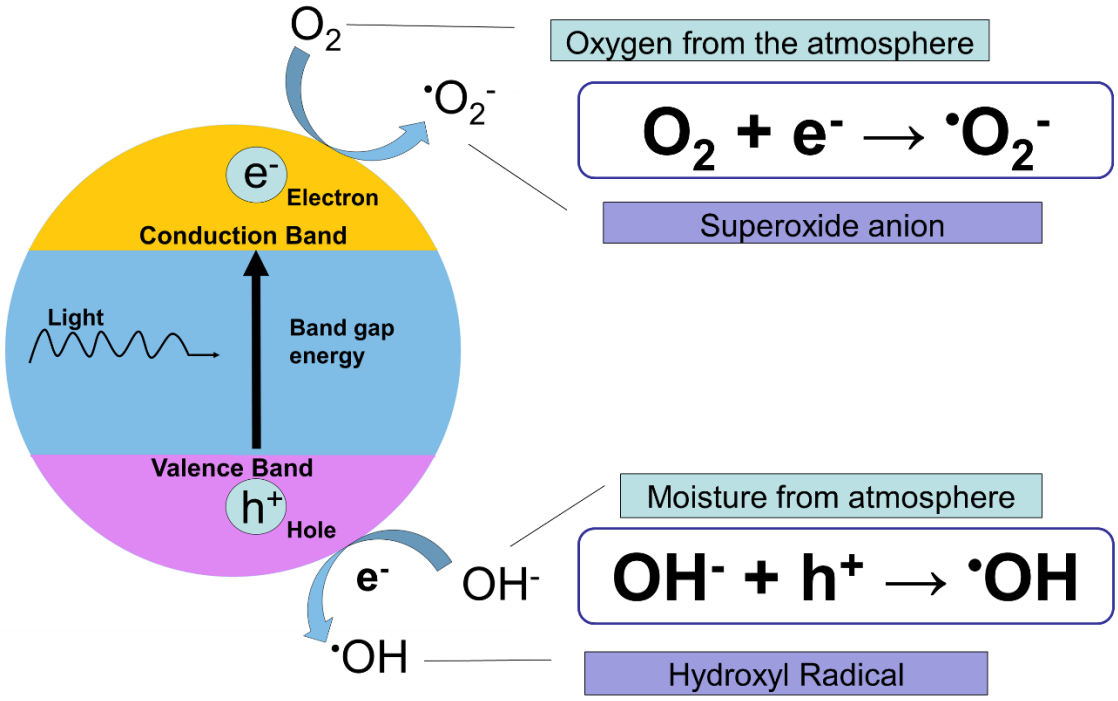

Figure 19. Reactive oxygen species formation as related to the energy band gap.[28]

4.4.5.1 Rhodamine-B Dye Degradation using Eu^{3+} doped ZnO Nanoparticles

An in-group collaboration was performed and photodegradation studies were completed by Joseph Lee in our laboratory. These photodegradation studies provide a way to analyze the nanoparticles ability to produce reactive oxygen species and therefore, their potential for antimicrobial activity. This is due to the fact that the production of reactive oxygen species is also responsible for the degradation of the dye of interest. These studies were performed using rhodamine-B dye at 4.11 x 10^{-6} M in nanopure water (35 mL). The nanoparticles (50 mg) were added to the rhodamine dye solution and stirred under ultraviolet (UV) light. Aliquots were taken once every five minutes to study the photodegradation of the dye. UV light increases the production of ROS because when UV light is absorbed the nanoparticle becomes photoexcited leading to energy storage by charge separation and formation of electron-hole pairs.[41] The

electron-hole pairs are discussed in section 4.4.5. Figures 20 shows the photodegradation studies performed on all nanoparticle doping percentages. As seen in Figure 20, the dye was degraded significantly for all doping percentages. However, undoped ZnO (E0) had the most pronounced degradation after 30 minutes. E1 ZnO nanoparticles were second best, decreasing the faster than the other Eu^{3+} doping percentages. All of the studies indicate that the nanoparticles would have the potential to produce ROS and therefore, all doping percentages have the potential to be antimicrobial.

Interestingly, the Eu^{3+} doped ZnO nanoparticles had a much more rapid degradation time compared to the Mn^{2+} doped ZnO nanoparticles. All Eu^{3+} doping percentages degraded the dye significantly within 30 minutes, however the Mn^{2+} ZnO was able to measured over a period of 7 hours, for all but small 5% Mn^{2+} doped ZnO and 15% Mn^{2+}. Large 15% Mn^{2+} showed only a slight decrease in extinction even after 9 hours. Therefore, the improved morphology of the Eu^{3+} doped ZnO nanoparticles yielded a greater probability of ROS formation, leading to a more rapid degradation of rhodamine-B dye.

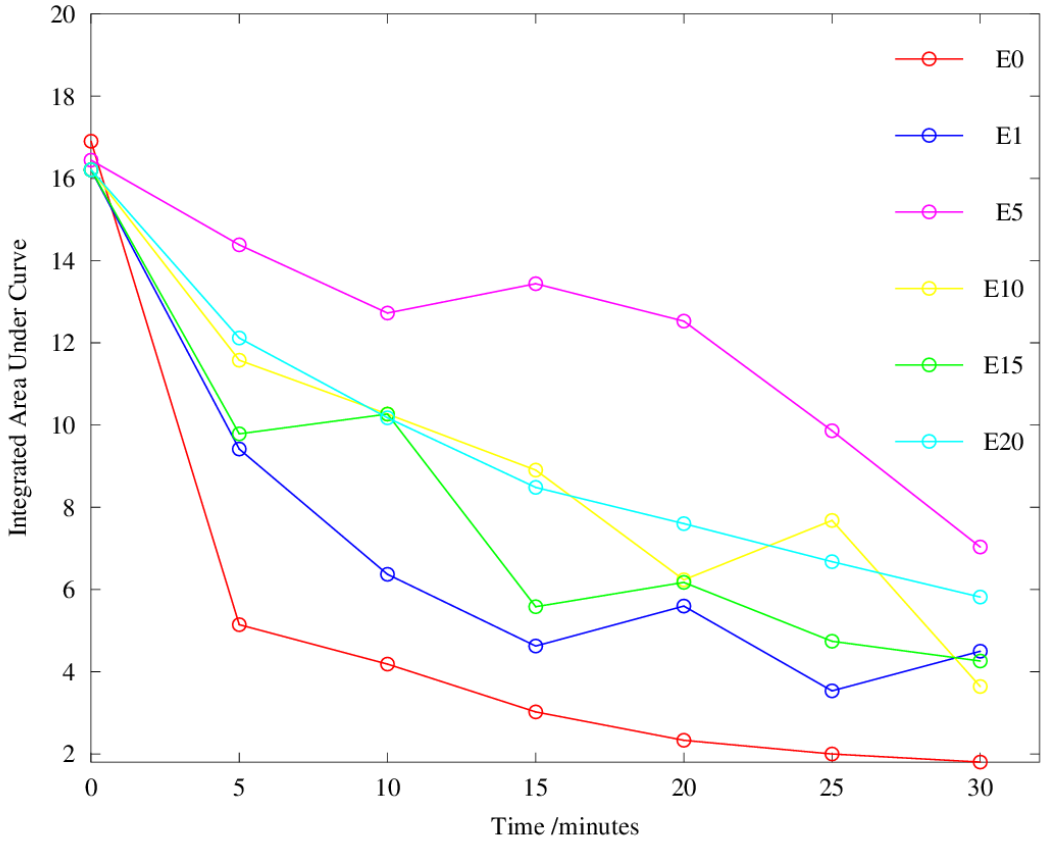

Figure 20. Photodegradation of rhodamine-B dye for all Eu^{3+} doping percentages as integrated area under the curve versus time.

4.5 Antimicrobial Susceptibility Testing for Eu^{3+} doped ZnO Nanoparticles

4.5.1 Agar Diffusion Test Results for Eu^{3+} doped ZnO Nanoparticles

Table 9 summarizes the average zone of inhibition (mm) after a 24 hour incubation. The zone of inhibition measurements in Table 9 were determined using a ruler against a dark background with the lid of the petri dish removed. Table 10 were measured using Adobe Photoshop CC to see if the area where nanoparticles can be seen in the agar makes a difference in the measurement. All of the agar diffusion tests were repeated in triplicate, and an average with standard deviation of the triplicate data is reported in Table 9 and 10. Agar diffusion is a

qualitative test, and mainly indicates whether the nanoparticles are antimicrobial or not. What we can see from Figures 21 through 25 is that all of the doping percentages exhibit some antimicrobial activity. Figure captions and labels contain the theoretical doping percentage, tables 9 and 10 indicate the actual doping percentages used in the testing. The differences between the control of ZnO and the Eu^{3+} doped ZnO are minute, and therefore, a quantitative test had to be completed to evaluate how the doping percentage affects the antimicrobial activity of the ZnO nanoparticles. However, one trend was notable, the gram-negative bacteria seems to be more resistant to the bacteria, as shown by a smaller zone of inhibition. Gram-negative bacteria tend to be more resistant to antibiotics due to their relatively impervious lipid membrane.[44] This means the gram-positive bacteria is more susceptible to the antimicrobial effect of the ZnO nanoparticles compared with the gram-negative species that was tested.

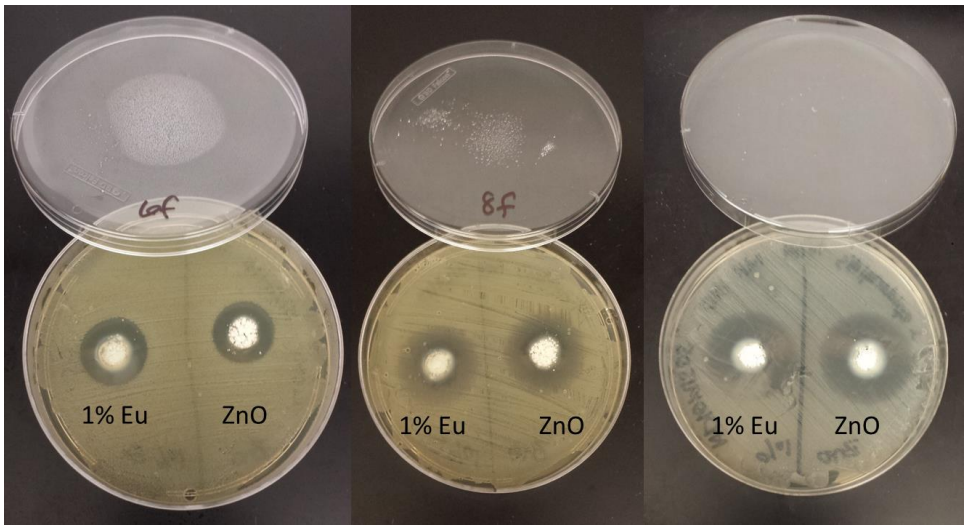

Figure 21. Agar diffusion testing of E1 (experimental 0.9%) nanoparticles against (A) *E. coli*, (B) *S. aureus*, and (C) *S. epidermidis*.

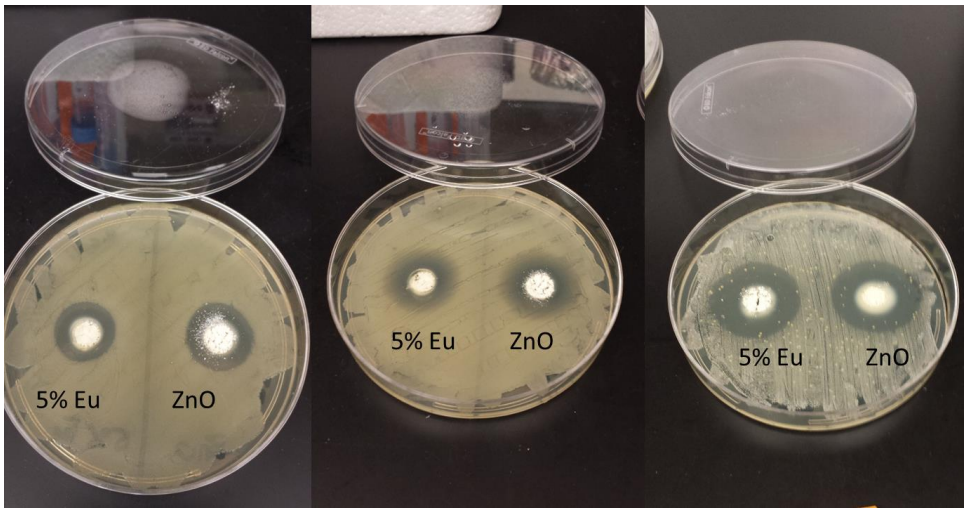

Figure 22. Agar diffusion testing of E5 (experimental 4.7%) nanoparticles against (A) *E. coli*, (B) *S. aureus*, and (C) *S. epidermidis*.

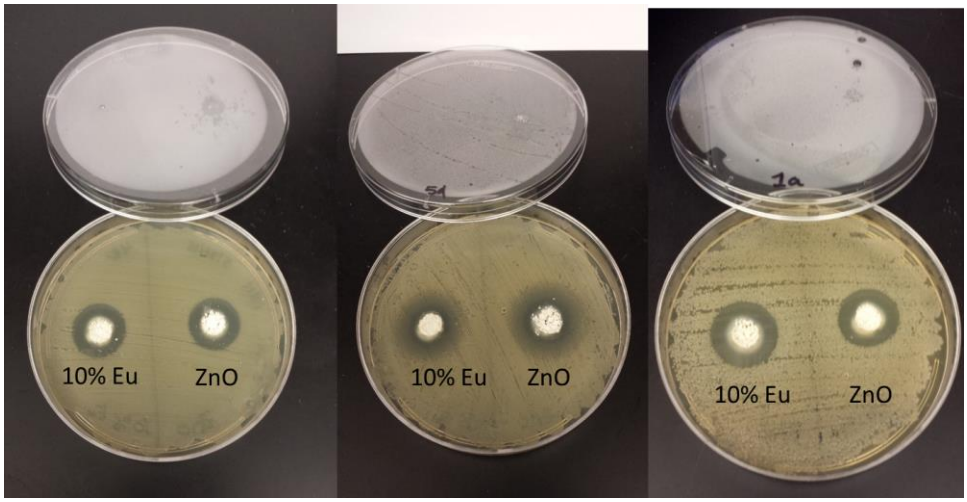

Figure 23. Agar diffusion testing of E10 (16% Eu^{3+}) nanoparticles against (A) *E. coli*, (B) *S. aureus*, and (C) *S. epidermidis*.

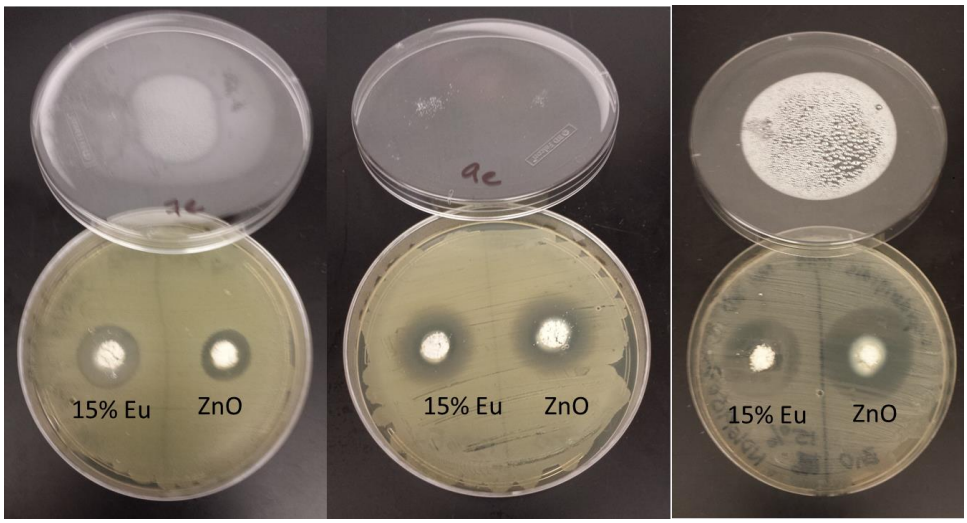

Figure 24. Agar diffusion testing of E15 (16% Eu^{3+}) nanoparticles against (A) *E. coli*, (B) *S. aureus*, and (C) *S. epidermidis*.

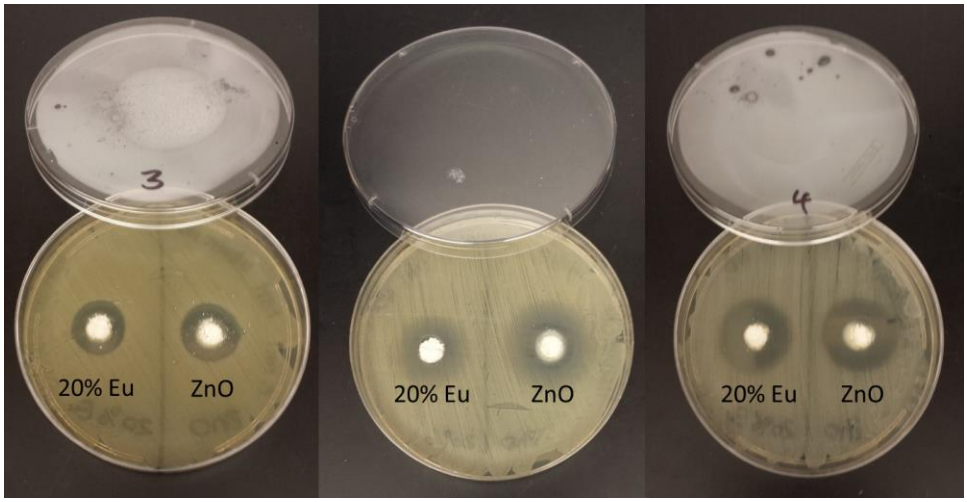

Figure 25. Agar diffusion testing of E20 (20% Eu^{3+}) nanoparticles against (A) *E. coli*, (B) *S. aureus*, and (C) *S. epidermidis*.

Table 10. Agar diffusion zone of inhibition data for Eu^{3+} doped ZnO nanoparticles versus undoped ZnO as a control.

Bacteria	Eu^{3+} Doping Percentage /%	Average Zone of Inhibition of 3 Trials /mm	Average Zone of Inhibition of ZnO /mm
E. coli	E1	19.0 ± 1.0	19.7 ± 0.6
S. aureus	E1	26.0 ± 0.6	27.0 ± 1.0
S. epidermidis	E1	31.0 ± 1.7	28.7 ± 1.5
E. coli	E5	21.0 ± 0.6	19.7 ± 0.6
S. aureus	E5	27.0 ± 1.7	24.7 ± 0.6
S. epidermidis	E5	28.0 ± 0.6	31.0 ± 2.6
E. coli	E10	19 ± 1.0	19.0 ± 1.0
S. aureus	E10	25.0 ± 0.6	24.0 ± 0.6
S. epidermidis	E10	21.0 ± 0.6	18.7 ± 0.6
E. coli	E15	19.0 ± 0.0	17.0 ± 0.0
S. aureus	E15	21.0 ± 0.7	22.5 ± 0.7
S. epidermidis	E15	32.0 ± 1.7	25.5 ± 0.7
E. coli	E20	18.7 ± 0.6	15.7 ± 1.5
S. aureus	E20	26.0 ± 0.6	21.7 ± 0.6
S. epidermidis	E20	26.0 ± 1.2	24.0 ± 0.0

Table 11. Agar diffusion zone of inhibition repeat data for Eu^{3+} doped ZnO nanoparticles versus undoped ZnO as a control.

Bacteria	Eu^{3+} Doping Percentage /%	Average Zone of Inhibition of 3 Trials /mm	Average Zone of Inhibition of ZnO /mm
E. coli	E1	3.9 ± 0.8	3.7 ± 0.7
S. aureus	E1	4.9 ± 1.3	4.7 ± 0.7
S. epidermidis	E1	6.1 ± 0.8	5.8 ± 0.5
E. coli	E5	3.6 ± 0.3	3.6 ± 0.2
S. aureus	E5	3.7 ± 0.5	4.0 ± 0.1
S. epidermidis	E5	6.2 ± 1.2	6.1 ± 1.2
E. coli	E10	-	-
S. aureus	E10	4.0 ± 0.5	4.3 ± 0.5
S. epidermidis	E10	-	-
E. coli	E15	2.4 ± 0.9	3.4 ± 0.2
S. aureus	E15	3.6 ± 0.3	3.9 ± 1.1
S. epidermidis	E15	6.1 ± 1.5	6.4 ± 0.1
E. coli	E20	3.7 ± 0.2	4.2 ± 0.8
S. aureus	E20	3.0 ± 0.6	3.3 ± 0.9
S. epidermidis	E20	4.2 ± 0.6	4.2 ± 0.9

4.5.2 Minimum Inhibitory Concentration Test Results for Eu^{3+} doped ZnO Nanoparticles

A minimum inhibitory concentration range was found for all nanoparticles against all three bacterial species: *E. coli*, *S. aureus* and *S. epidermidis*. Table 11 shows the MIC value range obtained during testing. The range indicated was found to be a pattern for the doping

percentages over multiple tests. Figures 26 - 28 show the minimum inhibitory concentration testing results for Eu^{3+} doped ZnO nanoparticles. The circles in the Figures indicate where the MIC range began. In Table 12, the calculated number of nanoparticles for the MIC range obtained is listed, where a conversion factor obtained from the ICP-OES data was used to determine the number of nanoparticles in the wells. This was calculated by multiplying the mass of nanoparticles in the stock solution by the volume that was transferred to the first well, the mass at the MIC range was calculated by the dilution at that point (i.e. if there was a two-fold dilution across all wells and 4 mg of nanoparticles was transferred to well one, then well two would contain 2 mg, well 3 would contain 1 mg, etc.). Table 13 indicates the doping percentage represented by the number in each image. A pattern was observed during the MIC testing that the 5% Eu^{3+} (experimental 4.7%) doped ZnO exhibited the lowest MIC for all three bacterial species. The E5 nanoparticles had an MIC range of 1.25 – 0.625 mg/mL, 2.50 – 1.25 mg/mL, and 0.625 mg/mL for *E. coli*, *S. aureus*, and *S. epidermidis*, respectively. In comparison, the undoped ZnO exhibited a slightly higher MIC range at 2.50 – 1.25 mg/mL for *E. coli*. However, the MIC range was significantly higher for *S. aureus*, and *S. epidermidis* of between 10.0 - 5.0 mg/mL and 5.0 – 2.50 mg/mL, respectively. This indicates that it takes at least twice the concentration of nanoparticles to inhibit the bacterial growth in *S. aureus*, and at least four times the concentration for *S. epidermidis*, compared to the results for the E5 nanoparticles. The E5 nanoparticles (calculated molar doping percentage of 5% Eu^{3+}) were then chosen for the cotton studies since they were the most effective compared to the other doping percentages.

Table 12. Minimum inhibitory concentrations for Eu^{3+} doped ZnO nanoparticles.

	Minimum Inhibitory Concentration Range (mg/mL)		
Eu^{3+} Doping %	***E. coli***	***S. aureus***	***S. epidermidis***
E0	2.50 -1.25	10.0 - 5.0	5.0 - 2.50
E1	1.25 - 0.625	4.0 - 2.0	1.25 - 0.625
E5	1.25 - 0.625	2.50 - 1.25	0.625-0.313
E10	6.0 - 4.0	6.0 - 4.0	2.50 -1.25
E15	4.0 - 2.0	10.0- 8.0	10.0 - 5.0
E20	10.0 - 5.0	20.0 – 10.0	5.0 – 2.5

Table 13. Number of nanoparticles at the reported MIC ranges for 0.71% Eu^{3+} and 3.41% Eu^{3+} doped ZnO nanoparticles.

	Number of Nanoparticles for MIC Range (x 10^{14})		
Experimental Eu^{3+} Doping %	***E. coli***	***S. aureus***	***S. epidermidis***
E1	0.771 – 0.386	2.47 – 1.23	0.771 – 0.386
E5	0.973 – 0.487	1.95 – 0.973	0.487 - 0.244

Table 14. Legend for Figures 35 - 37

Label	**Eu^{3+} Nanoparticle Doping Percentage /%**
1	E0
2	E1
3	E5
4	E10
5	E15
6	E20

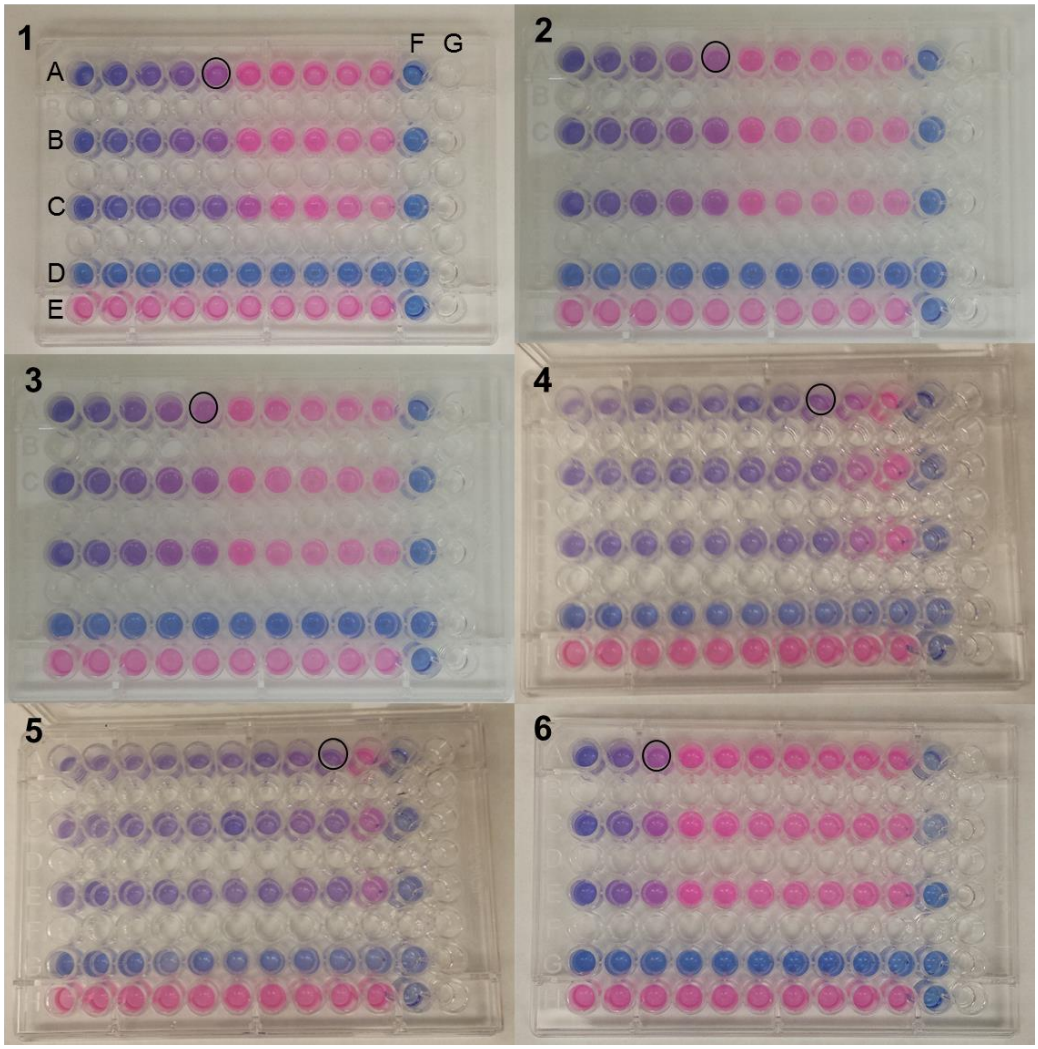

Figure 26. MIC test pictures of all nanoparticle doping percentages against *E. coli* where (A), (B), and (C) are triplicates of each sample, (D) is a control of nanoparticles with dye and no bacteria, (E) is dye with bacteria, (F) control of dye and MHB, (G) MHB only.

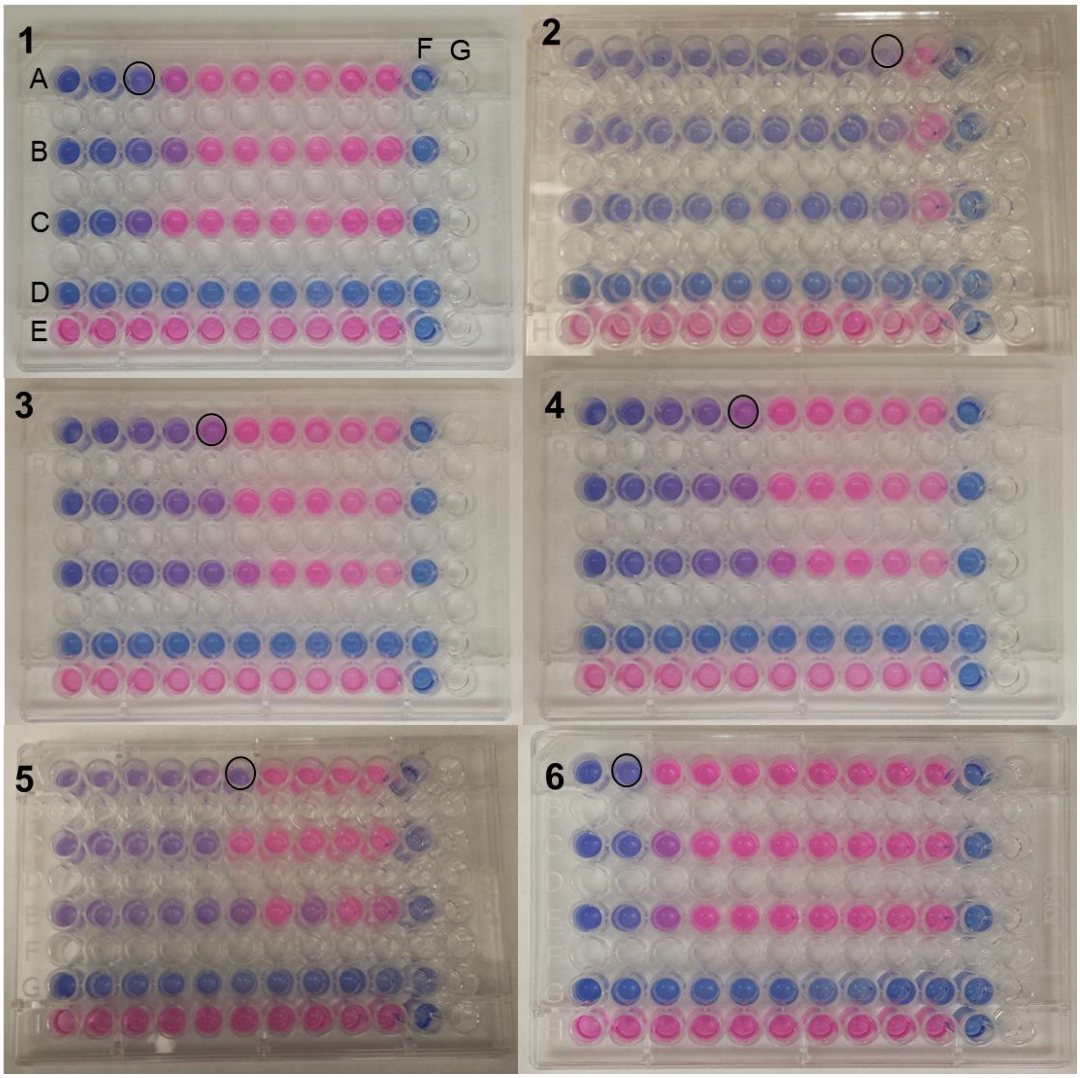

Figure 27. MIC test pictures of all nanoparticle doping percentages against *S. aureus* where (A), (B), and (C) are triplicates of each sample, (D) is a control of nanoparticles with dye and no bacteria, (E) is dye with bacteria, (F) control of dye and MHB, (G) MHB only.

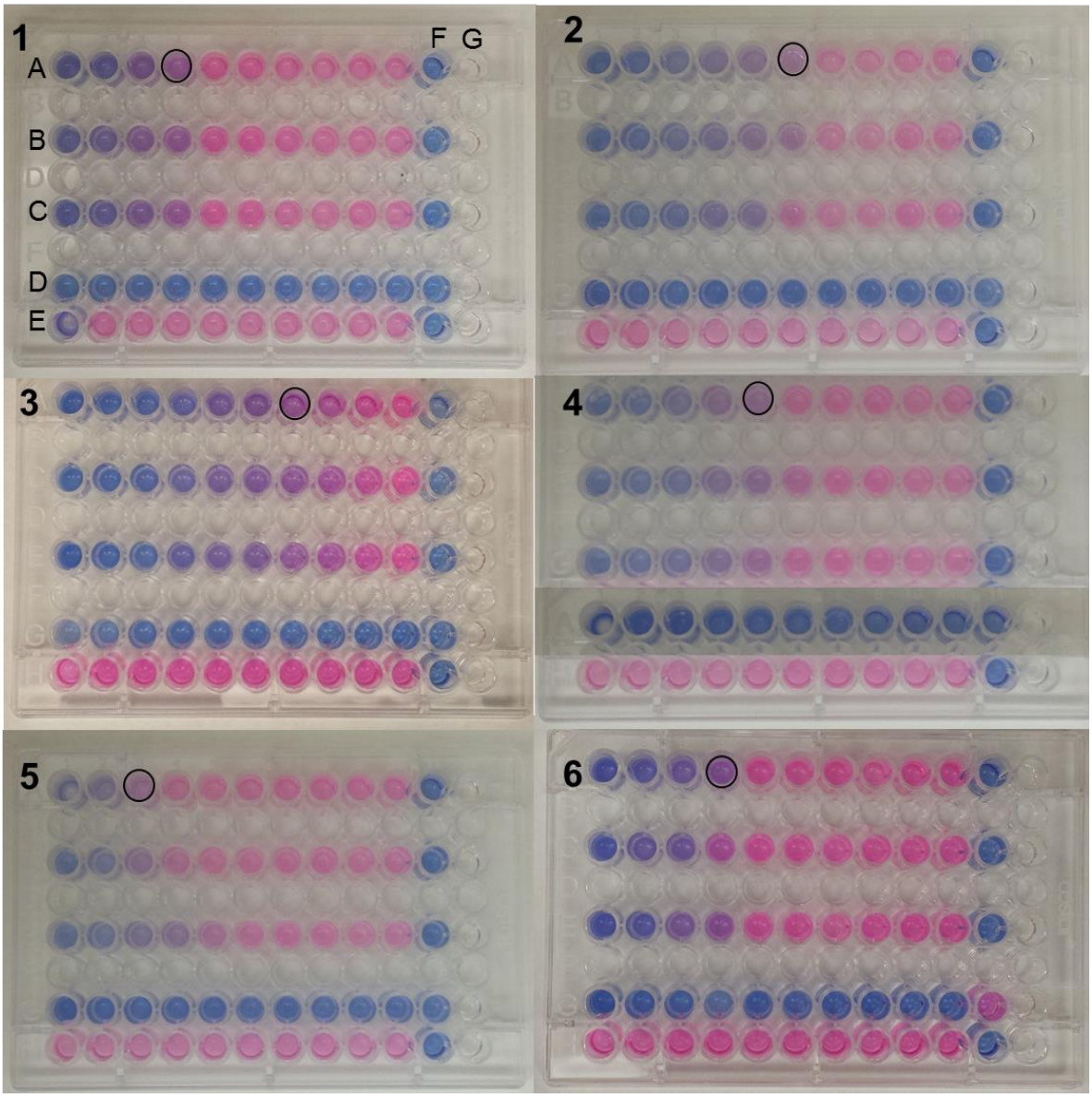

Figure 28. MIC test pictures of all nanoparticle doping percentages against *S. epidermidis* where (A), (B), and (C) are triplicates of each sample, (D) is a control of nanoparticles with dye and no bacteria, (E) is dye with bacteria, (F) control of dye and MHB, (G) MHB only.

4.6 Characterization of Nanoparticle Attachment to Cotton Textiles

Nanoparticles were attached to textiles using two different methods. The cotton textile material used was bleached, woven cotton purchased from TestFabrics, Inc. The first method

involved grafting β-cyclodextrin to the surface of the textile using citric acid as a crosslinker (Figure 29 – 30).[47] β-cyclodextrin, due to its structure, adds additional hydroxyl groups to the surface of the textile, thereby increasing the number of sites available for nanoparticles to bind.[47] Once this modification was performed, nanoparticle suspensions were prepared and the modified cotton was soaked in the suspension for four hours. The second method involved suspending prepared nanoparticles in 2-propanol and then placing clean, unmodified cotton in the suspension.[55]

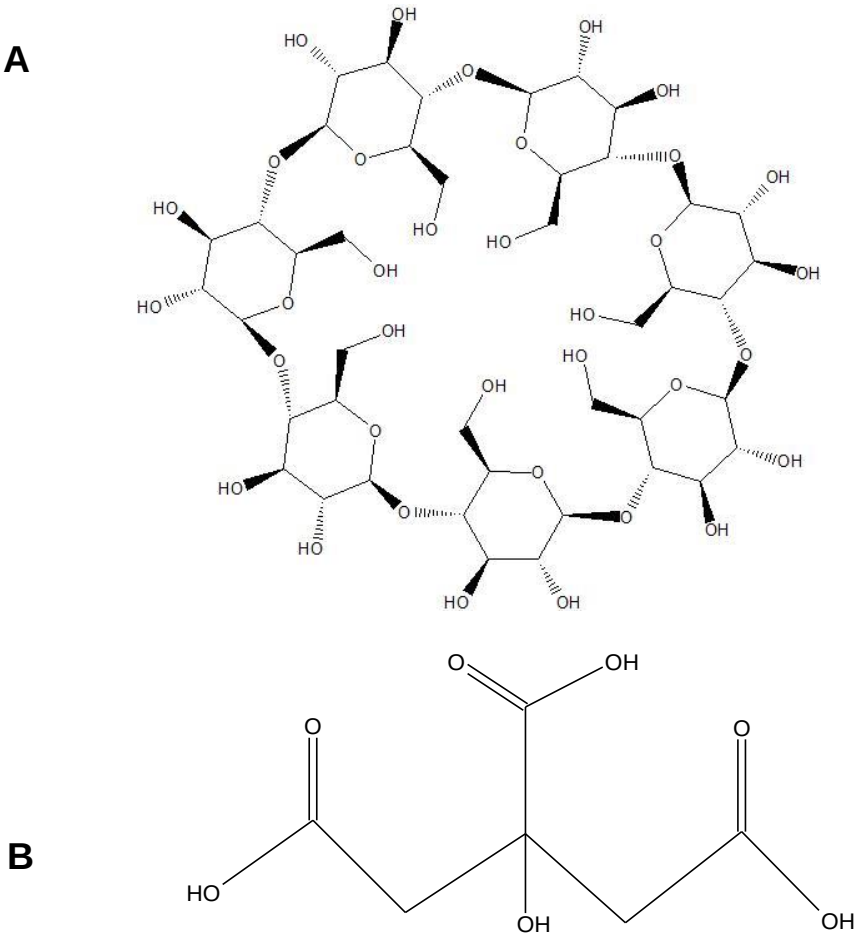

Figure 29. Structures of (a) β-cyclodextrin and (b) citric acid.

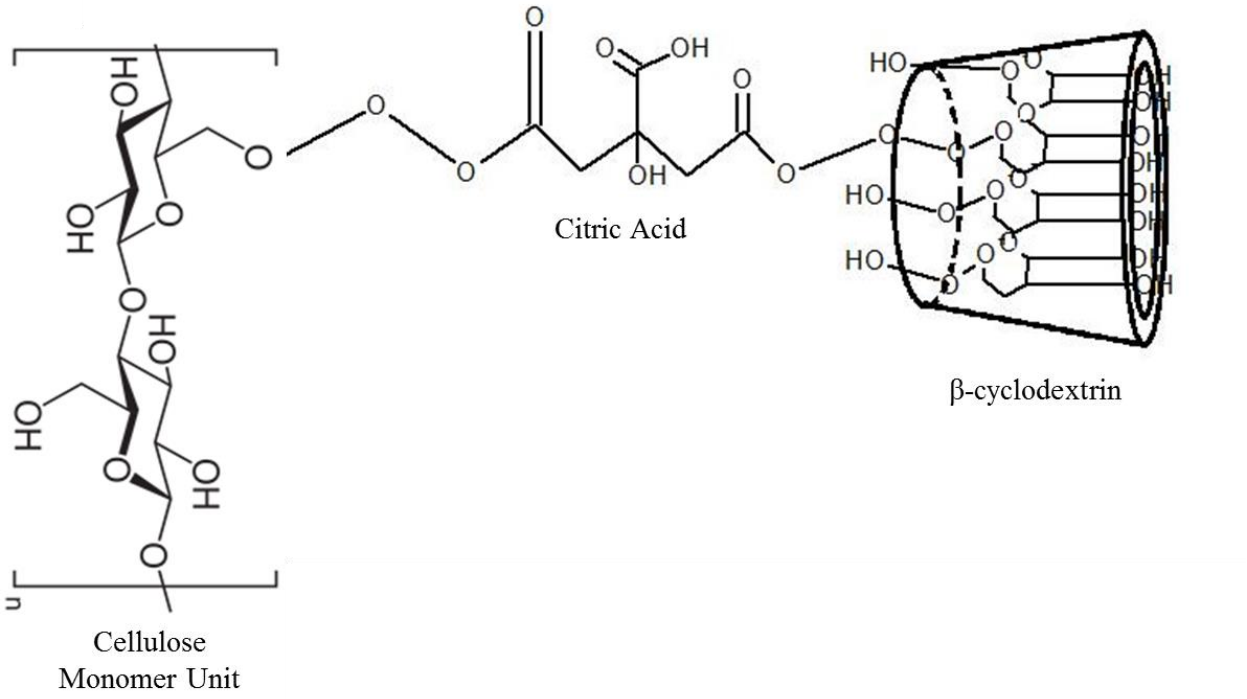

Figure 30. β-cyclodextrin bound to cellulose via a citric acid linker.

4.6.1 FT-IR of Modified Cotton Textile

FT-IR spectra were obtained of unmodified and modified cotton textile samples, to determine if β-cyclodextrin was present in the modified cotton sample. Figure 31 shows the FT-IR spectra of modified and unmodified cotton. As shown in Figure 31, the modified cotton contains an additional band at 1673 cm^{-1} (indicated by a) that is not present in the unmodified cotton, but is present in a literature FT-IR spectrum of β-cyclodextrin. The presence of this band indicates the presence of β-cyclodextrin in the modified cotton textile.

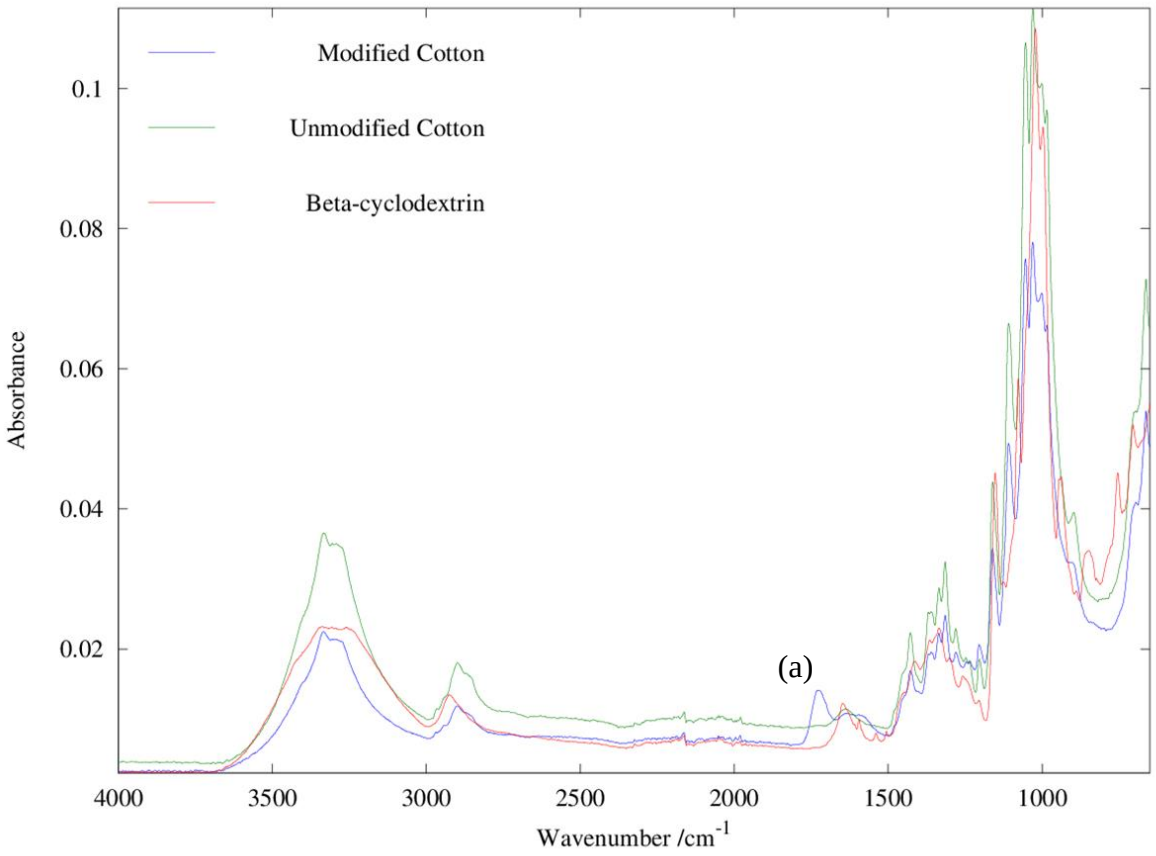

Figure 31. ATR FT-IR of unmodified and modified cotton.

4.6.2 ICP-OES Data for 5% Eu^{3+} doped ZnO Nanoparticles

One doping percentage was chosen for the cotton modification studies due to time constraints. The doping percentage was chosen due to the results obtained in the antimicrobial testing, and after examining the TEM images. The calculated 5% Eu^{3+} doped ZnO had the lowest MIC value of the prepared doping percentages, and from the TEM images we knew the average size was quite small and the particles formed well. Since such a large amount of nanoparticles was necessary to obtain antimicrobial data, several batches had to be prepared to complete the studies. Therefore, we wanted to know what the experimental doping percentage

was, since the cotton samples were being coated with nanoparticles. Since several batches were used during the studies, ICP-OES gave a good idea of the reproducibility of the batches. Table 14 shows the experimental doping percentage for six different batches of the theoretical 5% Eu^{3+} doped ZnO and the average of the six. The experimental doping percentages are all at the same magnitude and each value is within 10% of all other values, including the average. Therefore, the batches are very reproducible, making the synthetic method promising for future work. This result also means that it is unlikely that different batches should produce dissimilar results.

Table 15. Experimental doping percentages for several different batches of 5% Eu^{3+} doped ZnO nanoparticles.

Batch Number	Calculated Doping Percentage /%	Experimental Doping Percentage[a] /%	Average Number of Nanoparticles (x 10^{15})[b]
1	5	5.57 ± 0.02	1.23 ± 0.01
2	5	5.50 ± 0.04	1.217 ± 0.004
3	5	5.57 ± 0.03	1.118 ± 0.004
4	5	5.386 ± 0.006	0.950 ± 0.004
5	5	5.32 ± 0.05	0.799 ± 0.001
6	5	5.52 ± 0.05	0.982 ± 0.006
Average of All 6	5	5.5 ± 0.1	1.05 ± 0.1

[ab]Numbers are reported plus or minus standard deviation.

4.6.3 Scanning Electron Microscopy and Energy Dispersive X-Ray Spectroscopy Studies on Cotton Samples

Figure 32 shows the obtained SEM images of both attachment methods of unwashed, washed 1 and 3 times, respectively. The cotton modification method using β-cyclodextrin as a crosslinker does not lose many nanoparticles even after three washings, as shown in Figure 32. However, the 2-propanol attachment method looks to have lost many nanoparticles even after

just one wash. This tells us that the modified cotton would most likely be the preferred method of attachment of ZnO nanoparticles to woven cotton textiles. The longer the nanoparticles are attached to the cotton, the more resilient and robust the textile would be for antimicrobial activity in a clinical setting. What we also see is that the nanoparticle coverage is quite sporadic, so the method would need to be optimized to improve the nanoparticle coverage. If the nanoparticle coverage was improved, this could also lead to improved antimicrobial activity of the modified cotton.

Figures 33 through 38, show the obtained EDX spectra of the unwashed and washed cotton samples. Throughout the modified cotton sample studies (Figures 33 – 35) the amount does not change significantly after one washing, going from an overall weight percentage of Zn^{2+} of 16.3%, and a weight percent of Eu^{3+} of 7.8% to 14.1% and 6.8%, respectively. However, we see that the carbon to zinc ratio does not change significantly between washings at 0.424, 0.336 and 0.432 for unwashed, washed once and three washes, respectively. This is a decrease in weight percent of 2.2% for Zn^{2+} and 1.0% for Eu^{2+}. The Zn^{2+} and Eu^{3+} ion atomic percentages are much higher where the nanoparticles can be seen in the images, versus where there is little to no nanoparticle coverage, as is expected. The sodium and phosphorous in the modified cotton samples can be attributed to the modification technique, which uses sodium phosphate. However, as seen in Figures 36 – 38, the 2-propanl nanoparticle attachment method was less robust, and the nanoparticles begin to wash away after washing. The overall percentage of Zn^{2+}/Eu^{3+} ions decreases from 35.4 and 12.8 weight percent, respectively to 5.5 and 1.3 weight percent after three washes. This means a weight percent difference of 29.9 Zn^{2+} and 11.5 for Eu^{3+} which is a significant difference.

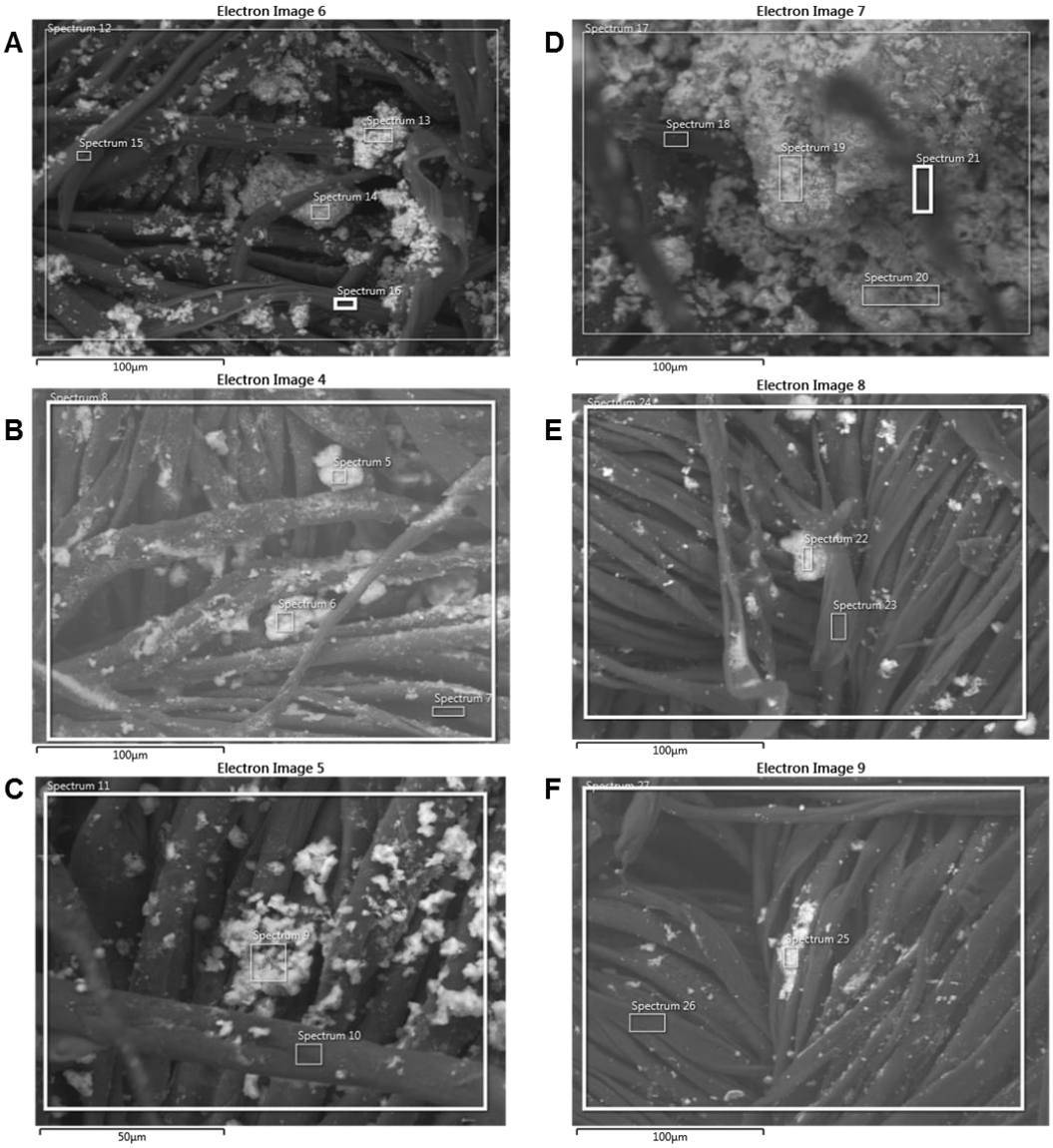

Figure 32. SEM images of (A) modified cotton (washed 0x), (B) modified cotton (washed 1x), (C) modified cotton (washed 3x), and 2-propanol cotton attachment method (D) washed 0x, (E) washed 1x, (D) washed 3x with E5 nanoparticles attached.

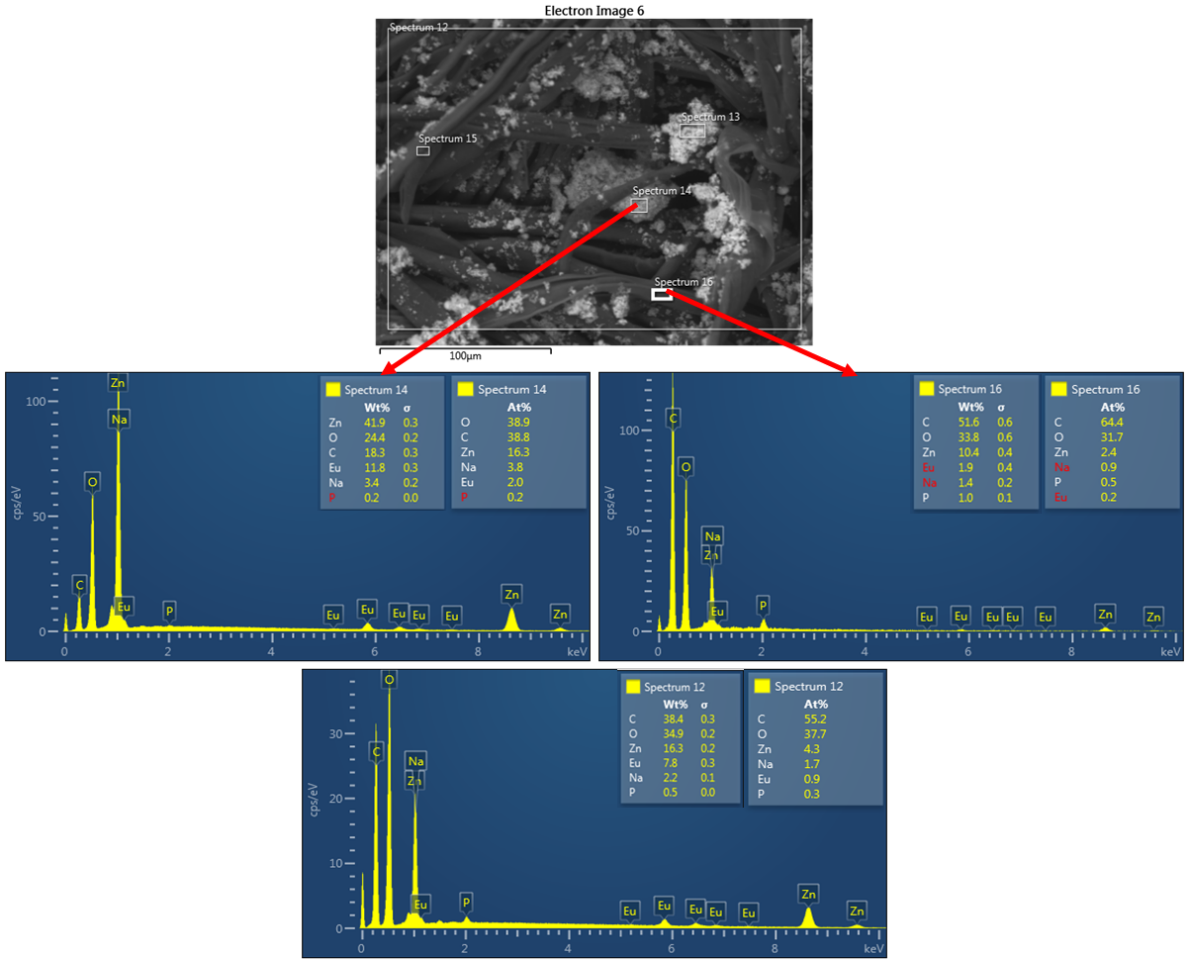

Figure 33. EDX results for modified cotton washed 0x.

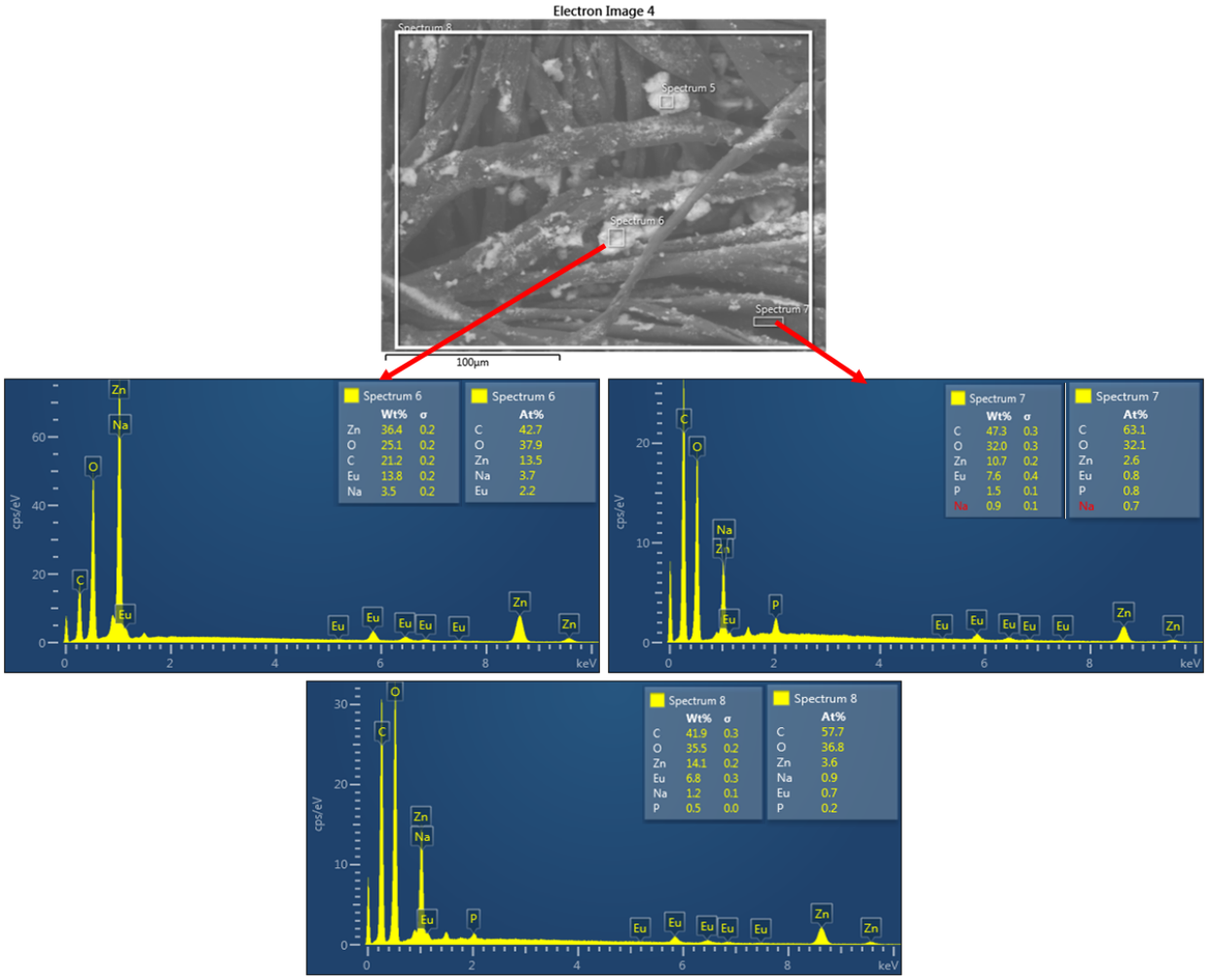

Figure 34. EDX results for modified cotton washed 1x.

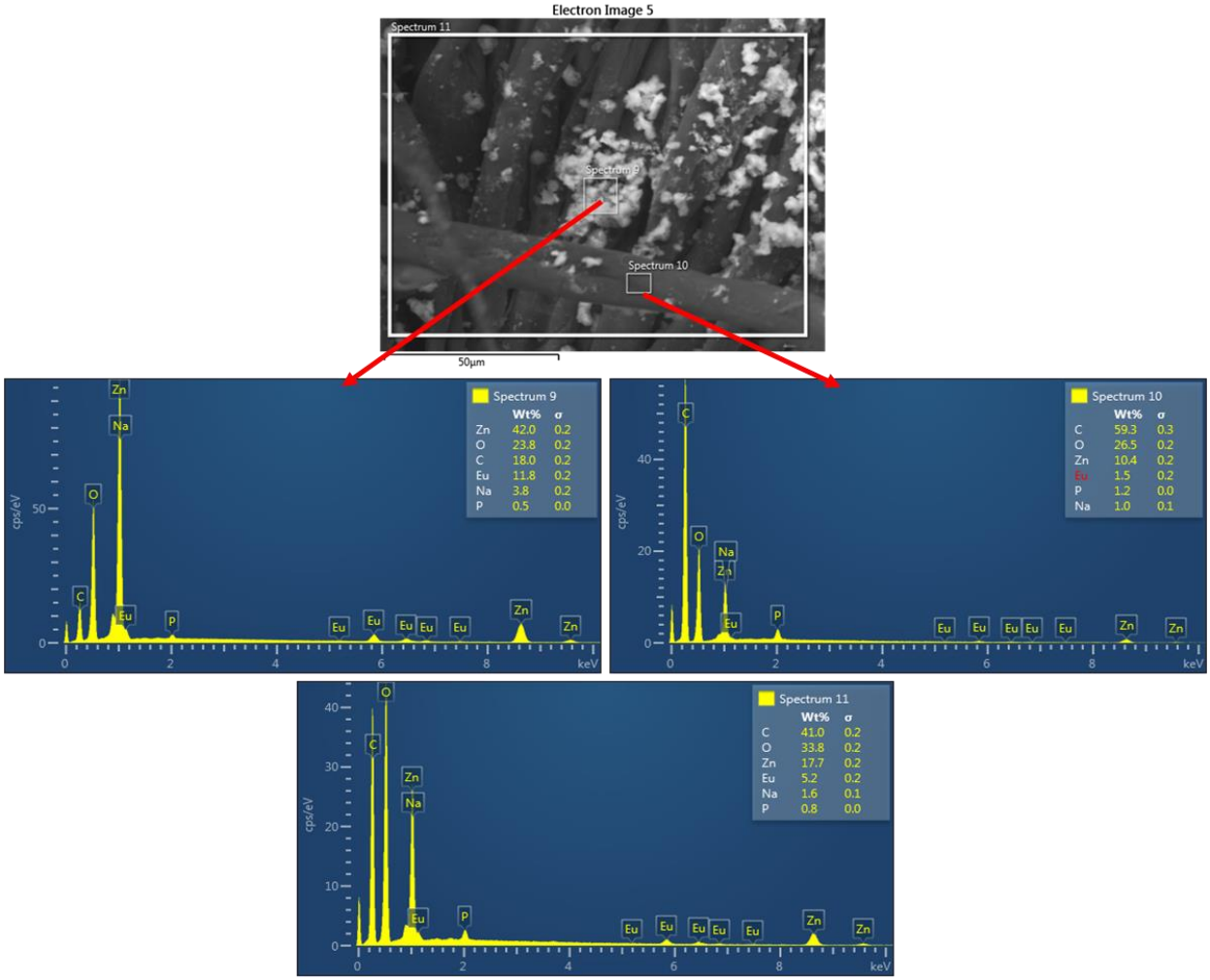

Figure 35. EDX results for modified cotton washed 3x.

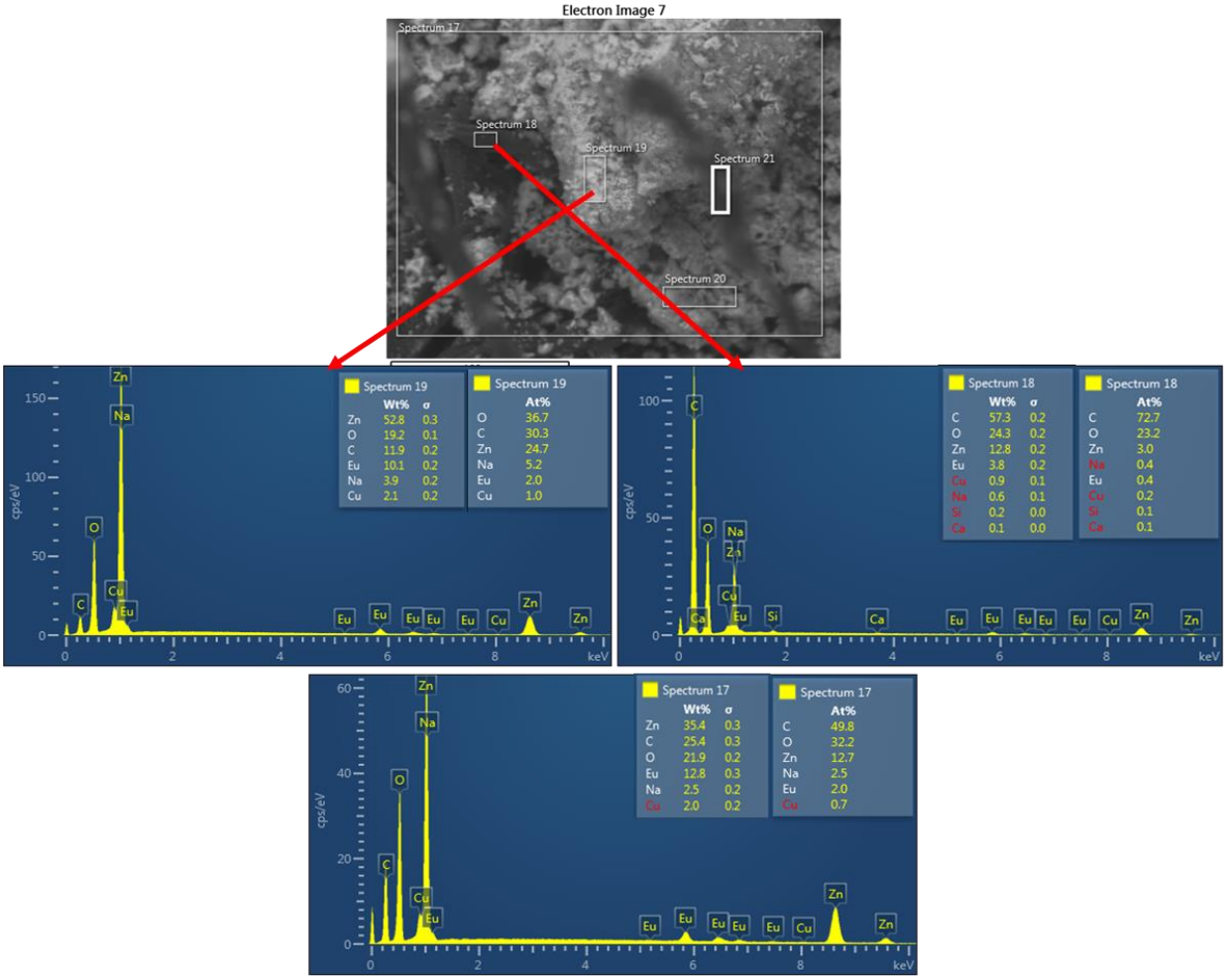

Figure 36. EDX results for 2-propanol nanoparticle attachment method, washed 0x.

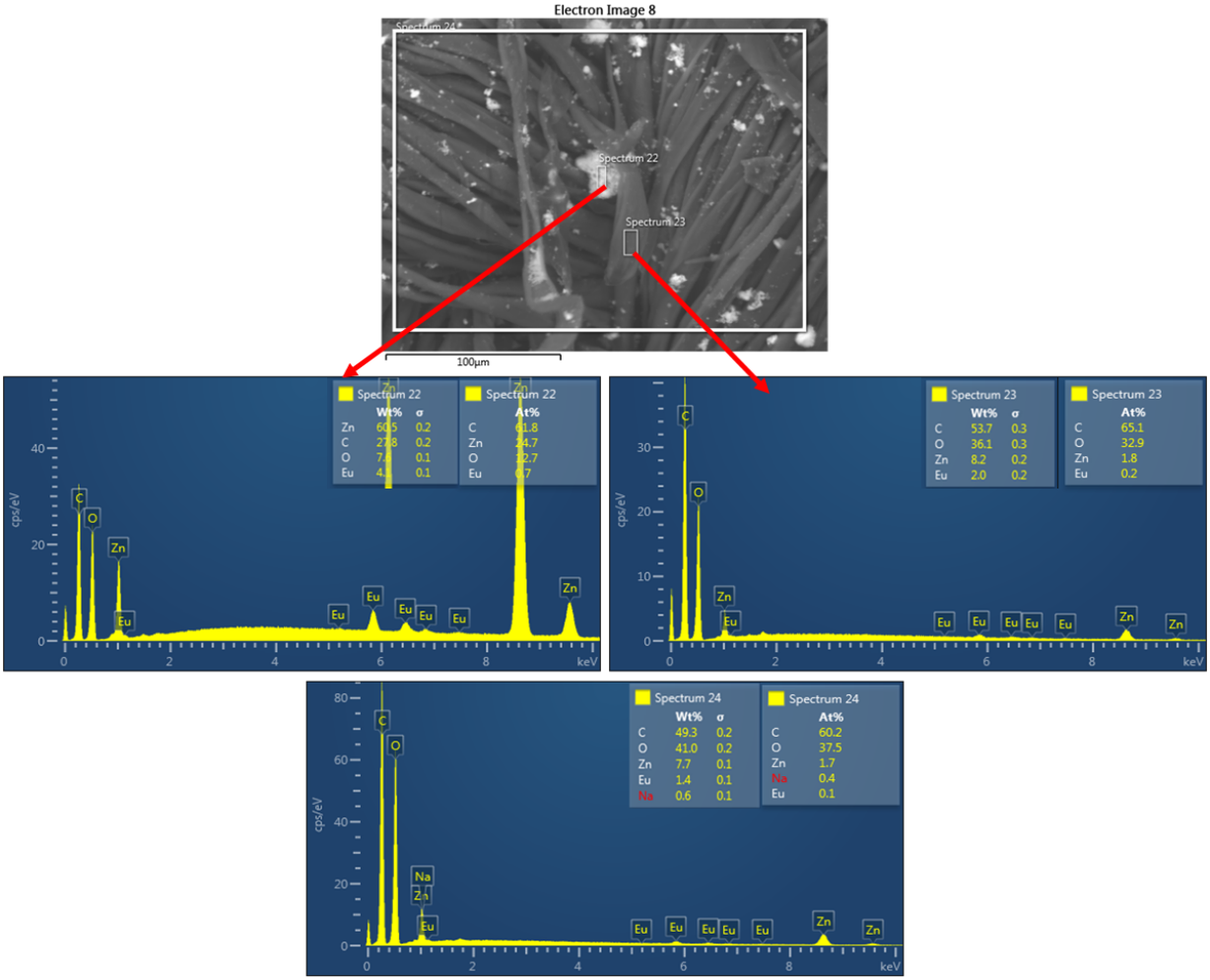

Figure 37. EDX results for 2-propanol nanoparticle attachment method, washed 1x.

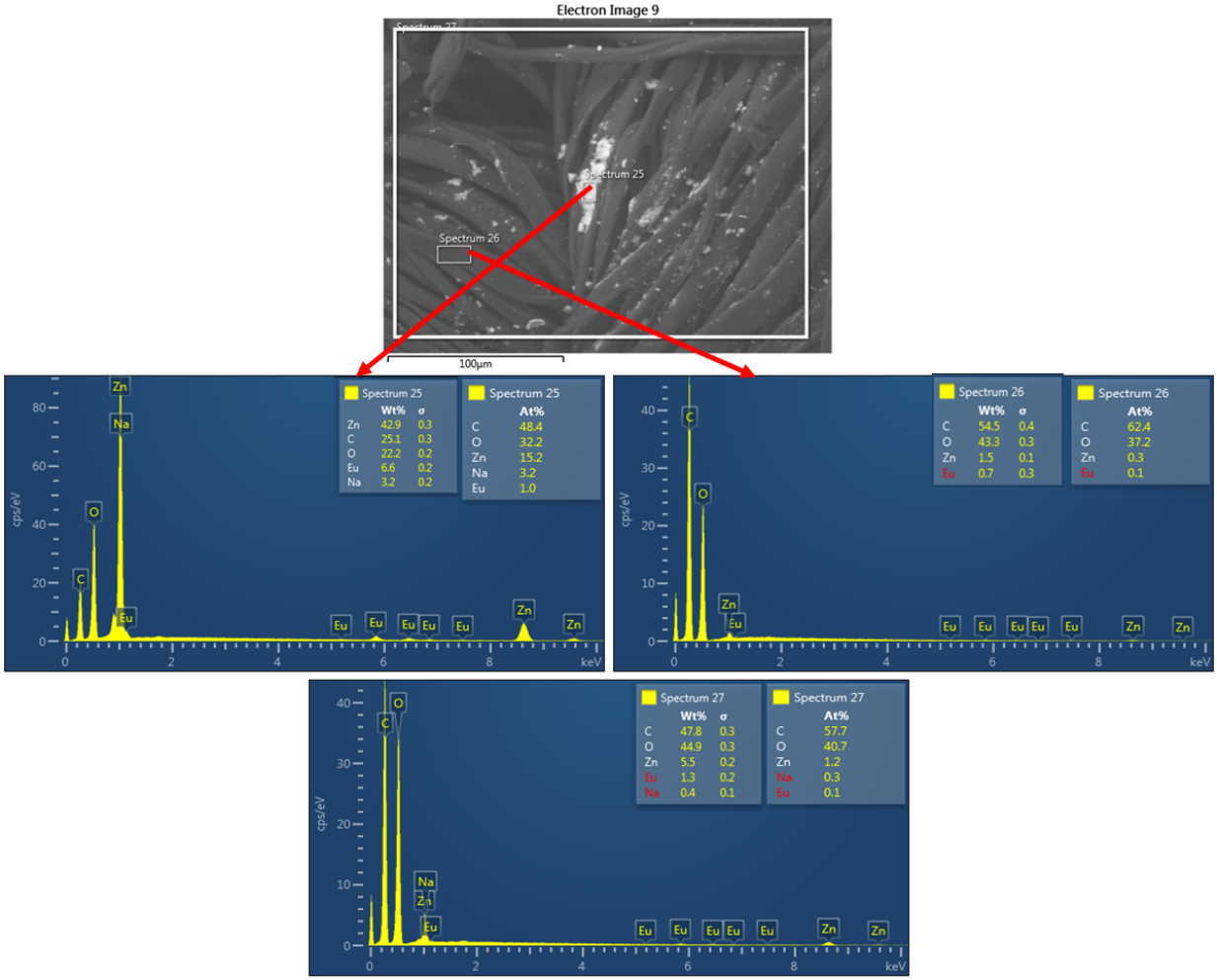

Figure 38. EDX results for 2-propanol nanoparticle attachment method, washed 3x.

4.6.4 Antimicrobial Susceptibility Testing

4.6.4.1 Agar Diffusion Test Results of Cotton Samples

The antimicrobial activities of the cotton samples with nanoparticles attached were evaluated by agar diffusion against *S. aureus* and are shown in Figure 39 and 40. Unwashed modified, and unmodified cotton with nanoparticles attached in the same manner both exhibited bacterial inhibition zones. As shown in Figure 39F, after one and two washes, there was a small amount of inhibition, but not enough to fully inhibit the bacterial growth. The images show that

perhaps the cotton samples are not fully saturated and an increased amount of nanoparticles on the cotton samples could improve the antimicrobial activity. After three washes, no inhibition zone is exhibited, therefore, at three washes or more we assume the majority of the nanoparticles have been removed, leading to a decrease in the antimicrobial activity. For the 2-propanol attachment method, this is supported by our EDX data, however, for the cotton modification method, only a small amount of nanoparticles is noticeably removed after three washes. In the case of the modified cotton, it may be that the small amount of nanoparticles that were removed were the loosely bound and therefore, more likely to diffuse through the agar.

Figure 40 shows the antimicrobial activity of the 2-propanol attachment method. The nanoparticle attached textiles that were unwashed, washed once and washed twice, again exhibit antimicrobial activity since there is a visible zone of inhibition. However, the textile washed three times does not show a zone of inhibition, therefore, we assume the nanoparticles began to be removed at three or more washes. The comparison between the two agar diffusion tests indicates that there is no major differences between the two attachment methods, both exhibit inhibition zones up to two wash cycles. Further examination of the antimicrobial activity, to compare the two attachment methods, was assessed using a time-dependent test.

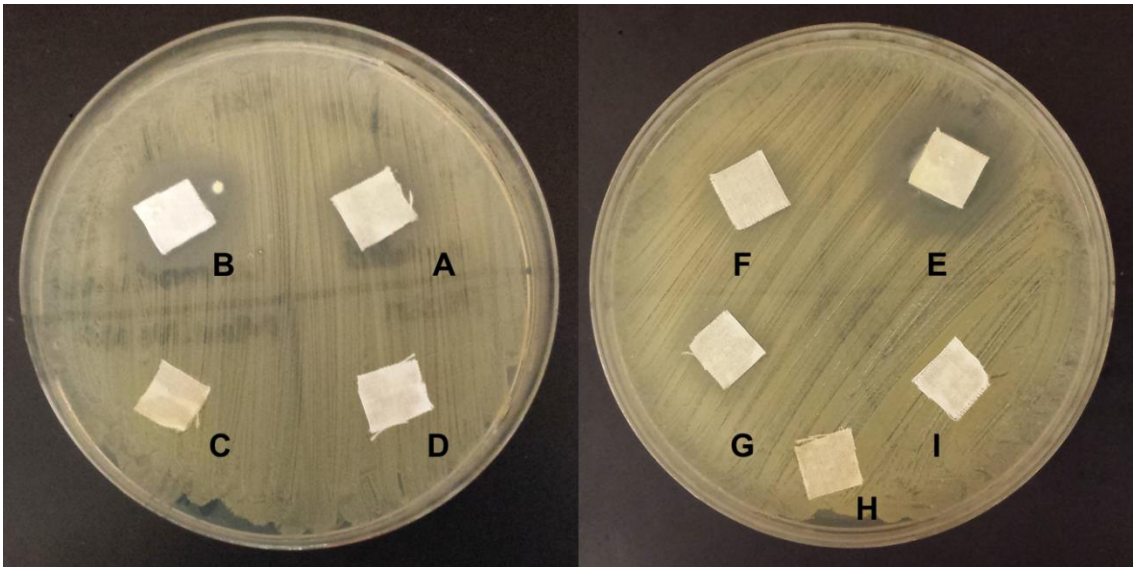

Figure 39. Agar diffusion testing of modified cotton samples (A) Modified cotton, and (B) Unmodified cotton with E5 nanoparticles, (C) Modified cotton without nanoparticles, (D) Plain cotton, (E) Modified Cotton (Washed 0x), (F) Modified cotton (washed 1x), (G) Modified cotton (washed 2x), (H) Modified cotton (washed 3x), (I) Plain cotton.

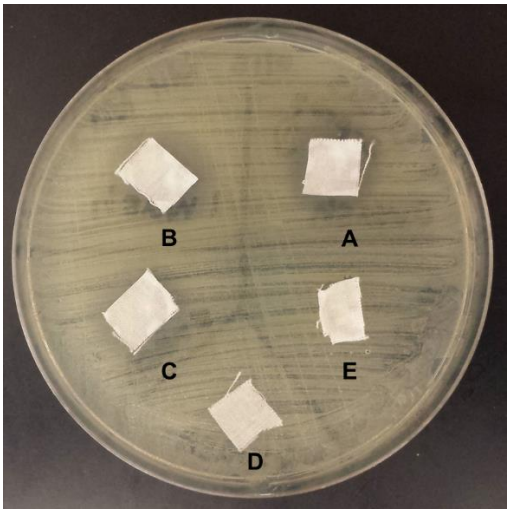

Figure 40. Agar diffusion testing of nanoparticle attached cotton samples using 2-propanol method (A) Washed 0x, (B) Washed 1x (C) Washed 2x (D) Washed 3x with E5 nanoparticles attached, and (E) Plain cotton.

4.6.4.2 Time-Dependent Test Results for Eu^{3+} doped ZnO Nanoparticles

The time-dependent antimicrobial susceptibility test evaluates the antimicrobial activity of samples over a period of time by measuring the optical density at time intervals. Optical density is measured since it is proportional to the amount of bacteria contained within the test tube. The cotton samples of interest were placed in the nutrient medium along with a liquid culture of *S. aureus* and the optical density of the culture tubes was monitored over a period of 24 hours. Four cotton samples were tested along with three controls. The modified cotton samples tested included unwashed modified cotton, modified cotton washed once, washed twice and washed 3 times. The three controls tested were modified cotton without nanoparticles attached, to evaluate if the modification method was contributing to the antimicrobial activity, *S. aureus* bacterial culture (no cotton or nanoparticles introduced), and plain cotton textile. The *S. aureus* culture was used to compare how the bacteria would grow without interference from cotton or nanoparticles, and the plain cotton was to compare the bacterial growth with untreated cotton.

Figure 41 shows the average of three time dependent tests for modified cotton over a period of 24 hours against *S. aureus*. Tables 15 and 16 show the averaged optical density values with their standard deviations over the 24 period. The time dependent testing exhibited something not shown in the agar diffusion test, that the bacterial growth was inhibited even after three washings. However, interestingly the unwashed cotton, which showed the largest zone of inhibition in the agar diffusion testing, showed bacterial growth at almost the same rate as the controls. Modified cotton after one washing had the lowest optical density after 24 hours, increasing to 0.432 ± 0.10. Modified cotton washed twice and three times increased to 0.447 ± 0.20 and 0.506 ± 0.10, respectively. Plain cotton had an optical density of 0.995 ± 0.04,

and *S. aureus* increased to an optical density of 0.979 ± 0.03. After one washing, the modified cotton decreased the bacterial growth to 44.1%, after three trials. After two washings the bacterial growth was decreased to 45.7% and after three washings to 51.7%. At three washes, the bacterial growth increases by 7.6%. With this, we are inhibiting the bacterial proliferation with these cotton textiles, but the inhibition is not complete.

In our previous studies, we found that poly(vinylpyrrolidinone) (PVP) coated 5% Mn^{2+} doped ZnO nanoparticles attached to cotton, stayed below an optical density of 0.3 over a seven hour period, even after two washes.[44] However, after three washes, the samples no longer exhibited antimicrobial activity. Ideally, we would like to see the washed cotton samples stay at very low optical density, even after 24 hours. Again, the cotton textiles are likely not being fully saturated with nanoparticles. One solution might be to heat the textiles during nanoparticle attachment to potentially expand the inner network of the cotton, thereby allowing more nanoparticles to attach within the core of the cotton. Other potential solutions include to increase the concentration of the nanoparticle suspension used to coat the cotton, or increase the time that the cotton is subjected to the nanoparticle suspension.

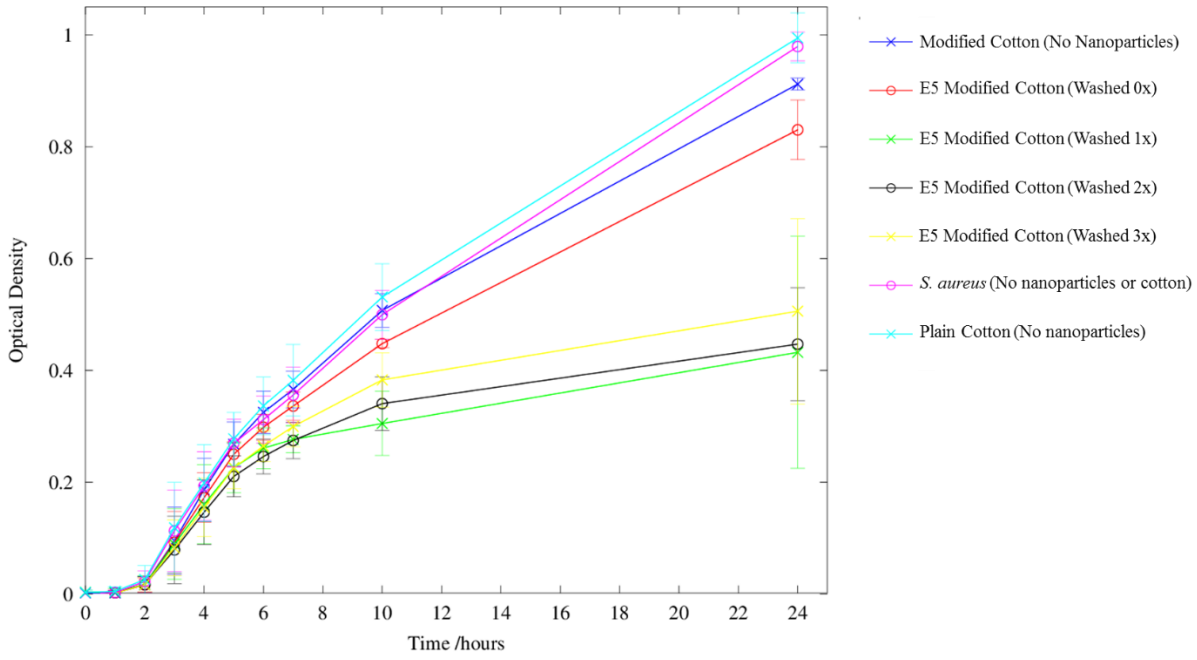

Figure 41. Optical density of cotton samples and controls measured over time against *S. aureus*.

Table 16. Average optical density with standard deviation over time for each sample.

Time	Modified Cotton	Washed 0x	Washed 1x	Washed 2x
0	0.002 ± 0.003	0.001 ± 0.001	0.003 ± 0.004	0.001 ± 0.001
1	0.002 ± 0.003	0.002 ± 0.003	0.004 ± 0.006	0.002 ± 0.004
2	0.017 ± 0.02	0.016 ± 0.01	0.017 ± 0.02	0.017 ± 0.02
3	0.095 ± 0.06	0.093 ± 0.06	0.089 ± 0.06	0.079 ± 0.06
4	0.187 ± 0.06	0.172 ± 0.04	0.160 ± 0.07	0.146 ± 0.06
5	0.268 ± 0.04	0.250 ± 0.02	0.226 ± 0.04	0.210 ± 0.04
6	0.325 ± 0.04	0.298 ± 0.02	0.261 ± 0.04	0.246 ± 0.03
7	0.366 ± 0.03	0.336 ± 0.03	0.277 ± 0.02	0.275 ± 0.03
10	0.507 ± 0.03	0.448 ± 0.007	0.305 ± 0.06	0.341 ± 0.05
24	0.912 ± 0.01	0.830 ± 0.053	0.432 ± 0.200	0.447 ± 0.100

Table 17. Average optical density with standard deviation over time for each sample.

Time	Washed 3x	*S. aureus*	Plain Cotton
0	0.001 ± 0.001	0.001 ± 0.001	0.003 ± 0.004
1	0.002 ± 0.003	0.003 ± 0.005	0.005 ± 0.008
2	0.017 ± 0.01	0.022 ± 0.02	0.026 ± 0.025
3	0.083 ± 0.05	0.113 ± 0.07	0.119 ± 0.08
4	0.155 ± 0.05	0.193 ± 0.06	0.199 ± 0.07
5	0.226 ± 0.04	0.270 ± 0.04	0.278 ± 0.05
6	0.265 ± 0.03	0.312 ± 0.04	0.337 ± 0.05
7	0.300 ± 0.05	0.356 ± 0.05	0.382 ± 0.06
10	0.383 ± 0.05	0.500 ± 0.04	0.531 ± 0.06
24	0.506 ± 0.2	0.979 ± 0.03	0.995 ± 0.05

CHAPTER 5. CONCLUSIONS AND FUTURE DIRECTIONS

At the beginning of this research, a selective precipitation method for Mn^{2+} doped ZnO nanoparticles was developed for narrowing their size distribution. Through TEM analysis, the selective precipitation technique was successful in separating small and large 10% Mn^{2+} ZnO nanoparticles in average sizes of 7 and 426 nm, respectively. ZnO and the 10% Mn^{2+} doped ZnO were used to carry out antimicrobial testing to evaluate the role of particle size in the antimicrobial activity. The agar diffusion testing showed that both undoped and Mn^{2+} doped ZnO nanoparticles exhibit antimicrobial activity against both *E. coli* and *S. aureus*. The MIC tests were inconclusive against *E. coli*, but *S. aureus* indicated that the medium ZnO nanoparticles were slightly more effective compared to the small and large ZnO. However, 10% Mn^{2+} doped ZnO nanoparticles exhibited the same MIC range for both medium and large nanoparticles. While small particles have a large surface to volume ratio, it is not only size that plays a role but the complete morphology of the nanoparticles. Thus, if the nanoparticles are small, then their shape, and lack of monodispersibility can inhibit their use as antimicrobial agents. These nanoparticles, even with the selective precipitation exhibited a high polydispersibility and thus we moved away from this nanoparticle synthesis method for future testing.

In the second part of this project, Eu^{3+} doped ZnO nanoparticles were synthesized by modifying a literature-based precipitation method for ZnO nanoparticles.[22] The design of the synthetic method was based on the ratios of ammonium carbonate to zinc nitrate hexahydrate in the literature method, but adapted to include europium nitrate hexahydrate as the Eu^{3+} metal ion doping agent. The nanoparticles were successfully synthesized and it was found that Eu^{3+}

doping does not alter the basic crystal structure of ZnO, as accessed by the X-ray powder diffraction patterns. Antimicrobial testing was performed on these nanoparticles using both agar diffusion and MIC testing. Through data analysis, we found that all of the nanoparticles exhibit antimicrobial activity, however, the MIC test results demonstrated that the theoretically calculated 5% Eu^{3+} doped ZnO nanoparticles showed the most inhibition of bacterial growth across all three bacterial species with MIC value ranges of 1.25 – 0.625 mg/mL, 2.50 – 1.25 mg/mL, and 0.625 – 0.313 mg/mL for *E. coli*, *S. aureus* and *S. epidermidis*, respectively. This percentage was then chosen for further study and attachment to cotton textile. We also observed that gram-negative bacteria was more resistant to the antimicrobial activity of the ZnO nanoparticles compared to the gram-positive bacteria. Thus in future studies, we would like to study several more gram-negative and gram-positive bacteria species to see if this trend holds true over multiple species.

At the latter of the project, two techniques for nanoparticle attachment to cotton textile were chosen. These two methods were used to attach E5 (5.5% Eu^{3+}) nanoparticles to bleached woven cotton and evaluated against one pathogenic bacterial species, *S. aureus*. The nanoparticle attachment to cotton showed promising results for both methods. The agar diffusion for both the 2-propanol attachment method, and the modified cotton (using citric acid as a crosslinker) showed small zones of inhibition even after two washes. However, the cotton modification method with citric acid as a crosslinker, showed the most promising results. The time-dependent studies showed that the *S. aureus* growth was inhibited to 51.7% of the normal bacterial growth, even after three washes. Due to this encouraging result, this part of the project is going to be continued with some optimization of the nanoparticle attachment to cotton through varying the concentration of the nanoparticle suspension used to coat the cotton, and varying the

attachment conditions. One method planned is to use heat to potentially expand the woven fibers of the cotton textile to allow for more nanoparticles to attach. Additionally, we would like to see results for all three bacterial species, and additional trials of the *S. aureus* time-dependent testing.

CHAPTER 6. REFERENCES

(1) Hensley, B. J.; Monson, J. R. T. Hospital-Acquired Infections. *Surg.* **2015**, *33* (11), 528–533.

(2) Hidron, A. I.; Edwards, J. R.; Patel, J.; Horan, T. C.; Sievert, D. M.; Pollock, D. A.; Fridkin, S. K. NHSN Annual Update: Antimicrobial-Resistant Pathogens Associated with Healthcare-Associated Infections: Annual Summary of Data Reported to the National Healthcare Safety Network at the Centers for Disease Control and Prevention, 2006-2007. *Infect.Control Hosp.Epidemiol.* **2008**, *29* (1559-6834 (Electronic)), 996–1011.

(3) Klevens, R. M.; Edwards, J. R.; Richards, C. L.; Horan, T. C.; Gaynes, R. P.; Pollock, D. A.; Cardo, D. M. Estimating Health Care-Associated Infections and Deaths in U.S. Hospitals, 2002. *Public Health Rep.* **2007**, *122* (April), 160–166.

(4) Magill, S. S.; Edwards, J. R.; Bamberg, W.; Beldavs, Z. G.; Dumyati, G.; Kainer, M. A.; Lynfield, R.; Maloney, M.; McAllister-Hollod, L.; Nadle, J.; Ray, S. M.; Thompson, D. L.; Wilson, L. E.; Fridkin, S. K. Multistate Point-Prevalence Survey of Health Care–Associated Infections. *N. Engl. J. Med.* **2014**, *370* (13), 1198–1208.

(5) Mehta, Y.; Gupta, A.; Subhash, T.; Myatra, S.; Samaddar, D. P.; Patil, V.; Bhattacharya, P.; Ramasubban, S. Guidelines for Prevention of Hospital-Acquired Infections. *Indian J. Crit. Care Med.* **2014**, *18* (3), 149–163.

(6) Fijan, S.; Turk, S. ??ostar. Hospital Textiles, Are They a Possible Vehicle for Healthcare-Associated Infections? *Int. J. Environ. Res. Public Health* **2012**, *9* (9), 3330–3343.

(7) Rajendran, S.; Anand, S. C. Application of Woven Structures in Hospitals. In *Woven Textiles: Principles, Developments and Applications*; Gandhi, K. L., Ed.; Woodhead

Publishing Limited: Oxford, 2012; pp 431–436.

(8) Neely, A. N.; Maley, M. P. Survival of Enterococci and Staphylococci on Hospital Fabrics and Plastic. *J. Clin. Microbiol.* **2000**, *38* (2), 724–726.

(9) Manivannan, G.; Sawan, S. P. Perspectives on Infectious Disease Challenges and Antimicrobial Answers. In *Antimicrobial/anti-infective Materials: Principles, Applications and Devices*; Sawan, S. P., Ed.; CRC Press: Lancaster, 2000; pp 1–20.

(10) Beyth, N.; Houri-haddad, Y.; Domb, A.; Khan, W.; Hazan, R. Alternative Antimicrobial Approach : Nano-Antimicrobial Materials. **2015**, *2015*.

(11) Blecher, K.; Nasir, A.; Friedman, A. The Growing Role of Nanotechnology in Combating Infectious Disease. *Virulence* **2011**, *2* (5), 395–401.

(12) Lakshmi Prasanna, V.; Vijayaraghavan, R. Insight Into the Mechanism of Antibacterial Activity of ZnO – Surface Defects Mediated Reactive Oxygen Species Even in Dark. *Langmuir* **2015**, 150729122119004.

(13) Rekha, K.; Nirmala, M.; Nair, M. G.; Anukaliani, a. Structural, Optical, Photocatalytic and Antibacterial Activity of Zinc Oxide and Manganese Doped Zinc Oxide Nanoparticles. *Phys. B Condens. Matter* **2010**, *405* (15), 3180–3185.

(14) Horikoshi, S.; Serpone, N. Introduction to Nanoparticles. In *Microwaves in Nanoparticle Synthesis: Fundamentals and Applications*; John Wiley & Sons, Ltd, 2013.

(15) Kang, S.; Pinault, M.; Pfefferle, L. D.; Elimelech, M. Single-Walled Carbon Nanotubes Exhibit Strong Antimicrobial Activity. *Langmuir* **2007**, *23* (17), 8670–8673.

(16) Dangge, G.; Xiying, D.; Chen, C.; Bin, L.; Jianzhong, M. Synthesis of Polymer Quaternary Ammonium Salt Containing Epoxy Group/Nano ZnO Long-Acting Antimicrobial Coating for Cotton Fabrics. *Ind. Eng. Chem. Res.* **2015**, *54* (43), 10560–

10567.

(17) Zinjarde, S. Bio-Inspired Nanomaterials and Their Applications as Antimicrobial Agents. *Chronicles Young Sci.* **2012**, *3* (1), 74.

(18) Sambhy, V.; MacBride, M. M.; Peterson, B. R.; Sen, A. Silver Bromide Nanoparticle/polymer Composites: Dual Action Tunable Antimicrobial Materials. *J. Am. Chem. Soc.* **2006**, *128* (30), 9798–9808.

(19) MubarakAli, D.; Thajuddin, N.; Jeganathan, K.; Gunasekaran, M. Plant Extract Mediated Synthesis of Silver and Gold Nanoparticles and Its Antibacterial Activity against Clinically Isolated Pathogens. *Colloids Surfaces B Biointerfaces* **2011**, *85* (2), 360–365.

(20) Kołodziejczak-Radzimska, A.; Jesionowski, T. Zinc Oxide—From Synthesis to Application: A Review. *Materials (Basel).* **2014**, *7* (4), 2833–2881.

(21) Lanje, A. S.; Sharma, S. J.; Ningthoujam, R. S.; Ahn, J.-S.; Pode, R. B. Low Temperature Dielectric Studies of Zinc Oxide (ZnO) Nanoparticles Prepared by Precipitation Method. *Adv. Powder Technol.* **2013**, *24* (1), 331–335.

(22) Raoufi, D. Synthesis and Microstructural Properties of ZnO Nanoparticles Prepared by Precipitation Method. *Renew. Energy* **2013**, *50*, 932–937.

(23) Talam, S.; Karumuri, S. R.; Gunnam, N. Synthesis, Characterization, and Spectroscopic Properties of ZnO Nanoparticles. *ISRN Nanotechnol.* **2012**, *2012*, 1–6.

(24) Hong, R.; Pan, T.; Qian, J.; Li, H. Synthesis and Surface Modification of ZnO Nanoparticles. *Chem. Eng. J.* **2006**, *119* (2-3), 71–81.

(25) Kolodziejczak-Radzimska, a.; Jesionowski, T.; Krysztafkiewicz, a. Obtaining Zinc Oxide from Aqueous Solutions of KOH and Zn(CH3COO)2. *Physiochemical Probl. Miner. Process.* **2010**, *44*, 93–102.

(26) Mei, Y.; Lu, Y.; Yan, B. Soft Materials Composed with Lanthanide (Eu, Tb) Beta-Diketonates and ZnO Nanoparticles through Ionic Liquid Linkage to Integrate White Luminescence. *J. Photochem. Photobiol. A Chem.* **2014**, *280*, 1–4.

(27) Zhao, X.; Zheng, B.; Li, C.; Gu, H. Acetate-Derived ZnO Ultrafine Particles Synthesized by Spray Pyrolysis. *Powder Technol.* **1998**, *100* (98), 20–23.

(28) Sirelkhatim, A.; Mahmud, S.; Seeni, A.; Kaus, N. H. M.; Ann, L. C.; Bakhori, S. K. M.; Hasan, H.; Mohamad, D. Review on Zinc Oxide Nanoparticles: Antibacterial Activity and Toxicity Mechanism. *Nano-Micro Lett.* **2015**, *7* (3), 219–242.

(29) Kreher, K. *Fundamentals of Semiconductors – Physics and Materials Properties*; 1997; Vol. 198.

(30) Jan, T.; Iqbal, J.; Ismail, M.; Zakaullah, M.; Haider Naqvi, S.; Badshah, N. Sn Doping Induced Enhancement in the Activity of ZnO Nanostructures against Antibiotic Resistant S. Aureus Bacteria. *Int. J. Nanomedicine* **2013**, *8*, 3679–3687.

(31) Saif, M.; Hafez, H.; Nabeel, A. I. Photo-Induced Self-Cleaning and Sterilizing Activity of Sm3+ Doped ZnO Nanomaterials. *Chemosphere* **2013**, *90* (2), 840–847.

(32) Ghaemi, B.; Mashinchian, O.; Mousavi, T.; Karimi, R.; Kharrazi, S.; Amani, A. Harnessing the Cancer Radiation Therapy by Lanthanide-Doped Zinc Oxide Based Theranostic Nanoparticles. *ACS Appl. Mater. Interfaces* **2016**, acsami.5b10056.

(33) Liu, Y.; Xu, C.; Yang, Q. White Upconversion of Rare-Earth Doped ZnO Nanocrystals and Its Dependence on Size of Crystal Particles and Content of Yb3+ and Tm3+. *J. Appl. Phys.* **2009**, *105* (8), 1–7.

(34) Zamiri, R.; Lemos, A. F.; Reblo, A.; Hossein, A. A.; Ferreira, J. M. F. Effects of Rare-Earth Doping on Morphology and Structure Properties of ZnO Nanostructures Prepared

by Wet Chemical Method. *Ceram. Int.* **2013**, *40*, 523–529.

(35) Shi, H.; Zhang, P.; Li, S. S.; Xia, J. B. Magnetic Coupling Properties of Rare-Earth Metals (Gd, Nd) Doped ZnO: First-Principles Calculations. *J. Appl. Phys.* **2009**, *106* (2), 1–6.

(36) Yang, L.; Jiang, Z.; Dong, J.; Pan, A.; Zhuang, X. The Study on Crystal Defects-Involved Energy Transfer Process of Eu Doped ZnO Lattice. *Mater. Lett.* **2014**, *129*, 65–67.

(37) Liu, Y.; Luo, W.; Li, R.; Liu, G.; Antonio, M. R.; Chen, X. Optical Spectroscopy of Eu Doped ZnO Nanocrystals. *J. Phys. Chem.* **2008**, *112*, 686–694.

(38) Yetisen, A. K.; Qu, H.; Manbachi, A.; Butt, H.; Dokmeci, M. R.; Hinestroza, J. P.; Skorobogatiy, M.; Khademhosseini, A.; Yun, S. H. Nanotechnology in Textiles. *ACS Nano* **2016**, acsnano.5b08176.

(39) Jorgensen, J. H.; Ferraro, M. J. Antimicrobial Susceptibility Testing: A Review of General Principles and Contemporary Practices. *Clin. Infect. Dis.* **2009**, *49* (11), 1749–1755.

(40) Rampersad, S. N. Multiple Applications of Alamar Blue as an Indicator of Metabolic Function and Cellular Health in Cell Viability Bioassays. *Sensors* **2012**, *12* (12), 12347–12360.

(41) He, W.; Kim, H. K.; Wamer, W. G.; Melka, D.; Callahan, J. H.; Yin, J. J. Photogenerated Charge Carriers and Reactive Oxygen Species in ZnO/Au Hybrid Nanostructures with Enhanced Photocatalytic and Antibacterial Activity. *J. Am. Chem. Soc.* **2014**, *136*, 750–757.

(42) Saif, M.; Abdel-Mottaleb, M. S. A. Titanium Dioxide Nanomaterial Doped with Trivalent Lanthanide Ions of Tb, Eu and Sm: Preparation, Characterization and Potential Applications. *Inorganica Chim. Acta* **2007**, *360* (9), 2863–2874.

(43) Wu, J.; Zhang, G.; Liu, J.; Gao, H.; Song, C.; Du, H.; Zhang, L.; Gong, Z.; L??, Y.

Synthesis, Characteristics, and Antibacterial Activity of a Rare-Earth Samarium/silver/titanium Dioxide Inorganic Nanomaterials. *J. Rare Earths* **2014**, *32* (8), 727–732.

(44) Darsanasiri, N. Synthesis and Property Investigation of Metal-Based Nanomaterials for Biotechnological Applications, Western Carolina University, 2014.

(45) M. P. Weinstein. *Methods for Dilution Antimicrobial Susceptibility Tests for Bacteria That Grow Aerobically ; Approved Standard — Ninth Edition*; 2012; Vol. 32.

(46) European Commitee of Antimicrobial Susceptibility Testing. Antimicrobial Susceptibility Testing: EUCAST Disk Diffusion Method. **2014**, No. June, 1–18.

(47) Ambika, S.; Sundrarajan, M. Synthesis of β-cyclodextrin/ZnO Nanocomposites and Its Improved Antibacterial Activity on Cotton Fabric. *World J. Pharm. Pharm. Sci.* **2014**, *3* (4), 751–761.

(48) Voncina, B.; Le Marechal, A. M. Grafting of Cotton with B- Cyclodextrin via Poly(carboxylic Acid). *J. Appl. Polym. Sci.* **2005**, *96* (4), 1323–1328.

(49) Martel, B.; Weltrowski, M.; Ruffin, D.; Morcellet, M. Polycarboxylic Acids as Crosslinking Agents for Grafting Cyclodextrins onto Cotton and Wool Fabrics: Study of the Process Parameters. *J. Appl. Polym. Sci.* **2002**, *83* (7), 1449–1456.

(50) Wang, C. M.; He, J. X. Research on the Multifunction Fabric Loaded with Nano-ZnO and β-Cyclodextrin. *Adv. Mater. Res.* **2011**, *332-334*, 1439–1442.

(51) Martel, B.; Morcellet, M.; Ruffin, D.; Vinet, F.; Weltrowski, L. Capture and Controlled Release of Fragrances by CD Finished Textiles. *J. Incl. Phenom. Macrocycl. Chem.* **2002**, *44* (1/4), 439–442.

(52) Becheri, A.; Dürr, M.; Lo Nostro, P.; Baglioni, P. Synthesis and Characterization of Zinc

Oxide Nanoparticles: Application to Textiles as UV-Absorbers. *J. Nanoparticle Res.* **2008**, *10* (4), 679–689.

(53) Yin, M.; Li, Z.; Kou, J.; Zou, Z. Mechanism Investigation of Visible Light-Induced Degradation in a Heterogeneous TiO 2 /Eosin Y/Rhodamine B System. *Environ. Sci. Technol.* **2009**, *43* (21), 8361–8366.

(54) Rahman, Q. I.; Ahmad, M.; Misra, S. K.; Lohani, M. Effective Photocatalytic Degradation of Rhodamine B Dye by ZnO Nanoparticles. *Mater. Lett.* **2013**, *91*, 170–174.

(55) Becheri, A.; Dürr, M.; Lo Nostro, P.; Baglioni, P. Synthesis and Characterization of Zinc Oxide Nanoparticles: Application to Textiles as UV-Absorbers. *J. Nanoparticle Res.* **2008**, *10* (4), 679–689.

(56) "Physical Constants of Inorganic Compounds." In *CRC Handbook of Chemistry and Physics*; Haynes, W. M., Ed.; CRC Press/Taylor and Francis: Boca Raton, FL.

(57) Darsanasiri, N. D. Synthesis and Property Investigation of Metal-Based Nanomaterials for Biotechnological Applications, Western Carolina University, 2014.

(58) Miessler, G. L.; Tarr, D. A. *Inorganic Chemistry*, 4th ed.; Folchetti, N., DuPont, C., Neumann, J., Eds.; Pearson Prentice Hall: Glenview, 2011.

(59) Nowak, M.; Kauch, B.; Szperlich, P. Determination of Energy Band Gap of Nanocrystalline SbSI Using Diffuse Reflectance Spectroscopy. *Rev. Sci. Instrum.* **2009**, *80* (4), 046107.

(60) Goodall, J. B. M.; Illsley, D.; Lines, R.; Makwana, N. M.; Darr, J. A. Structure-Property-Composition Relationships in Doped Zinc Oxides: Enhanced Photocatalytic Activity with Rare Earth Dopants. *ACS Comb. Sci.* **2015**, *17* (2), 100–112.